Neural Reorganisation During Monroe Institute Hemi-Sync Inner Earth 'Plant Kingdom' Sessions: A Multiscale EEG Analysis

Michael McLeod - The Line Group Ltd

This study characterises the EEG dynamics during Hemi-Sync Inner Earth auditory entrainment using a baseline-referenced, multiscale analytical framework. The analysis quantifies spectral redistribution, spatial differentiation, informational complexity, cross-frequency coordination, temporal persistence, and dynamical state-space behaviour across defined recording epochs. All results derive from consistently preprocessed EEG data and are evaluated relative to the resting eyes-closed baseline. The study is descriptive in scope, with conclusions limited to measurable properties of neural activity and their systematic variation across conditions. No inferences are made regarding subjective experience, cognitive states, environmental interaction, or underlying mechanisms.

Scope and Limitations

This work makes no claims regarding consciousness, perception, subjective experience, or internal mental states. No inferences are drawn about environmental interaction, nonlocal effects, or information exchange beyond measured neural signals. The analyses do not propose causal mechanisms beyond association with the auditory entrainment protocol. Neurochemical, psychological, and phenomenological interpretations are outside scope. The study is not positioned as a clinical or therapeutic investigation and does not evaluate behavioural outcomes. Conclusions are limited to quantitative properties of neural activity and their variation relative to baseline.

Analytical Structure and Script Mapping

The analyses are organised to characterise neural activity during Monroe Institute's Hemi-Sync Inner Earth entrainment across progressively higher levels of organisation.

The framework begins with time-resolved spectral modulation, establishing band-level dynamics and their redistribution relative to resting baseline. Spatially resolved, baseline-anchored maps define the foundational pattern of reorganisation across channels and frequency bands.

Signal complexity is then examined to determine whether observed spectral changes reflect increased dispersion or more constrained temporal structure. Power spectral density analyses verify that envelope-level findings correspond to underlying frequency-domain characteristics rather than artefactual transformations.

Cross-frequency coupling metrics assess hierarchical coordination between bands across cortical regions, while dwell-time and autocorrelation measures quantify the persistence and stability of emerging regimes.

State-space reorganisation velocity provides a global summary of neural trajectory evolution, integrating spectral, spatial, and temporal dimensions within a unified dynamical framework.

Together, these analyses describe neural signal organisation across scales while remaining restricted to observable EEG dynamics.

Data and Methods

All data were acquired from a single participant (author) across multiple recording days using a consistent EEG hardware and preprocessing pipeline. EEG signals were recorded with the Emotiv Flex 2.0, a 32-channel research-grade wireless EEG system configured according to the international 10–20 electrode layout. The sampling rate for raw EEG data was 256 Hz, and band-power (FFT) metrics were calculated at an 8 Hz cadence.

The participant had approximately eight years of prior experience using Monroe Institute Hemi-Sync auditory protocols. This extended familiarity reduces novelty-related confounds and supports interpretation of observed signal dynamics within a stable experiential context.

Baseline recordings consisting of eyes-closed (EC) and brief eyes-open (EO) conditions were collected on 5 October. These segments served as reference distributions for baseline-referenced normalisation and z-scoring. The Plant Kingdom Outdoor session was recorded on 30 October, and the Plant Kingdom Indoor session on 31 October. All analysed epochs were of equal duration (2 minutes), corresponding to the full length of the auditory prompt used in each session.

Five indoor recordings were acquired in total; the session with the lowest residual EMG contamination was selected as the primary indoor dataset. Selection was based solely on artefact burden and not on the magnitude or direction of any reported outcome features. A single outdoor recording was obtained under matched protocol conditions. A localised EMG-contaminated segment in the outdoor dataset was manually inspected and corrected prior to analysis; no other manual signal manipulation was performed.

All analyses are descriptive and baseline-referenced. No inferential statistical testing was conducted. The results are presented as an exploratory, single-participant case study characterising signal-level organisation across conditions.

Frequency Band Power Dynamics Across Time

This analysis tracks canonical EEG band power across time to characterise the temporal evolution of spectral dynamics during each experimental condition. Continuous band-power estimates preserve sustained states, gradual transitions, and transient events rather than collapsing activity into condition-level summaries. Band-limited power was analysed for theta (4–8 Hz), alpha (8–12 Hz), low beta (12–16 Hz), high beta (16–25 Hz), and gamma (25–45 Hz). Estimates were sampled at 8 Hz (125 ms resolution) from device-derived band-power streams. For each band, power values were aggregated across electrodes using the median to capture dominant system-level behaviour while reducing sensitivity to isolated channel fluctuations. Analyses were restricted to defined experimental epochs to ensure context alignment. The results presented here reflect absolute band-power dynamics rather than baseline-normalised values, allowing intrinsic temporal organisation within each session to be examined directly. Baseline-referenced comparisons and higher-order metrics are introduced in subsequent sections. These trajectories establish the spectral foundation for later analyses of entropy, cross-frequency coordination, and state-space reorganisation.

Theta Band Difference: Outdoor Minus Indoor (Baseline-Referenced)

Theta-band power differs between outdoor and indoor sessions in a predominantly negative and spatially heterogeneous pattern. Extended intervals of reduced theta activity are visible across many channels, interspersed with brief, channel-specific increases, indicating non-uniform modulation across cortex and time.

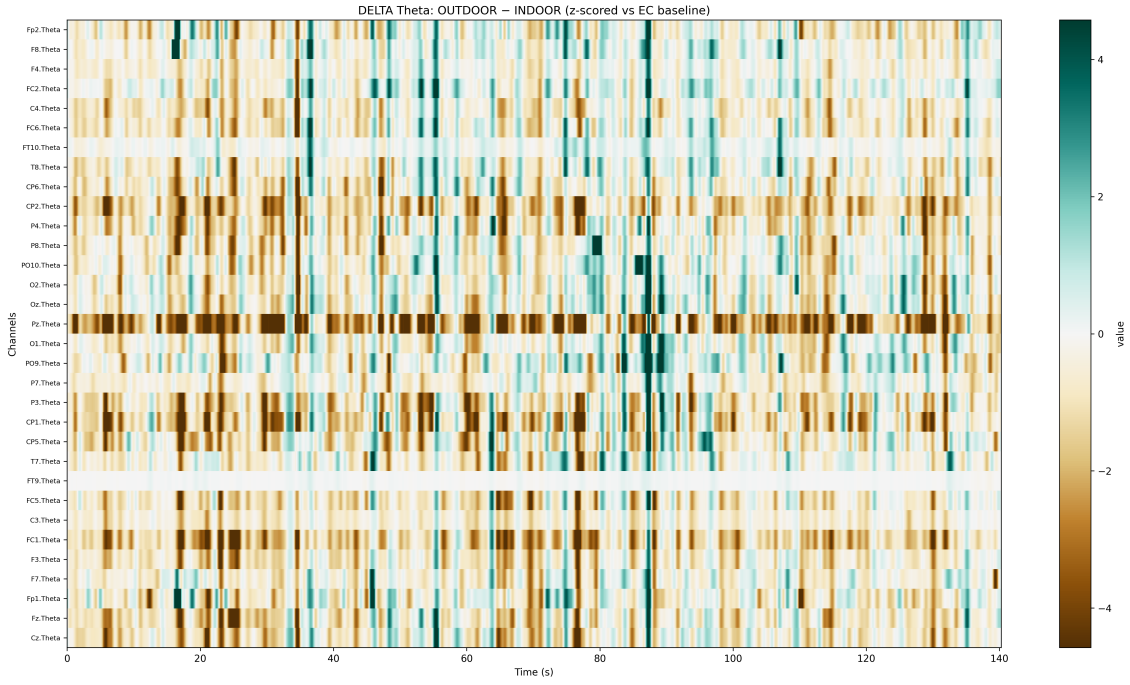

Figure 1: Theta-band power difference (Outdoor minus Indoor), expressed as z-scored deviation relative to the eyes-closed baseline.

Suppression is most pronounced in parietal and posterior midline electrodes, where negative deviations persist across longer segments of the epoch. Frontal and fronto-central channels show

more variable behaviour, alternating between mild enhancement and suppression and suggesting less stable theta organisation in these regions. Rather than forming sustained plateaus, theta differences fluctuate over shorter intervals, with polarity reversals occurring across multiple time scales. This pattern indicates transient, region-dependent modulation rather than a globally stable shift in theta power. The overall reduction in theta during the outdoor condition is compatible with reduced dominance of slower, integrative rhythms relative to the indoor session. Interpretation is restricted to signal-level redistribution and does not assume specific cognitive or environmental mechanisms.

Alpha Band Difference: Outdoor Minus Indoor (Baseline-Referenced)

Alpha power is reduced outdoors relative to the indoor session across most channels, with the strongest and most sustained suppression in parietal and occipital regions. These posterior deviations persist across extended portions of the epoch rather than appearing as brief or isolated events.

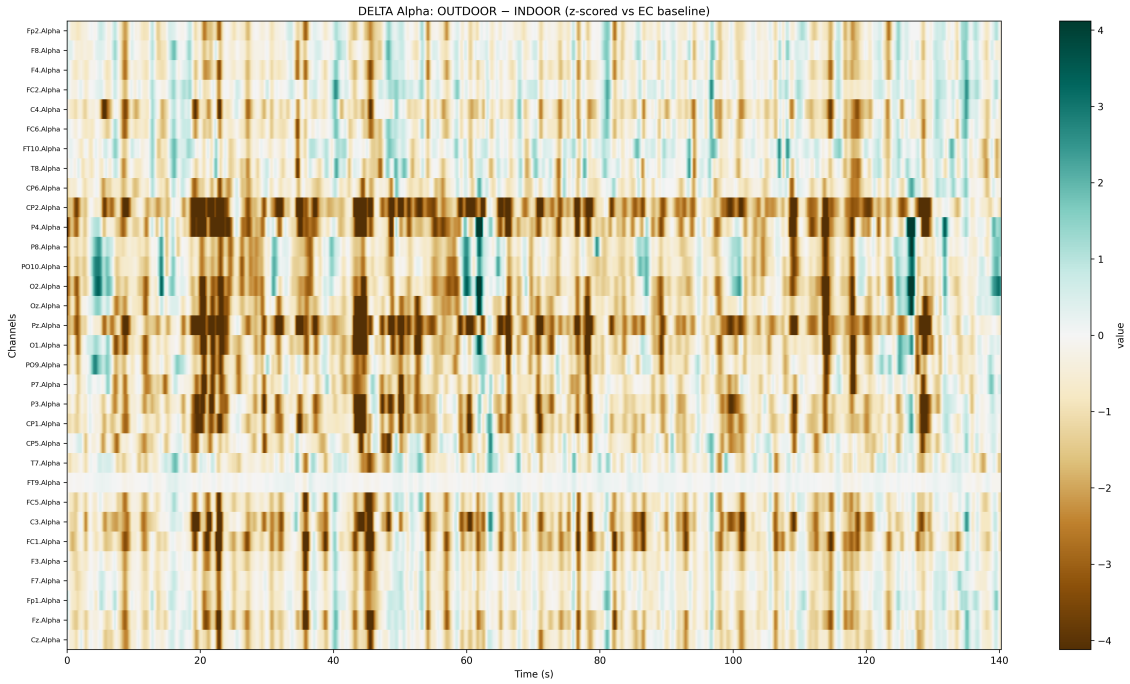

Figure 2: Alpha-band power difference (Outdoor minus Indoor), expressed as z-scored deviation relative to the eyes-closed baseline.

The effect is topographically structured rather than uniform. Posterior electrodes show continuous negative deviation, while frontal and fronto-central sites exhibit weaker and more intermittent changes, indicating regionally differentiated modulation rather than a global amplitude shift. Alpha suppression unfolds as a distributed, long-duration pattern with only brief partial recoveries, indicating a sustained redistribution of spectral energy rather than discrete onset–offset transitions. The temporal continuity and spatial specificity of the effect argue against transient artefact as a primary driver. The outdoor session therefore shows reduced dominance of posterior alpha rhythms relative to indoor conditions. Interpretation is restricted to signal-level redistribution and does not assume specific cognitive or environmental mechanisms.

Low-Beta Band Difference: Outdoor Minus Indoor (Baseline-Referenced)

Low-beta power shows a spatially mixed and time-varying pattern across the outdoor session relative to indoor. Periods of enhancement and suppression alternate across channels, with no single polarity dominating the epoch.

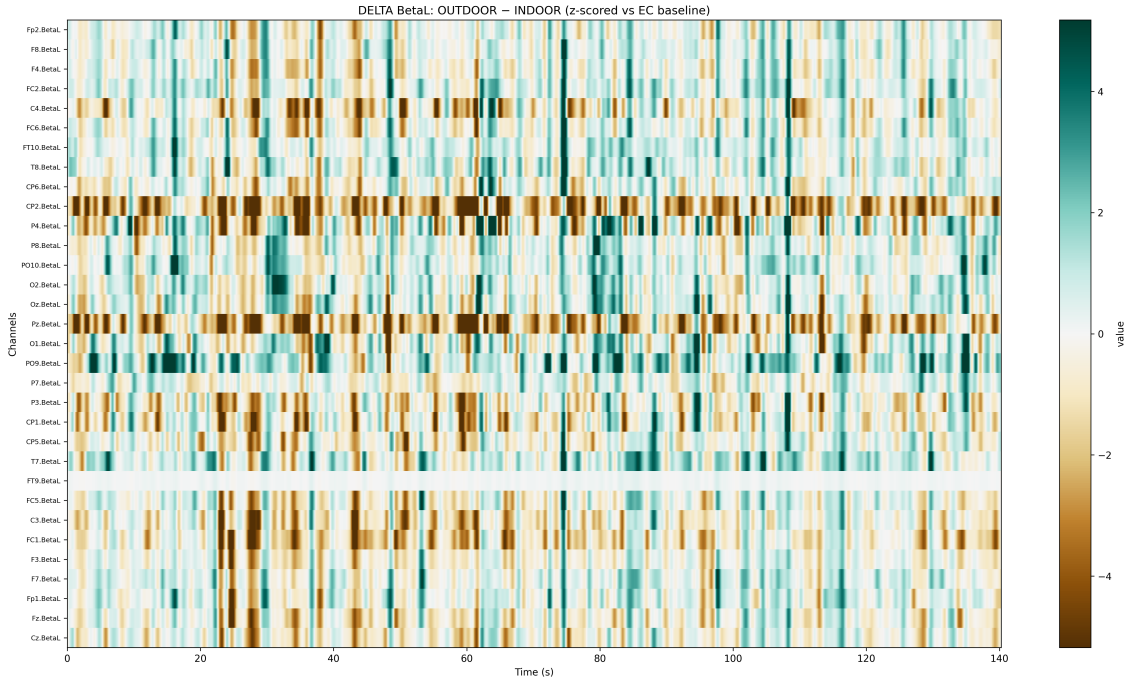

Figure 3: Low-beta (12–16 Hz) band power difference (Outdoor minus Indoor), expressed as z-scored deviation relative to the eyes-closed baseline.

Posterior and parietal electrodes display alternating bands of increased and reduced power, while frontal and fronto-central regions exhibit weaker and more intermittent deviations. The effect is therefore locally variable rather than globally coherent, indicating region-dependent modulation within this frequency range. Low-beta differences occur as shorter excursions rather than sustained plateaus, with polarity reversals appearing across multiple time scales. This contrasts with bands showing prolonged suppression and indicates a more transient and locally sensitive redistribution of activity. The outdoor condition does not produce a uniform shift in low-beta power but instead alters its spatial and temporal distribution relative to the indoor session. Interpretation is restricted to signal-level modulation and does not assume specific functional or behavioural mechanisms.

High-Beta Band Difference: Outdoor Minus Indoor (Baseline-Referenced)

High-beta power is elevated outdoors relative to the indoor session across much of the recording. Positive deviations dominate the map, particularly in temporal, parietal, and posterior regions where enhancement persists across extended segments of the epoch.

The distribution is regionally differentiated rather than uniform. Posterior and lateral electrodes show continuous high-beta elevation, whereas central and frontal sites display more heterogeneous behaviour, including intermittent reductions. This pattern indicates spatially selective modulation rather than a global amplification of activity. The increase is sustained over time, with relatively

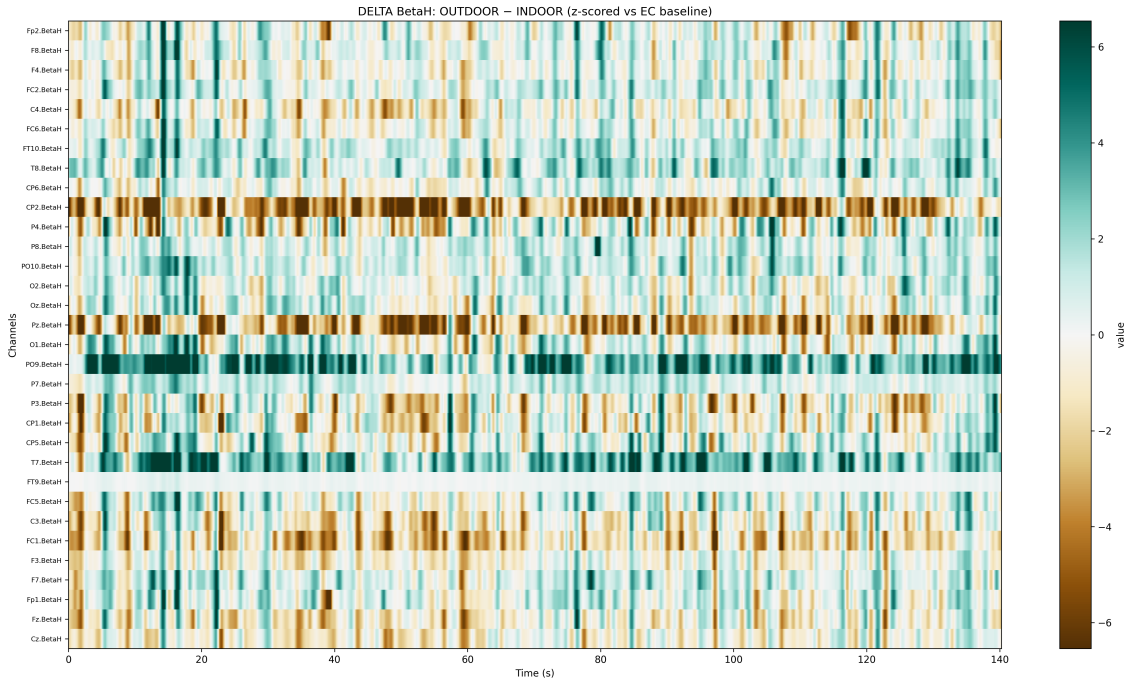

Figure 4: High-beta (16–25 Hz) band power difference (Outdoor minus Indoor), expressed as z-scored deviation relative to the eyes-closed baseline.

few brief reversals and no prominent transient spikes. The stability of the effect across channels and windows argues against isolated artefact as the primary source of the observed enhancement. Relative to the indoor session, the outdoor condition therefore shows increased expression of mid-to-high frequency activity within specific cortical regions. Interpretation remains limited to measurable spectral redistribution and does not assume specific cognitive or environmental mechanisms.

Gamma Band Difference: Outdoor Minus Indoor (Baseline-Referenced)

Gamma power is elevated outdoors relative to the indoor session across a substantial subset of channels, with sustained positive deviations visible throughout much of the epoch. The strongest increases occur in temporal, parietal, and posterior regions, where enhancement persists across extended time segments rather than appearing as isolated bursts.

The effect is spatially organised rather than uniform. Posterior and lateral electrodes show continuous bands of elevated gamma activity, while frontal and fronto-central sites exhibit weaker and more diffuse increases. This distribution indicates regionally specific modulation of high-frequency activity rather than a global gain effect. The enhancement remains stable across time, with relatively few polarity reversals and no prominent transient spikes. The persistence and channel consistency of the pattern are not characteristic of brief, irregular artefactual events. Relative to the indoor session, the outdoor condition therefore shows increased expression of high-frequency activity in posterior and temporal regions. Interpretation is limited to signal-level redistribution and does not assume specific cognitive or environmental mechanisms.

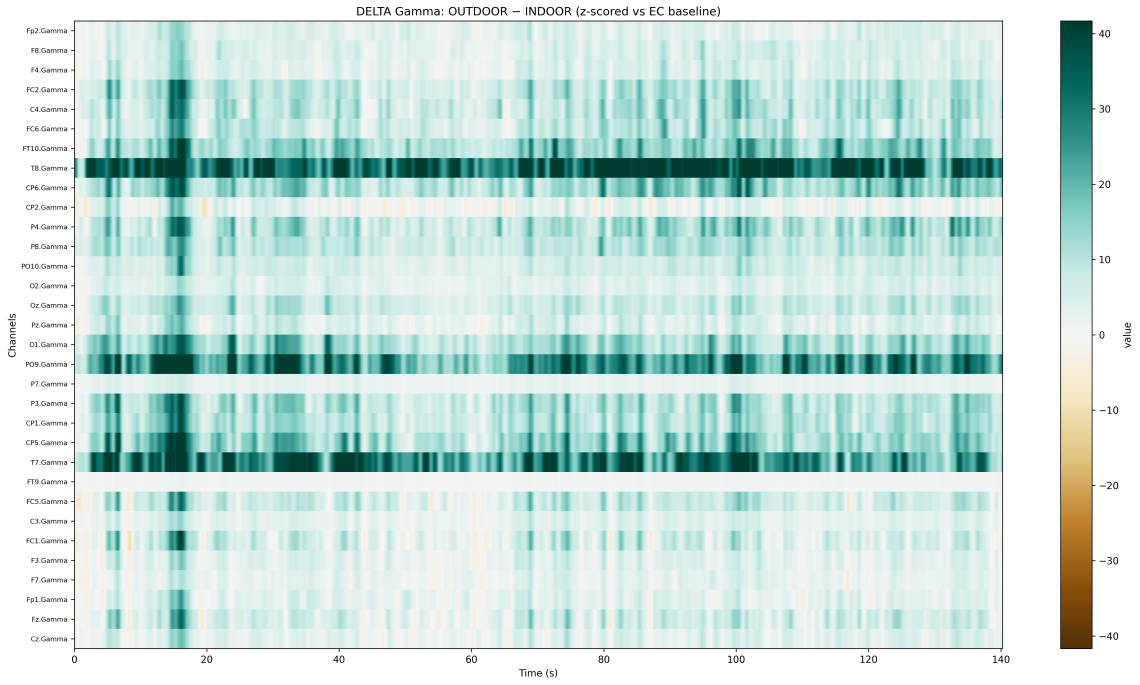

Figure 5: Gamma-band (25–45 Hz) power difference (Outdoor minus Indoor), expressed as z-scored deviation relative to the eyes-closed baseline.

Integrated Interpretation of Outdoor–Indoor Spectral Differences

Outdoor–Indoor comparisons reveal a frequency-dependent redistribution of spectral power rather than a uniform change in overall signal amplitude. Slower rhythms, particularly theta and alpha, are reduced during the outdoor session, while faster activity in the high-beta and gamma ranges is elevated across extended portions of the epoch. This opposing behaviour across bands indicates a shift in how spectral energy is distributed across frequency ranges.

The bands differ not only in direction but also in temporal stability and spatial structure. Theta and alpha reductions are sustained and most prominent in posterior regions, whereas high-beta and gamma elevations are stable and regionally organised across posterior and lateral channels. Low-beta activity occupies an intermediate position, showing greater temporal variability and spatial heterogeneity relative to the other bands.

The selectivity of these effects across frequency ranges and regions argues against a uniform global shift in activation. Instead, the outdoor session is associated with a redistribution of spectral expression across frequencies and cortical areas relative to the indoor session. Interpretation is restricted to signal-level reorganisation and does not assume specific cognitive, behavioural, or environmental mechanisms.

These band-power dynamics provide a time-resolved foundation for subsequent analyses of complexity, cross-frequency coordination, and state-space behaviour, which examine how the observed spectral redistribution relates to changes in neural stability and organisation across scales.

Baseline-Referenced Spectral Power Within Indoor and Outdoor Conditions

To complement the Outdoor–Indoor difference maps, band-power heatmaps were examined separately for the Indoor and Outdoor sessions relative to the eyes-closed baseline. These plots characterise the temporal evolution and spatial organisation of spectral activity within each condition independently of direct subtraction.

Panels (a–e) show baseline-referenced band power for the Indoor session across canonical frequency ranges, while panels (f–j) display the corresponding Outdoor session. In both conditions, spectral activity exhibits structured, channel-specific organisation rather than uniform fluctuation. Notable contrasts emerge in the stability and spatial distribution of alpha and high-frequency activity across sessions.

These baseline-referenced maps provide internal context for interpreting the Outdoor–Indoor difference analyses presented above.

Indoor Condition: Baseline-Referenced Band Power

Figures 6–10. Indoor Condition: Baseline-Referenced Band Power.

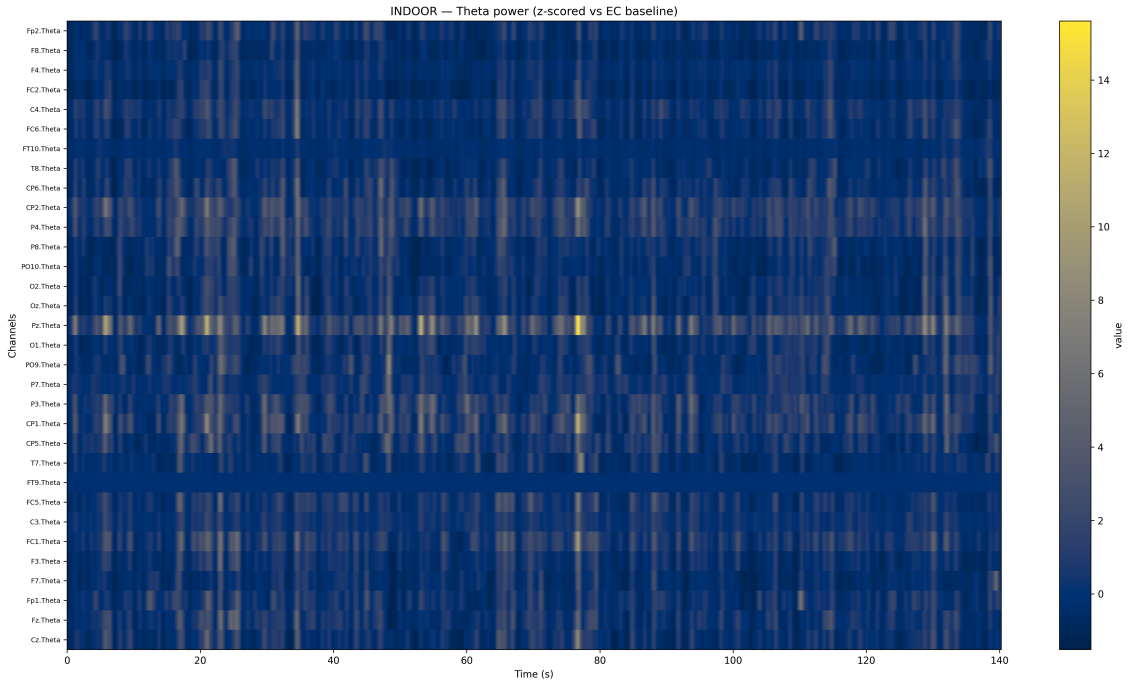

Figure 6: Panel a - Baseline-referenced theta-band (4–8 Hz) power within the Indoor condition (z-scored relative to eyes-closed baseline).

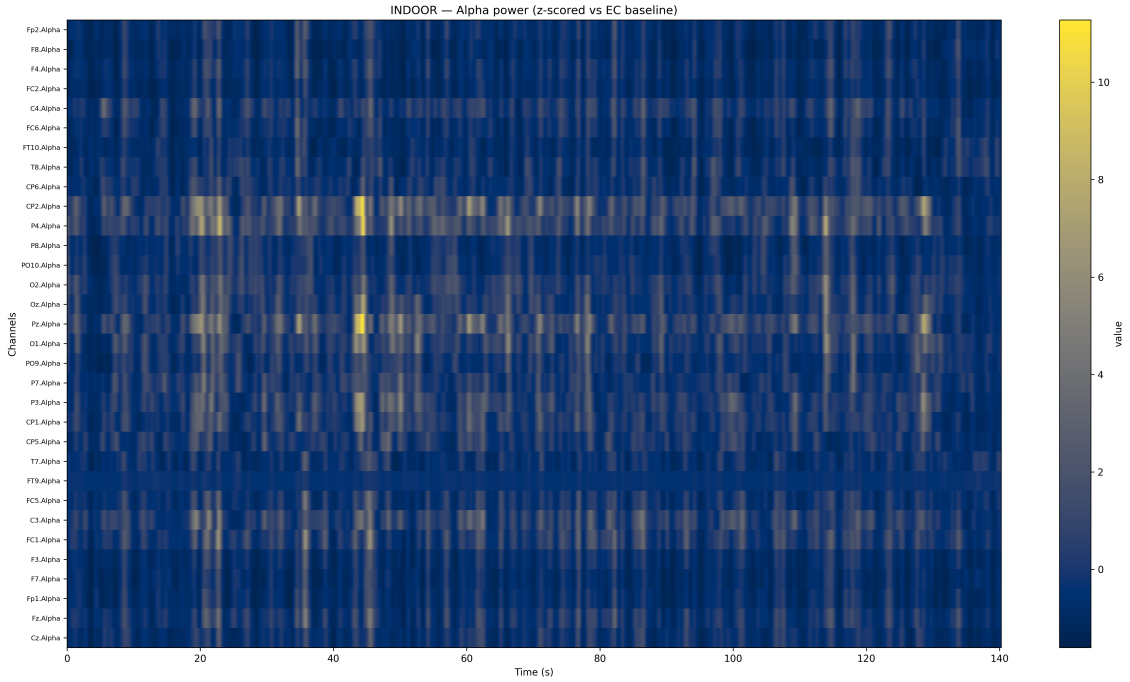

Figure 7: Panel b - Baseline-referenced alpha-band (8–12 Hz) power within the Indoor condition (z-scored relative to eyes-closed baseline).

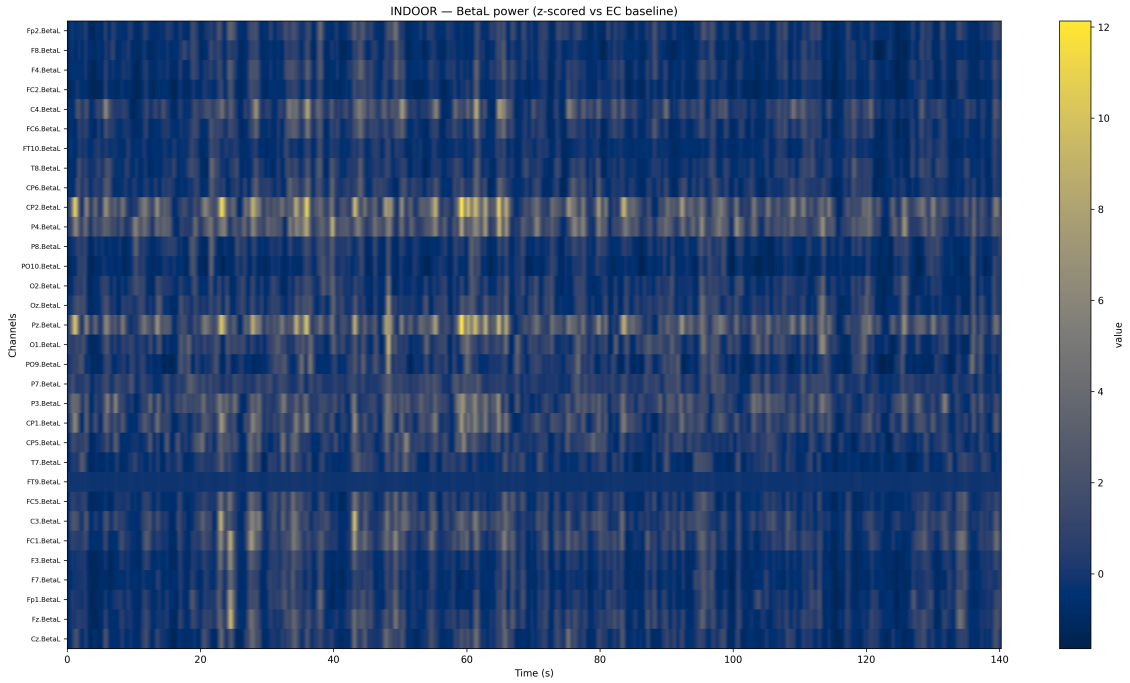

Figure 8: Panel c - Baseline-referenced low-beta (12–16 Hz) power within the Indoor condition (z-scored relative to eyes-closed baseline).

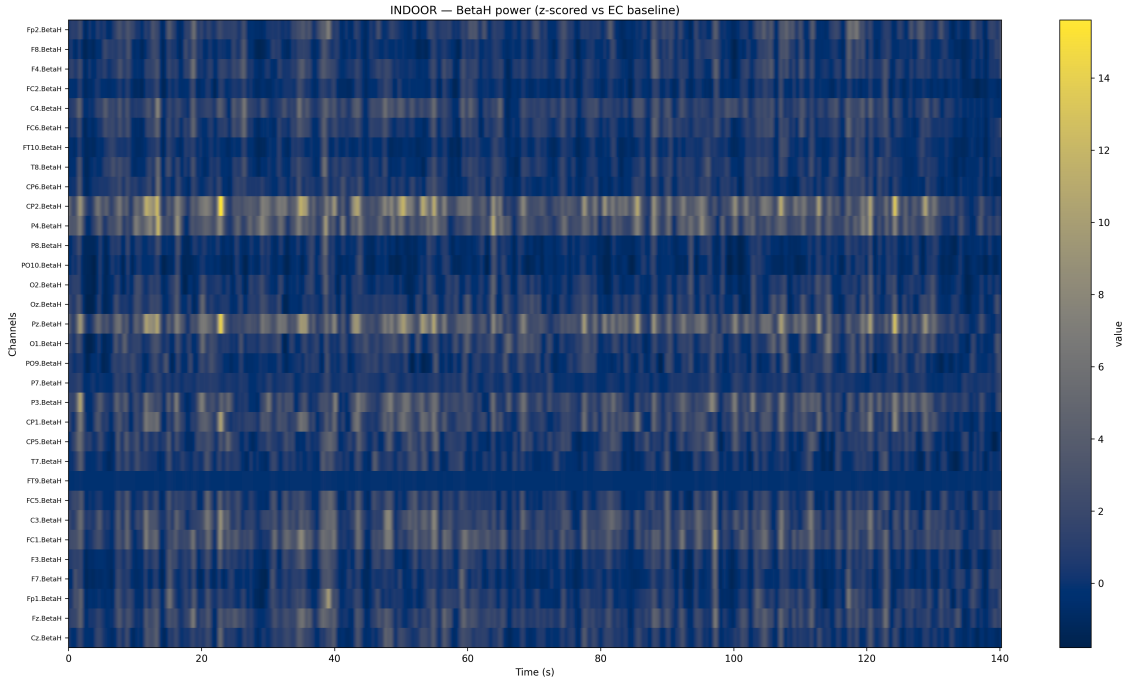

Figure 9: Panel d - Baseline-referenced high-beta (16–25 Hz) power within the Indoor condition (z-scored relative to eyes-closed baseline).

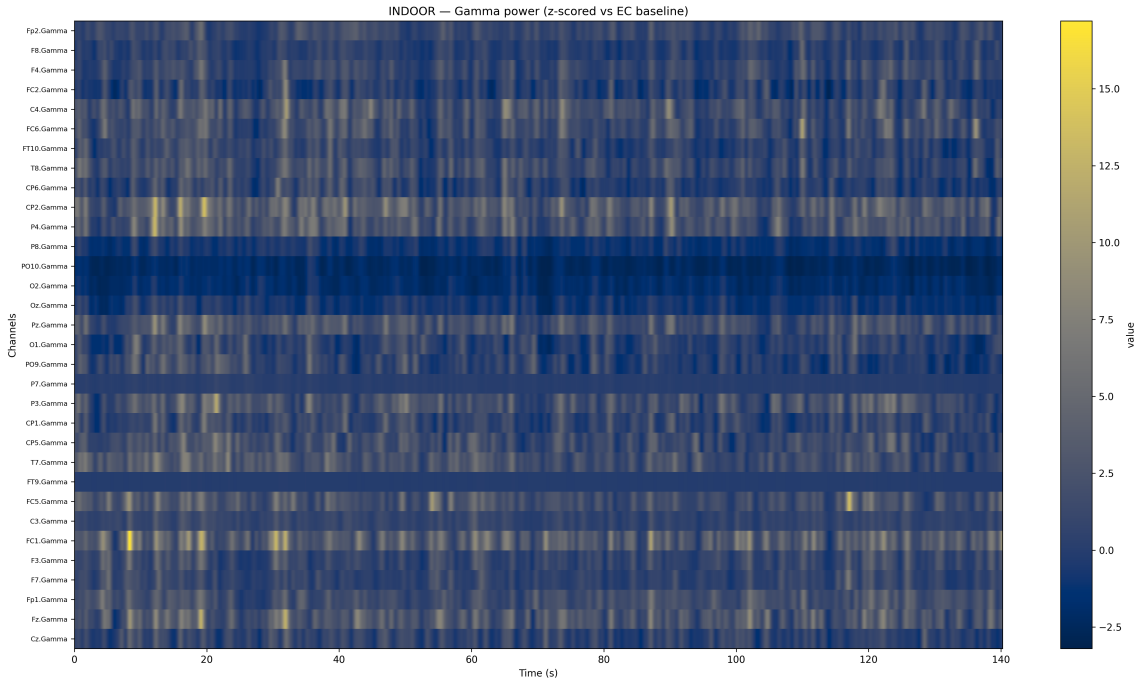

Figure 10: Panel e - Baseline-referenced gamma-band (25–45 Hz) power within the Indoor condition (z-scored relative to eyes-closed baseline).

Outdoor Condition: Baseline-Referenced Band Power

Figures 11–15. Outdoor Condition: Baseline-Referenced Band Power.

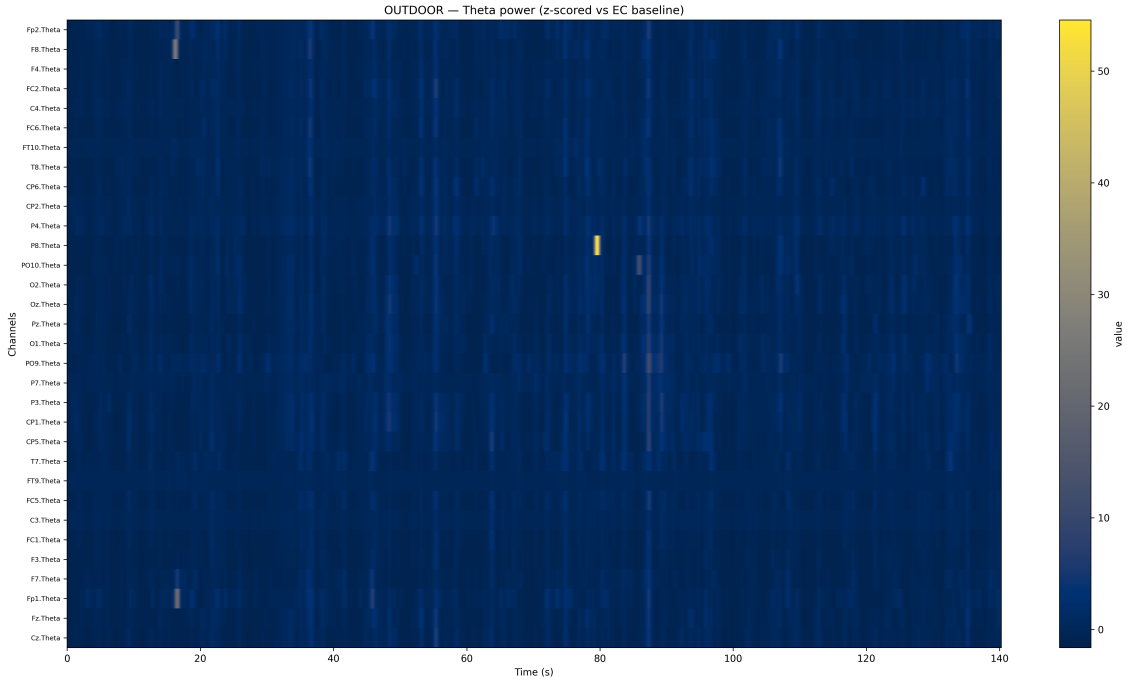

Figure 11: Panel f - Baseline-referenced theta-band (4–8 Hz) power within the Outdoor condition (z-scored relative to eyes-closed baseline).

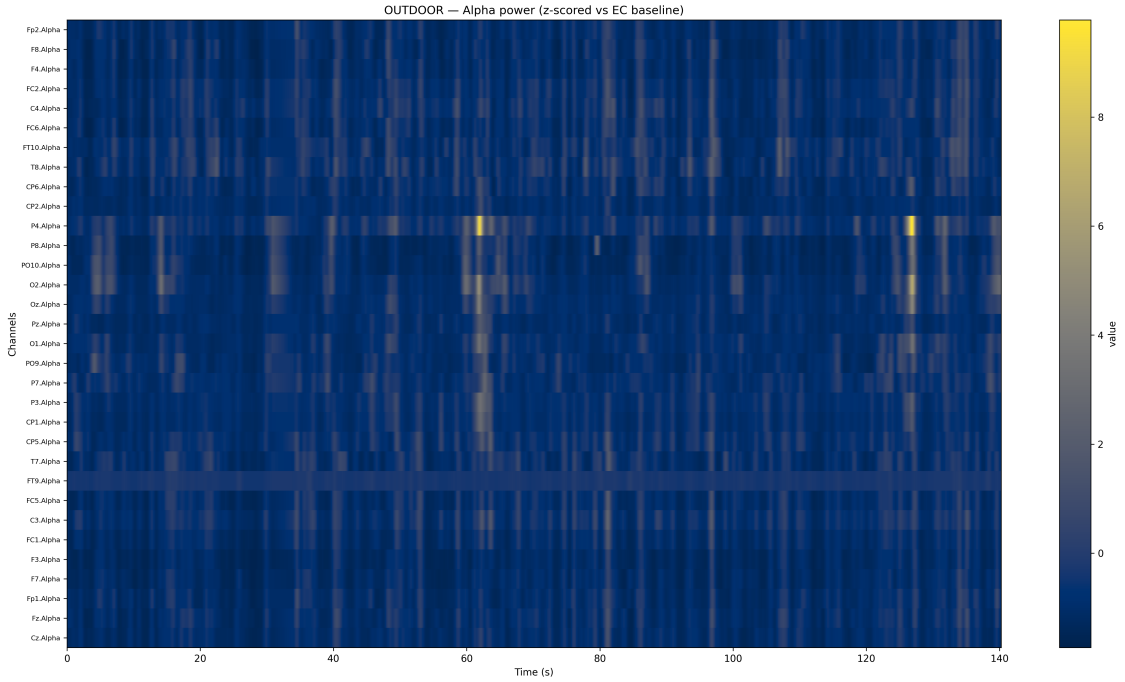

Figure 12: Panel g - Baseline-referenced alpha-band (8–12 Hz) power within the Outdoor condition (z-scored relative to eyes-closed baseline).

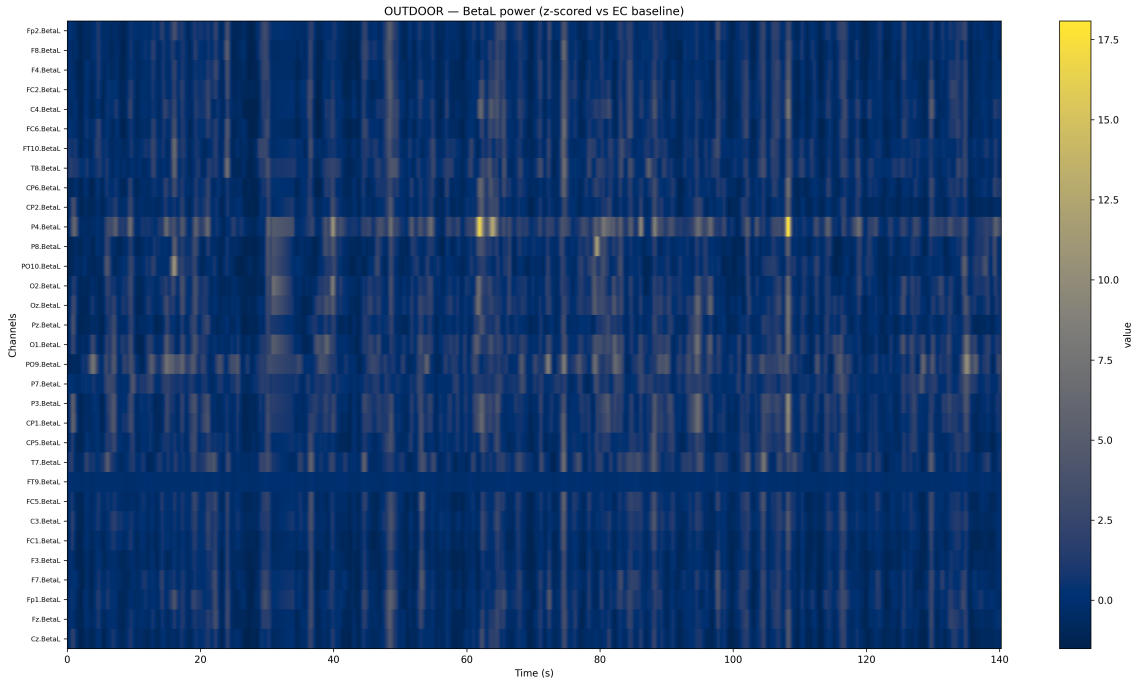

Figure 13: Panel h - Baseline-referenced low-beta (12–16 Hz) power within the Outdoor condition (z-scored relative to eyes-closed baseline).

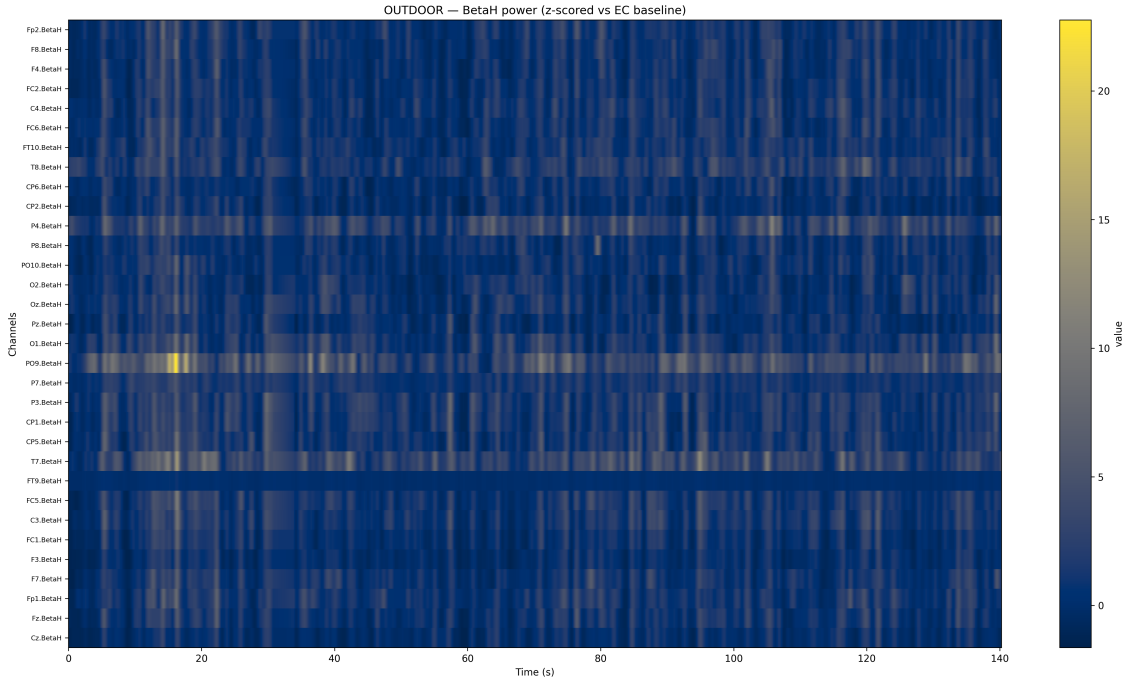

Figure 14: Panel i - Baseline-referenced high-beta (16–25 Hz) power within the Outdoor condition (z-scored relative to eyes-closed baseline).

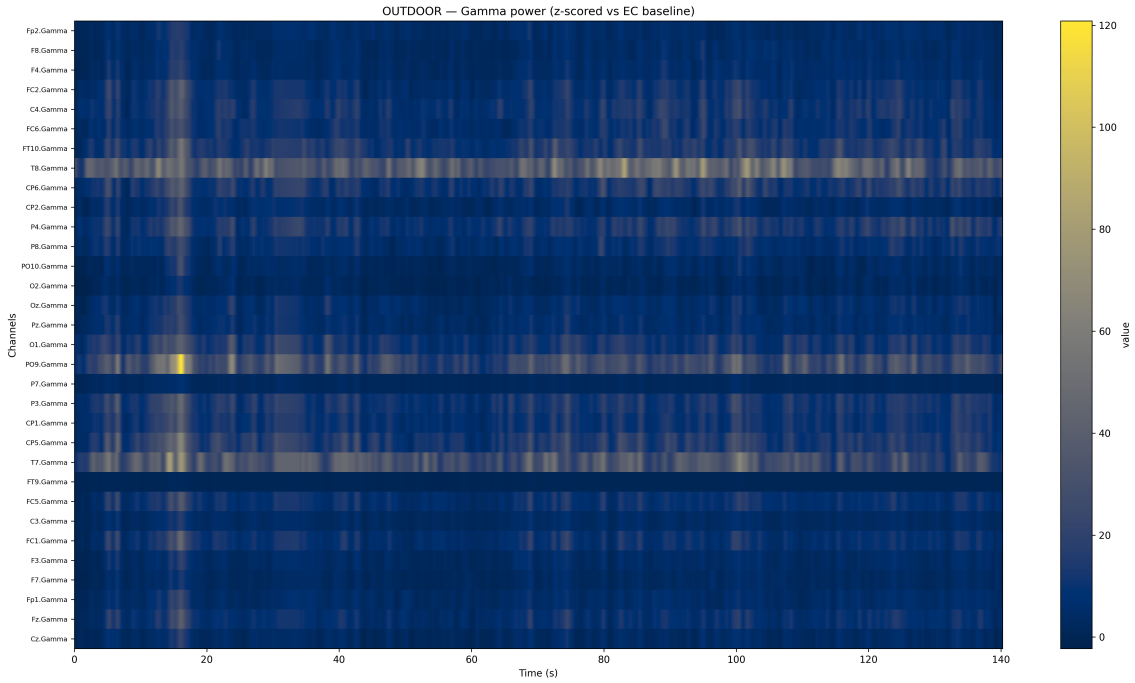

Figure 15: Panel j - Baseline-referenced gamma-band (25–45 Hz) power within the Outdoor condition (z-scored relative to eyes-closed baseline).

Examination of the baseline-referenced heatmaps shows that both Indoor and Outdoor sessions exhibit organised spectral structure across time and channels. Dominant rhythms form spatially consistent patterns with temporal continuity, indicating stable condition-specific organisation rather than transient fluctuation.

Relative to baseline, the Outdoor session shows reduced prominence of theta and alpha activity alongside more sustained expression of higher-frequency power, whereas the Indoor session retains stronger slow-rhythm expression. These patterns are consistent with the Outdoor–Indoor difference maps and indicate that the observed contrasts reflect differences in within-condition spectral organisation.

These time-resolved dynamics motivate subsequent analyses of signal complexity, cross-frequency coordination, and dynamical stability, which examine how the observed redistribution of power relates to broader changes in neural organisation.

Baseline-Normalized Band×Channel State Maps

Plant Kingdom Indoor: Whole-session band × channel mean z-scores relative to the eyes-closed baseline

Whole-session mean band-power deviations for the Indoor session show a structured, frequency-dependent departure from baseline across channels.

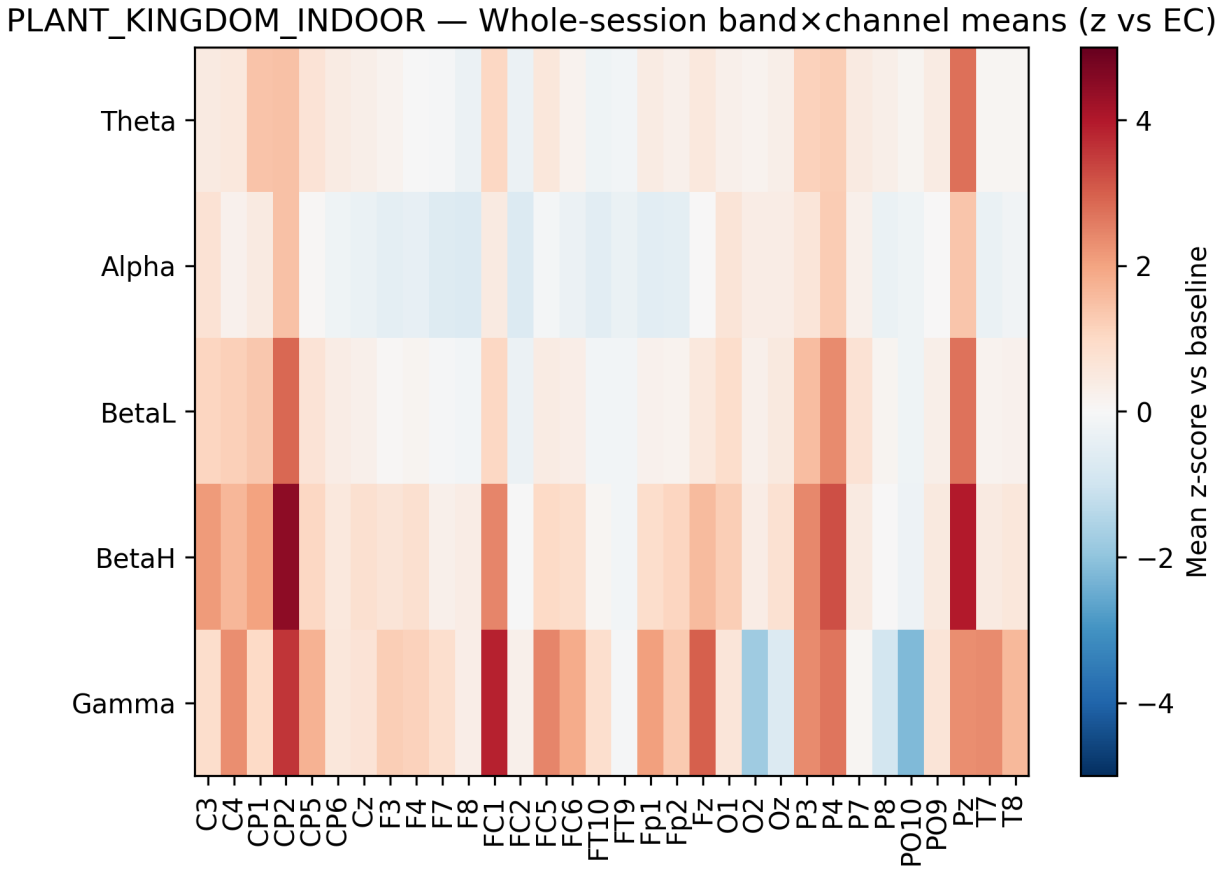

Figure 16: Plant Kingdom Indoor: whole-session band × channel mean z-scores relative to the eyes-closed baseline.

High-frequency activity is elevated overall, most prominently in the gamma range. Gamma power increases are spatially structured, with stronger deviations in specific regions rather than uniform elevation across all channels. High beta shows a similar but lower-magnitude pattern, with heterogeneous increases across multiple sites. Low beta deviations are comparatively modest and lack a consistent global pattern.

Alpha power is broadly reduced relative to baseline across much of the scalp, with spatial variation in magnitude but consistent direction. Theta activity remains heterogeneous and low in magnitude overall, showing only mild regional increases.

Taken together, the session-averaged map reflects a shift away from baseline slow-rhythm dominance toward increased high-frequency expression with regionally differentiated structure.

Plant Kingdom Outdoor: Whole-session band × channel mean z-scores relative to the eyes-closed baseline

Whole-session mean band-power deviations for the Outdoor session show a pronounced shift in spectral balance relative to baseline under the same aggregation and normalisation procedures used for the Indoor condition.

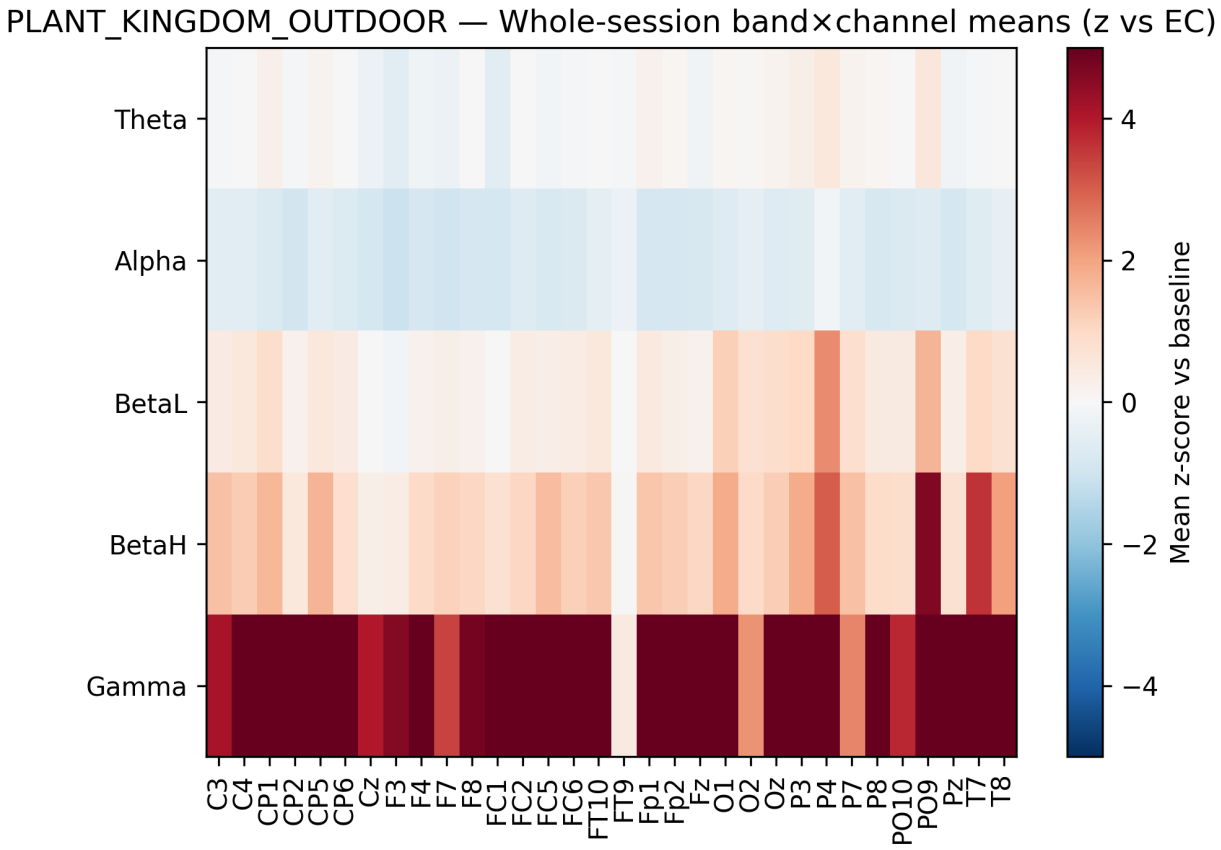

Figure 17: Plant Kingdom Outdoor: whole-session band × channel mean z-scores relative to the eyes-closed baseline.

High-frequency activity is prominently elevated, particularly in the gamma range, with positive deviations visible across most channels. Unlike the Indoor session, the elevation appears broadly distributed rather than regionally concentrated. High beta shows a similarly widespread increase, while low beta exhibits more modest deviations.

Alpha power is uniformly suppressed across the scalp relative to baseline, with few channels remaining near zero deviation. Theta activity remains close to baseline or mildly reduced at the session-averaged level, without clear global elevation.

Overall, the Outdoor map reflects a whole-session state characterised by reduced slow-rhythm expression and broadly increased high-frequency activity relative to baseline.

Summary: Indoor vs Outdoor

Figures 16 and 17 show that both sessions deviate substantially from the eyes-closed baseline. In each case, elevated high-frequency activity and reduced alpha power define the dominant spectral

state, indicating sustained departure from resting dynamics.

The sessions differ in spatial distribution and magnitude. The Indoor condition shows more regional differentiation, with localised peaks and heterogeneous engagement across channels. The Outdoor condition exhibits a more globally distributed and higher-magnitude high-frequency profile. These contrasts are visible directly in the whole-session maps.

These figures describe the average spectral state rather than its temporal evolution or stability. Questions of persistence, variability, and cross-frequency organisation are addressed in subsequent analyses, which build on the baseline-anchored state descriptions established here.

Entropy and Complexity Metrics — Band-Level (Five-Band Decomposition)

This section examines entropy and related complexity measures computed separately within canonical EEG frequency bands (Theta, Alpha, BetaL, BetaH, Gamma). Each band is treated as a distinct signal domain, allowing variability and structure to be assessed within bands prior to any cross-band synthesis.

In this context, entropy is used as a descriptive measure of variability and organisation in band-limited power signals. Higher values indicate greater dispersion or irregularity, whereas lower values indicate more stable or regular temporal structure. These metrics are presented without assuming specific cognitive or behavioural interpretations.

Figures are band-specific and visualise how entropy and related measures evolve across time, channels, or regions depending on the analysis. This separation allows band-dependent structure, stability, and variability to be examined without conflating dynamics across frequency ranges.

The analyses are exploratory and diagnostic, providing a reference for later comparison with measures of coordination, stability, and cross-frequency interaction. At this stage, interpretation remains restricted to signal-level behaviour within individual bands.

Entropy and Complexity Metrics: Baseline Eyes-Open vs Baseline Eyes-Closed

This figure compares Shannon entropy and Lempel–Ziv (LZ) complexity across canonical EEG bands during baseline eyes-open (EO) and eyes-closed (EC) conditions. Values are summarised at the band level for each baseline state.

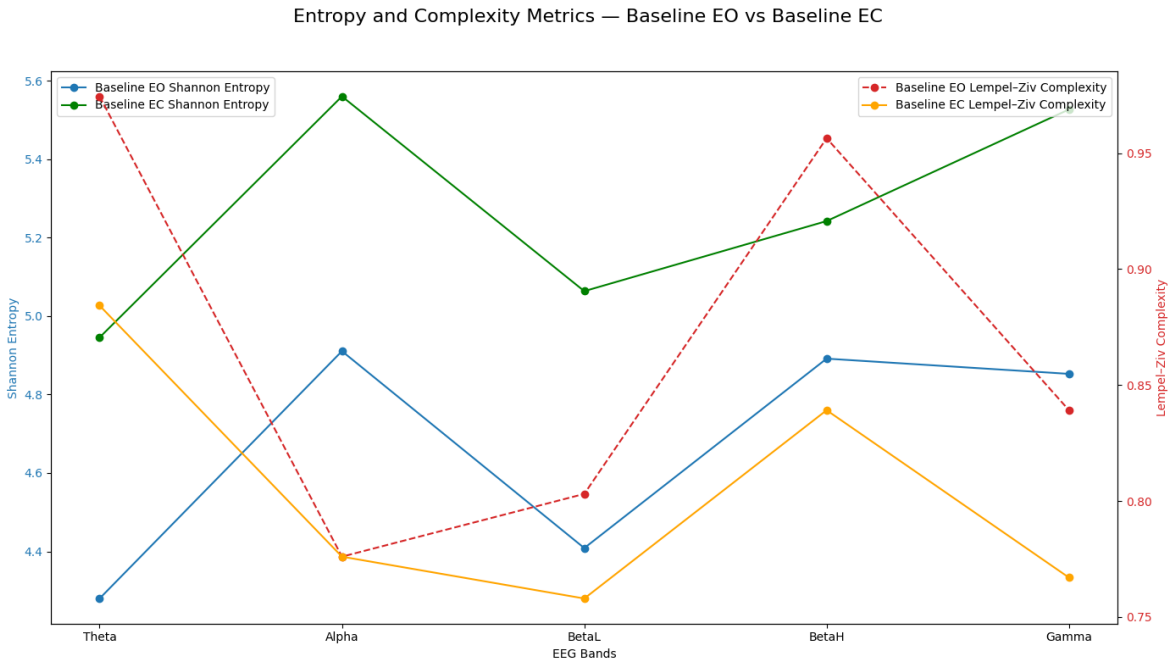

Figure 18: Band-level Shannon entropy and Lempel–Ziv complexity: baseline eyes-open (EO) vs baseline eyes-closed (EC).

Across bands, Shannon entropy is consistently higher during EC than EO, indicating greater

variability in band-limited power under eyes-closed rest. The separation is most pronounced in the alpha and gamma ranges.

In contrast, LZ complexity is generally higher during EO across most bands, suggesting increased sequence diversity despite lower magnitude variability. The difference is particularly visible in high beta, where EO complexity exceeds EC.

These comparisons establish baseline distinctions between EO and EC states and serve as reference points for subsequent condition-specific analyses. Interpretation is restricted to descriptive differences in variability and symbolic complexity within baseline recordings.

Entropy and Complexity Metrics: Indoor Session vs Baseline Eyes-Closed

This figure compares band-level Shannon entropy and Lempel–Ziv (LZ) complexity during the indoor session relative to the baseline eyes-closed (EC) condition, which serves as the reference anchor.

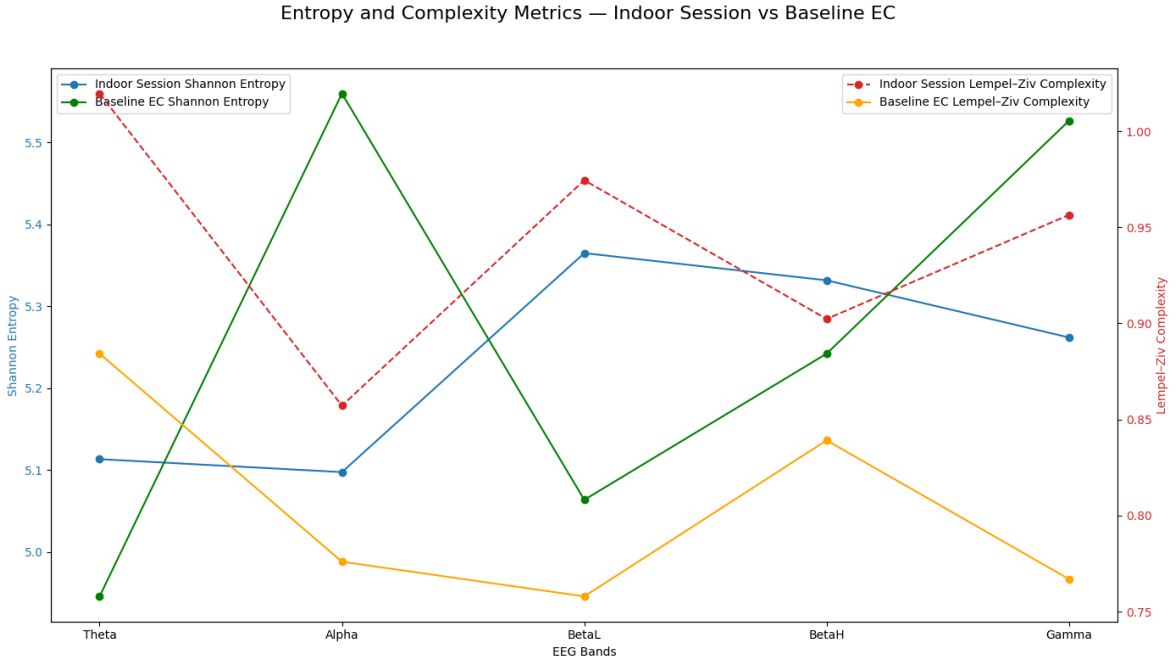

Figure 19: Band-level Shannon entropy and Lempel–Ziv complexity: indoor session vs baseline eyes-closed (EC).

Relative to baseline EC, Shannon entropy is elevated in the low- and high-beta ranges during the indoor session, indicating increased variability in mid-frequency band-power dynamics. Theta and alpha entropy remain closer to baseline levels, suggesting comparatively stable structure in lower-frequency bands.

LZ complexity shows increased values in theta and low beta during the indoor session, with moderate elevation in higher bands. These differences indicate greater sequence diversity in selected frequency ranges relative to baseline.

The comparison characterises deviations from the eyes-closed baseline at the band level. Interpretation is restricted to descriptive differences in variability and complexity and does not attribute these changes to specific cognitive or environmental factors.

Entropy and Complexity Metrics: Indoor vs Outdoor Sessions

This figure compares Shannon entropy and Lempel–Ziv (LZ) complexity across canonical EEG bands between the indoor and outdoor sessions.

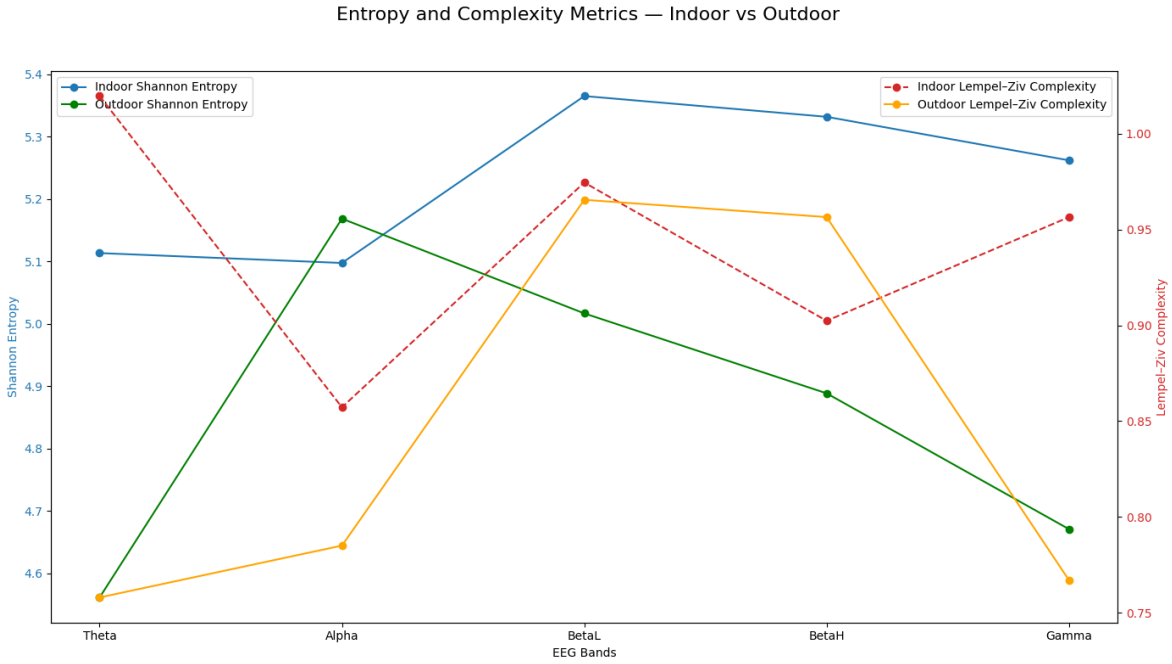

Figure 20: Band-level Shannon entropy and Lempel–Ziv complexity: indoor vs outdoor sessions.

Across bands, Shannon entropy is higher during the indoor session, with the largest differences in low beta, high beta, and gamma. Outdoor entropy decreases progressively from alpha through gamma, indicating comparatively lower high-frequency variability relative to the indoor condition.

LZ complexity shows a similar pattern, with indoor values exceeding outdoor values across all bands, most prominently in theta and gamma.

These comparisons describe band-level differences in variability and sequence diversity between sessions. Interpretation remains restricted to descriptive contrasts and does not attribute the observed differences to specific environmental or behavioural factors.

Entropy and Complexity Metrics: Outdoor Session vs Baseline Eyes-Closed

This figure compares Shannon entropy and Lempel–Ziv (LZ) complexity across canonical EEG bands between the outdoor session and the baseline eyes-closed (EC) condition.

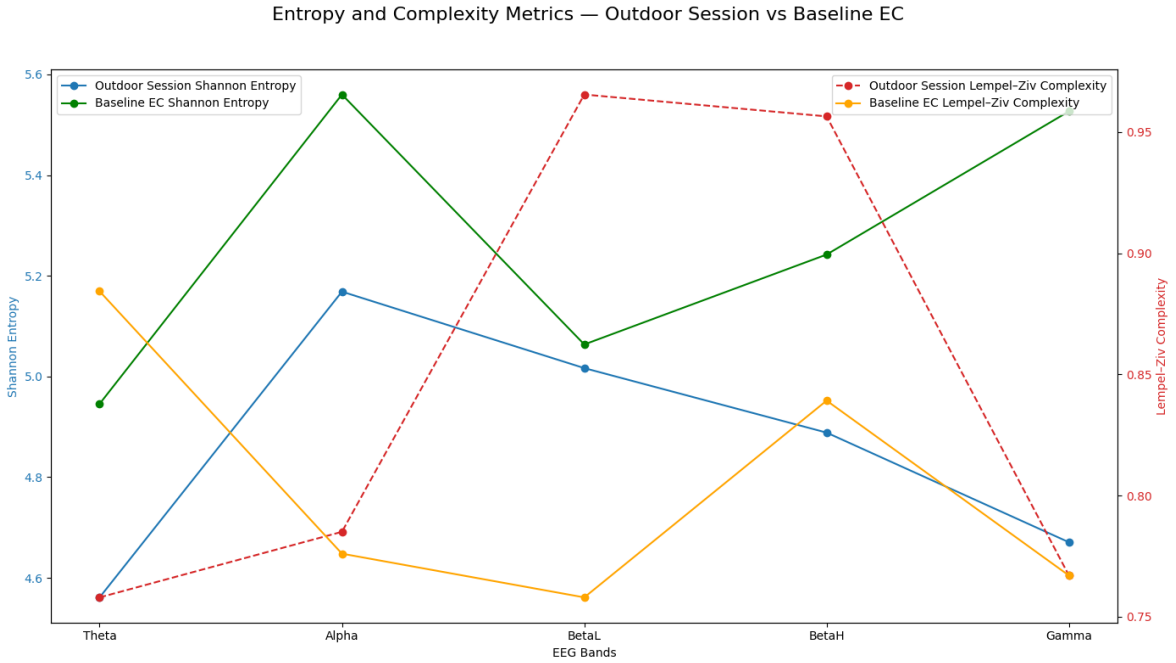

Figure 21: Band-level Shannon entropy and Lempel–Ziv complexity: outdoor session vs baseline eyes-closed (EC).

Relative to baseline EC, Shannon entropy is reduced across all bands during the outdoor session, with the largest decreases in high beta and gamma. This indicates lower variability in band-limited power compared with eyes-closed rest.

LZ complexity shows a mixed pattern: values are elevated relative to baseline in low and high beta, while remaining comparable to or slightly reduced in theta and gamma.

These results describe band-level differences in variability and sequence diversity relative to baseline EC. Interpretation is restricted to descriptive properties of signal organisation and does not assign functional or cognitive meaning to the observed entropy differences.

Entropy & Complexity (ALL POW Features): Baseline Eyes-Open vs Baseline Eyes-Closed

This figure compares Shannon entropy and Lempel–Ziv (LZ) complexity across all POW features, where each feature corresponds to a channel × frequency-band combination. Unlike the band-averaged summaries, this analysis preserves feature-level granularity across the full spatial–spectral space.

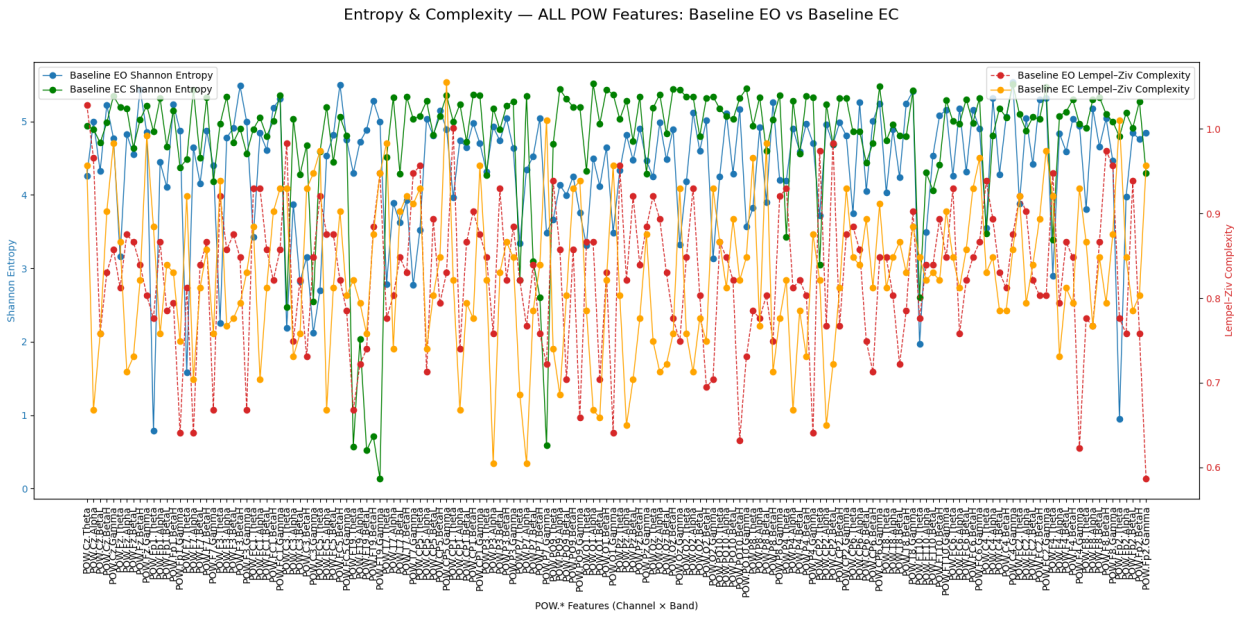

Figure 22: Feature-level Shannon entropy and Lempel–Ziv complexity (all POW features): baseline eyes-open (EO) vs baseline eyes-closed (EC).

Across the majority of features, Shannon entropy is higher during baseline eyes-closed (EC) than eyes-open (EO), indicating greater variability in band-limited power under eyes-closed rest. This elevation is spatially widespread rather than confined to a limited subset of channels or bands.

LZ complexity shows greater dispersion across features, with EO frequently exhibiting higher values than EC at individual channel–band combinations. The divergence between entropy and complexity patterns reflects the distinct aspects of signal organisation captured by each metric at the feature level.

This analysis characterises the distribution and dispersion of variability and sequence diversity across the full POW feature set and serves as a high-resolution baseline reference for subsequent condition comparisons. Interpretation is restricted to descriptive properties of signal organisation.

Entropy & Complexity (ALL POW Features): Indoor Session vs Baseline Eyes-Closed

This figure compares Shannon entropy and Lempel–Ziv (LZ) complexity across all POW features between the indoor session and the baseline eyes-closed (EC) condition, preserving full spatial–spectral granularity.

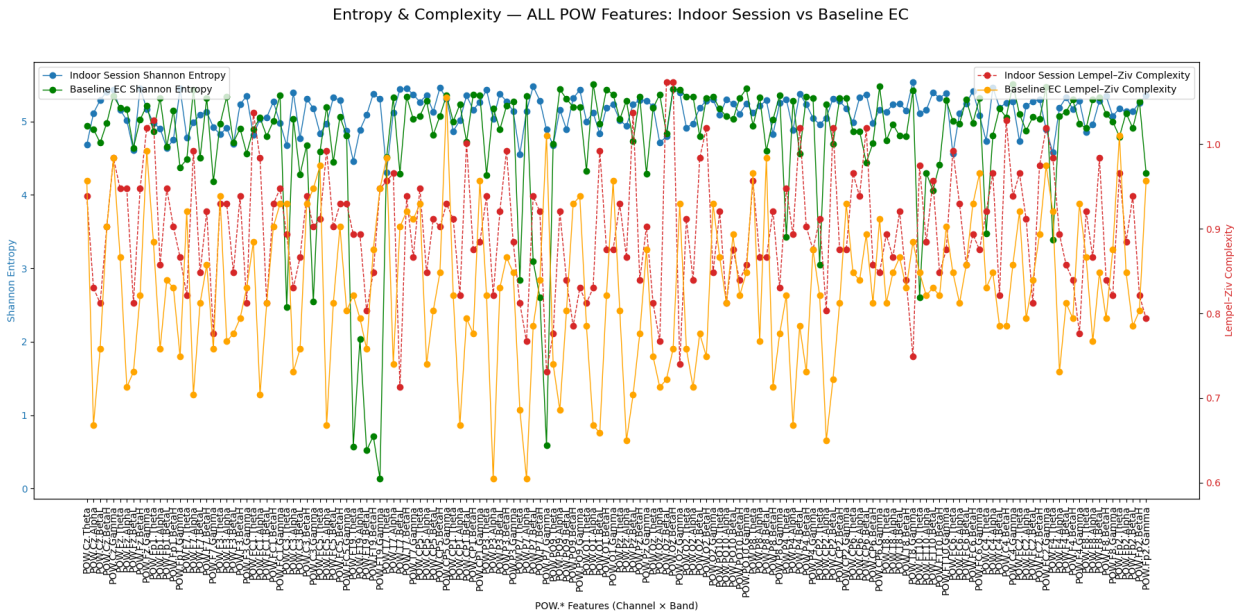

Figure 23: Feature-level Shannon entropy and Lempel–Ziv complexity (all POW features): indoor session vs baseline eyes-closed (EC).

Relative to baseline EC, Shannon entropy is elevated across a substantial portion of POW features during the indoor session, particularly within mid- and higher-frequency components. This indicates increased variability distributed across the spatial–spectral feature space.

LZ complexity is likewise higher for many features in the indoor session, though with greater dispersion and feature-level heterogeneity. The effect reflects reshaping of the variability landscape rather than a uniform upward shift across all channel–band combinations.

These results describe global deviation within the full POW feature set without aggregating by band or region. Interpretation remains restricted to descriptive differences in variability and sequence diversity relative to baseline EC.

Entropy & Complexity (ALL POW Features): Indoor vs Outdoor Sessions

This figure compares Shannon entropy and Lempel–Ziv (LZ) complexity across all POW features between the indoor and outdoor sessions, preserving full spatial–spectral resolution and without baseline anchoring.

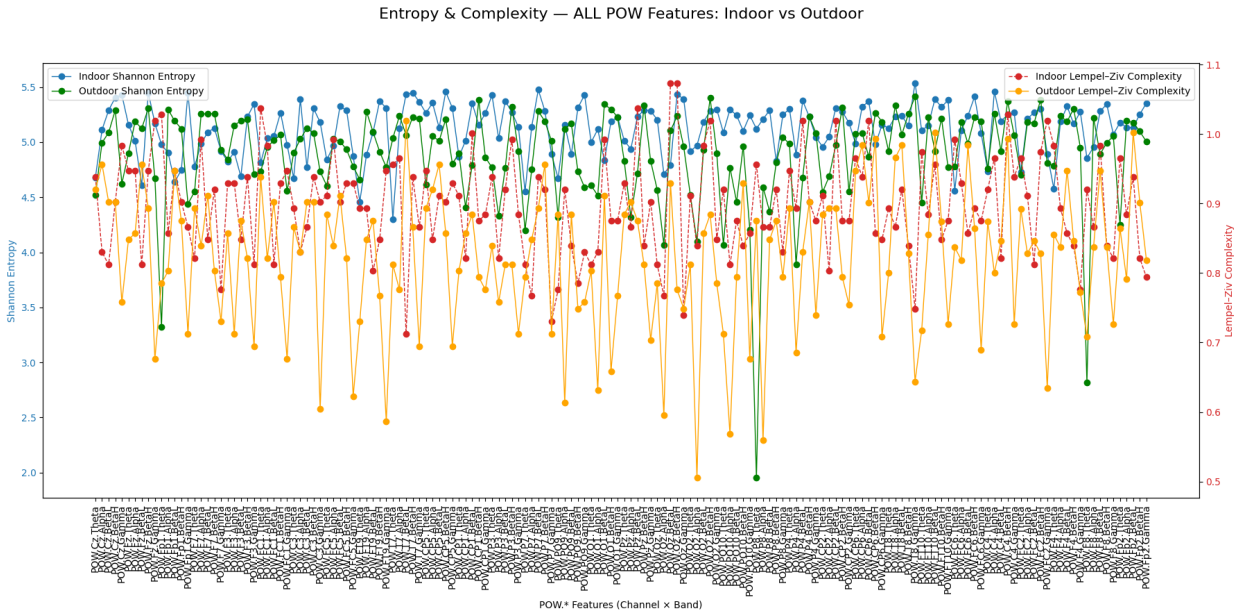

Figure 24: Feature-level Shannon entropy and Lempel–Ziv complexity (all POW features): indoor vs outdoor sessions.

Across the feature space, Shannon entropy is generally higher and more tightly clustered during the indoor session, whereas the outdoor session shows broader dispersion and more pronounced downward deviations, particularly within higher-frequency components.

LZ complexity follows a similar pattern, with indoor values exceeding outdoor values across many features, alongside substantial feature-level heterogeneity in both conditions. Outdoor complexity exhibits deeper troughs at select channel–band combinations, indicating reduced sequence diversity in those components relative to indoor.

These contrasts describe global differences in variability and complexity across the POW feature space between sessions. Interpretation remains restricted to descriptive differences in signal organisation and does not attribute causality to environmental context.

Entropy & Complexity (ALL POW Features): Outdoor Session vs Baseline Eyes-Closed

This figure compares Shannon entropy and Lempel–Ziv (LZ) complexity across all POW features between the outdoor session and the baseline eyes-closed (EC) condition, preserving full spatial–spectral resolution.

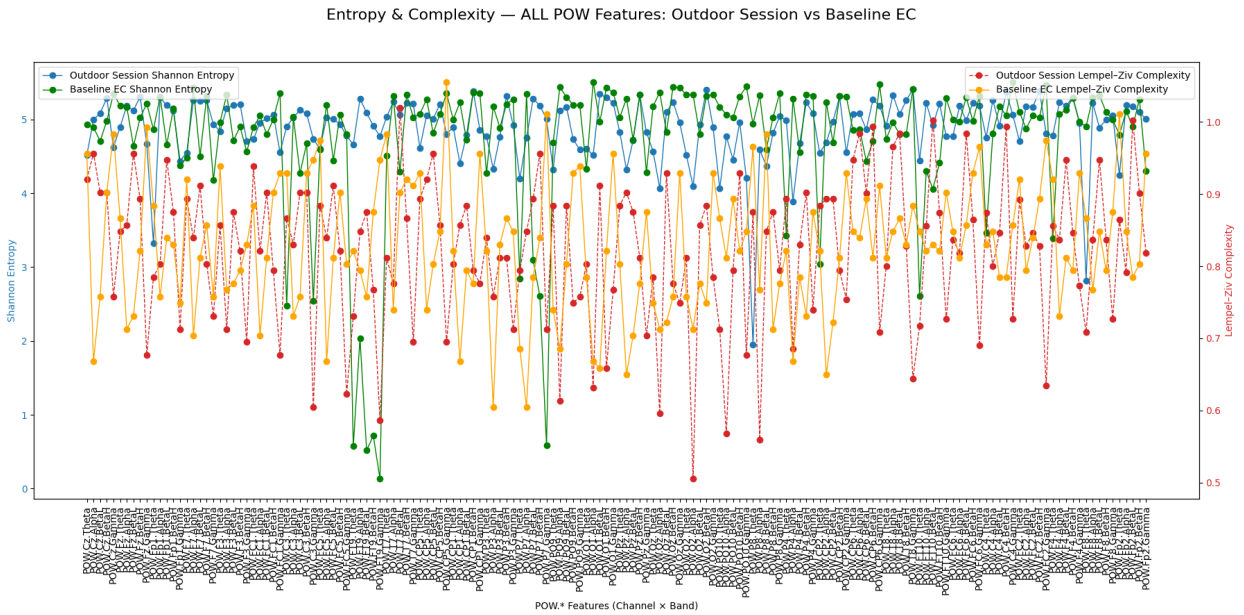

Figure 25: Feature-level Shannon entropy and Lempel–Ziv complexity (all POW features): outdoor session vs baseline eyes-closed (EC).

Relative to baseline EC, Shannon entropy is generally reduced across many POW features during the outdoor session, with the largest decreases in higher-frequency components. This indicates lower variability in band-limited power across the spatial–spectral feature space compared with eyes-closed rest.

LZ complexity exhibits a mixed pattern, with some features exceeding baseline EC and others falling below, resulting in broader dispersion relative to the entropy profile. The divergence between entropy and complexity again reflects complementary aspects of signal organisation captured by each metric.

These results describe feature-level deviations in variability and sequence diversity relative to baseline EC. Interpretation remains restricted to descriptive properties of signal organisation and does not assign functional or cognitive meaning to the observed differences.

ALL POW Feature Analyses

The ALL POW feature analyses provide a high-resolution characterisation of entropy and complexity across the full spatial–spectral space. The following sections introduce more structured spectral representations to facilitate interpretation and cross-metric comparison.

Absolute and Relative Power Spectral Density (PSD)

This section examines EEG spectral composition using power spectral density (PSD) estimates derived from the recorded signals. PSD provides a frequency-domain representation of signal power distribution, enabling inspection of broadband spectral structure as well as band-specific contributions.

Two complementary representations are used. Absolute PSD reflects the raw distribution of energy across frequencies, capturing overall spectral shape, dominant components, and the balance between slow and fast activity. Relative (baseline-referenced) PSD expresses spectral changes with respect to defined resting conditions (eyes closed or eyes open), highlighting frequency-specific increases or decreases associated with the session context. Relative PSD is expressed in logarithmic (dB) units to permit symmetric interpretation of power shifts and facilitate comparison across frequencies and channels.

PSD is computed at the channel level and summarised using robust statistics (e.g., medians and interquartile ranges) to limit the influence of transient artefacts or outlier channels. Figures include both continuous spectral curves and band-collapsed representations depending on the analytical focus. Where relevant, distinctions between raw EEG-derived PSD and band-power-derived PSD are made explicit.

The purpose of this section is descriptive: to characterise spectral structure, cross-frequency balance, and baseline-referenced shifts without assigning mechanistic interpretation. Individual figures are interpreted independently with emphasis on stable versus variable features of the spectral profile.

Band-Integrated Power (Absolute) — BASELINE EC [RAW]

This figure shows absolute band-integrated power computed from raw EEG during the eyes-closed (EC) baseline, with power integrated across canonical frequency bands. Bars represent the central tendency across channels and error bars reflect between-channel variability.

Alpha power is the dominant component under baseline EC, exceeding all other bands and consistent with a stable eyes-closed resting state. Theta and high beta exhibit moderate absolute power, while low beta and gamma contribute comparatively less to overall spectral energy.

Between-channel variability is largest in the alpha range, indicating spatial heterogeneity across the scalp even during baseline. Gamma shows lower absolute power with comparatively tighter dispersion across channels.

This figure establishes the absolute spectral reference profile for subsequent comparisons with session-based PSD estimates.

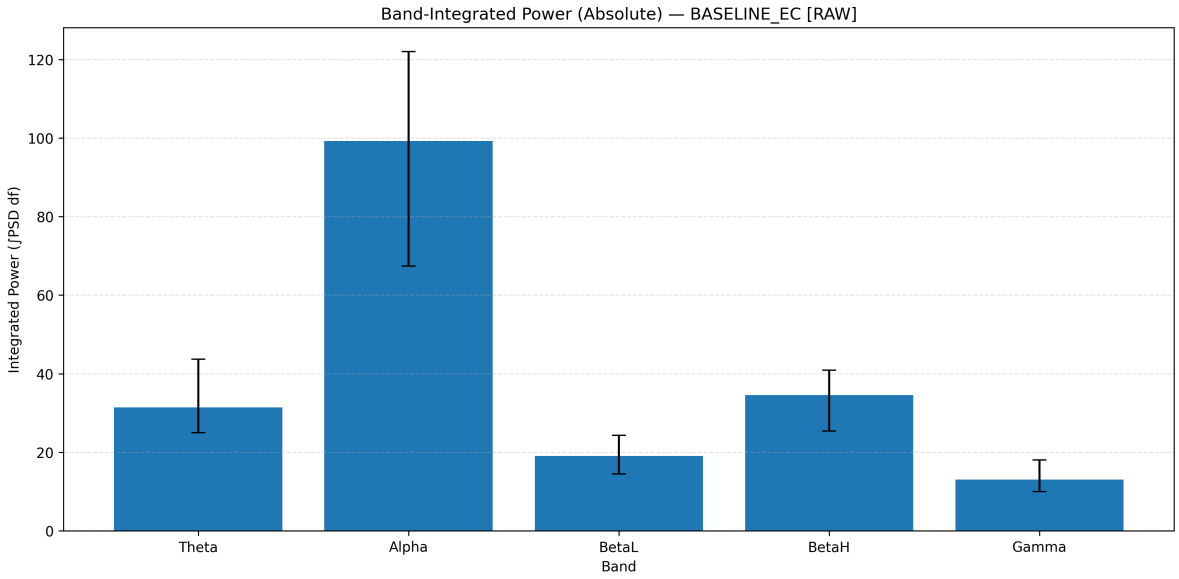

Figure 26: Absolute band-integrated power (RAW): baseline eyes-closed (EC).

Band-Integrated Power (Absolute) — PLANT KINGDOM INDOOR [RAW]

This figure shows absolute band-integrated power for the Plant Kingdom indoor session computed from raw EEG using the same integration procedure as the baseline. Bars represent central tendency across channels and error bars reflect between-channel variability.

Alpha remains the dominant band in absolute terms, but its central value is reduced relative to the eyes-closed baseline and is accompanied by increased between-channel variability. Theta power is elevated compared with baseline, while high beta also shows increased absolute power. Low beta and gamma increase modestly but remain lower than theta and high beta in absolute magnitude.

Relative to baseline, the spectral profile is less alpha-dominant and more distributed across frequency bands. Variability is particularly pronounced in alpha and high beta, indicating greater spatial differentiation across channels during the indoor session.

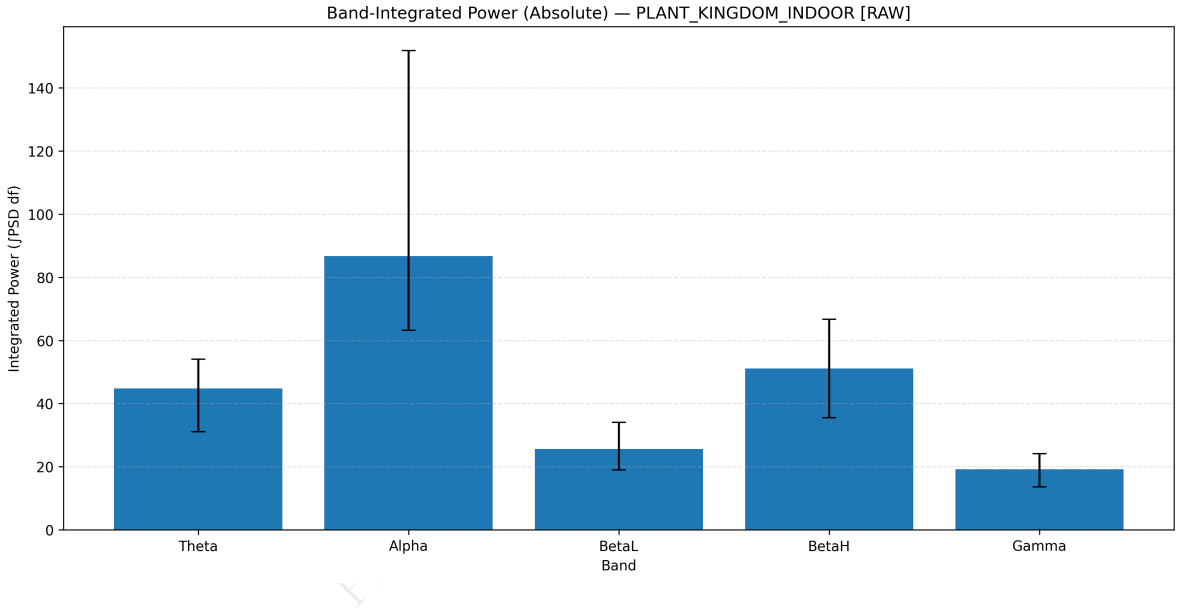

Figure 27: Absolute band-integrated power (RAW): Plant Kingdom indoor session.

Band-Integrated Power (Absolute) — PLANT KINGDOM OUTDOOR [RAW]

This figure shows absolute band-integrated power for the Plant Kingdom outdoor session computed from raw EEG using the same integration procedure as previous conditions. Bars represent central tendency across channels and error bars reflect between-channel variability.

Alpha is no longer the dominant spectral component and is comparable in magnitude to theta and high beta. Gamma power is elevated relative to both baseline and indoor sessions and constitutes a major contributor to total spectral energy in this condition. High beta also remains elevated with substantial between-channel variability, while theta and low beta occupy intermediate positions.

The overall profile indicates a shift in absolute power distribution toward higher frequencies. Gamma shows both high central power and broad dispersion across channels, indicating spatial heterogeneity. Relative to baseline and indoor sessions, the outdoor condition exhibits reduced alpha dominance and increased high-frequency contribution to the spectral profile.

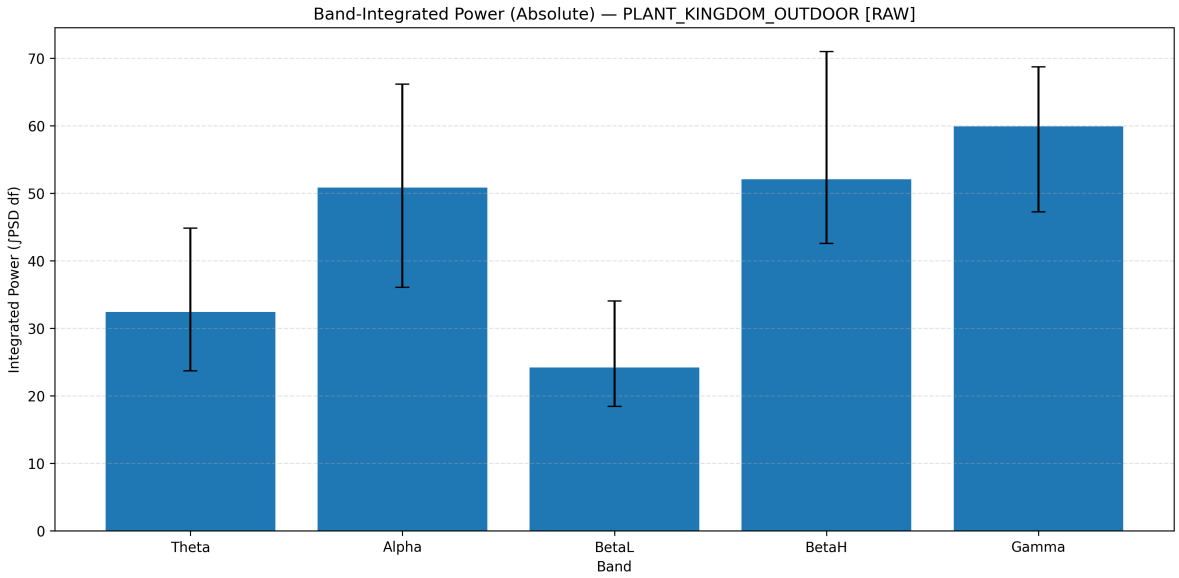

Figure 28: Absolute band-integrated power (RAW): Plant Kingdom outdoor session.

Absolute PSD (Welch) — BASELINE EC [RAW]

This figure shows the absolute power spectral density (PSD) estimated using Welch's method for the eyes-closed (EC) baseline. PSD is summarised across channels using the median, with the shaded region indicating the interquartile range (25th–75th percentile).

The spectrum is dominated by strong low-frequency power, including a pronounced low-frequency component and a clear alpha-band peak in the 8–12 Hz range. Beyond the alpha range, spectral power decreases rapidly with increasing frequency, producing a steep spectral slope characteristic of resting-state EEG.

The interquartile range is narrow across most frequencies, indicating consistent spectral structure across channels. Variability increases around the alpha peak, reflecting spatial heterogeneity in alpha expression. At higher frequencies, power approaches the noise floor with minimal dispersion, consistent with low-amplitude high-frequency activity in this condition.

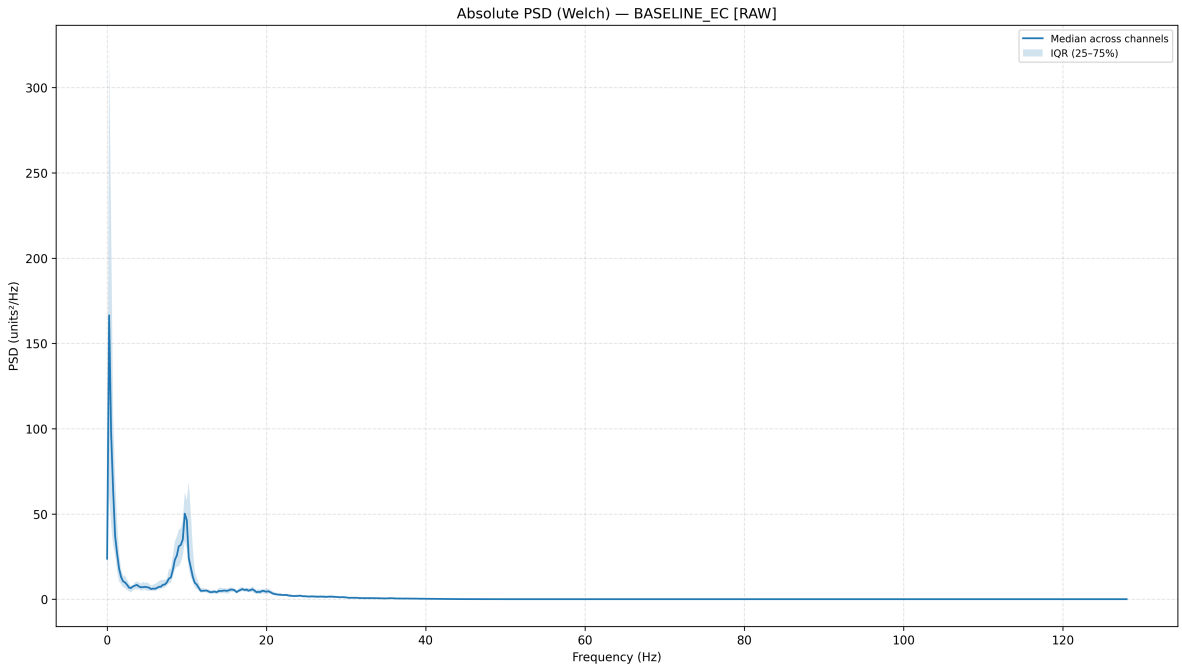

Figure 29: Absolute PSD (Welch; RAW): baseline eyes-closed (EC), median across channels with interquartile range.

Absolute PSD (Welch) — PLANT KINGDOM INDOOR [RAW]

This figure shows the absolute power spectral density (PSD) for the Plant Kingdom indoor session estimated using Welch's method and summarised across channels by the median, with the interquartile range (25th–75th percentile) shown as shading.

The low-frequency component remains prominent; however, the overall spectral profile is flatter relative to the eyes-closed baseline, with reduced dominance of the alpha peak. Alpha power remains clearly identifiable but appears broader and less pronounced, accompanied by increased interquartile spread, indicating greater spatial variability across channels.

Power in the theta and low-beta ranges is elevated relative to baseline, contributing to a more distributed low- and mid-frequency profile. At higher frequencies, power declines toward low levels, with slightly greater dispersion than baseline, consistent with modest increases in high-frequency variability during the indoor session.

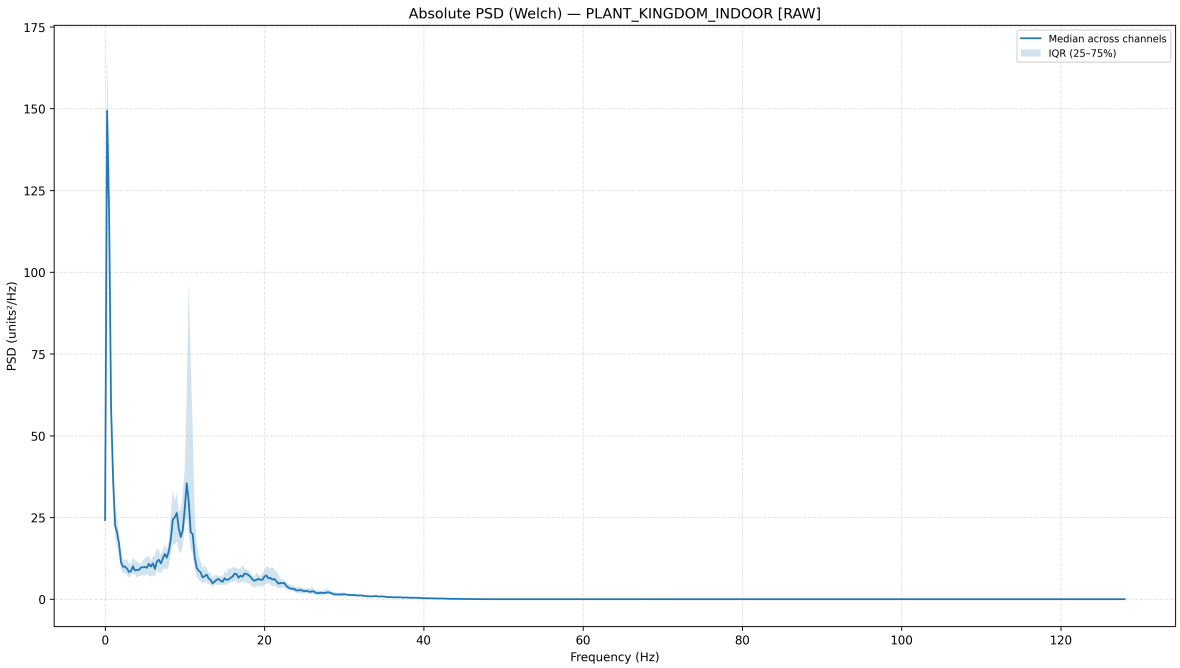

Figure 30: Absolute PSD (Welch; RAW): Plant Kingdom indoor session, median across channels with interquartile range.

Absolute PSD (Welch) — PLANT KINGDOM OUTDOOR [RAW]

This figure shows the absolute power spectral density (PSD) for the Plant Kingdom outdoor session estimated using Welch's method and summarised across channels by the median, with the interquartile range (25th–75th percentile) shown as shading.

The spectrum is dominated by very high power at the lowest frequencies, producing a steep low-frequency peak that exceeds the scale observed in both baseline and indoor conditions. Beyond this initial component, spectral power declines rapidly and remains comparatively low across mid and high frequencies.

An alpha peak is not clearly distinguishable at this scale, indicating that very low-frequency activity dominates the absolute spectral energy in this session. The interquartile range is not prominently visible across most frequencies, suggesting that between-channel variability is small relative to the dominant low-frequency component or compressed by the plotting scale.

Relative to baseline and indoor sessions, the outdoor condition exhibits a markedly different absolute spectral profile characterised by strong low-frequency dominance.

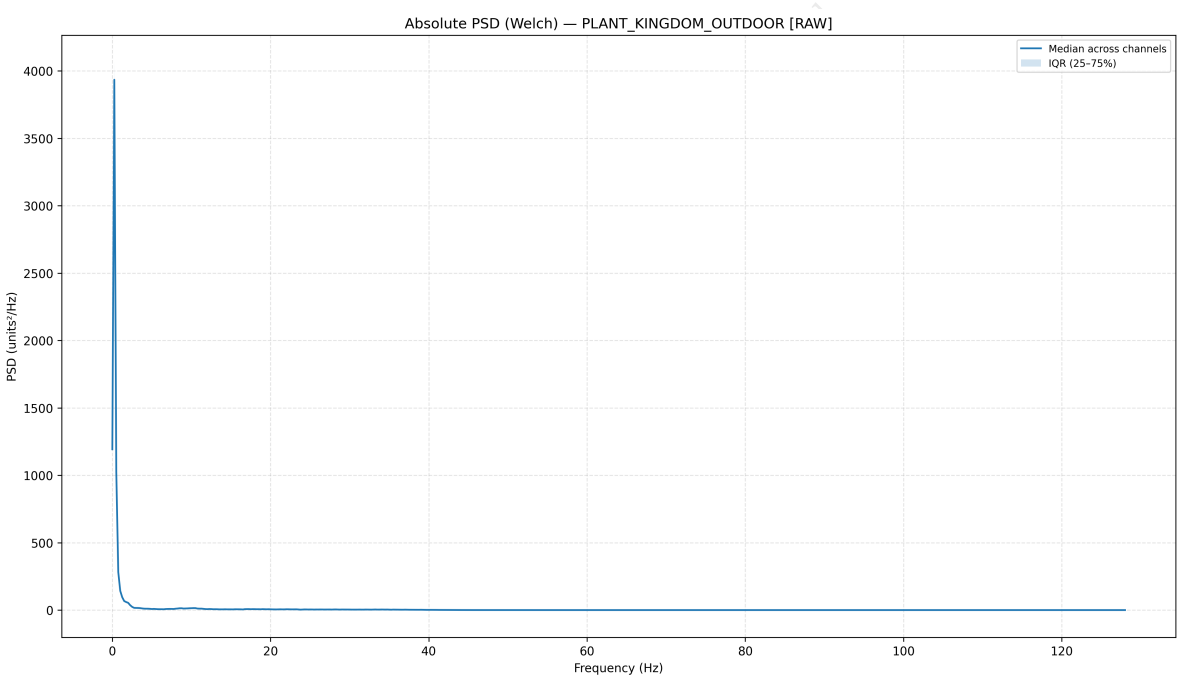

Figure 31: Absolute PSD (Welch; RAW): Plant Kingdom outdoor session, median across channels with interquartile range.

Band-Integrated Power (dB) — PLANT KINGDOM INDOOR vs BASELINE EC [RAW]

This figure shows baseline-normalised band-integrated power for the Plant Kingdom indoor session expressed in decibels relative to the eyes-closed (EC) baseline. Positive values indicate increased power relative to baseline and negative values indicate reductions.

Theta shows a modest positive shift relative to baseline. Alpha is near zero and slightly negative on average, indicating a mild reduction compared with baseline, with error bars spanning zero and reflecting between-channel variability. Low beta and high beta both show positive deviations, with high beta exhibiting the strongest increase among mid-frequency bands. Gamma also shows a consistent positive shift, indicating elevated high-frequency power during the indoor session.

Overall, these results reflect moderate redistribution of power across bands rather than large-amplitude changes, with between-channel variability captured by the error bars.

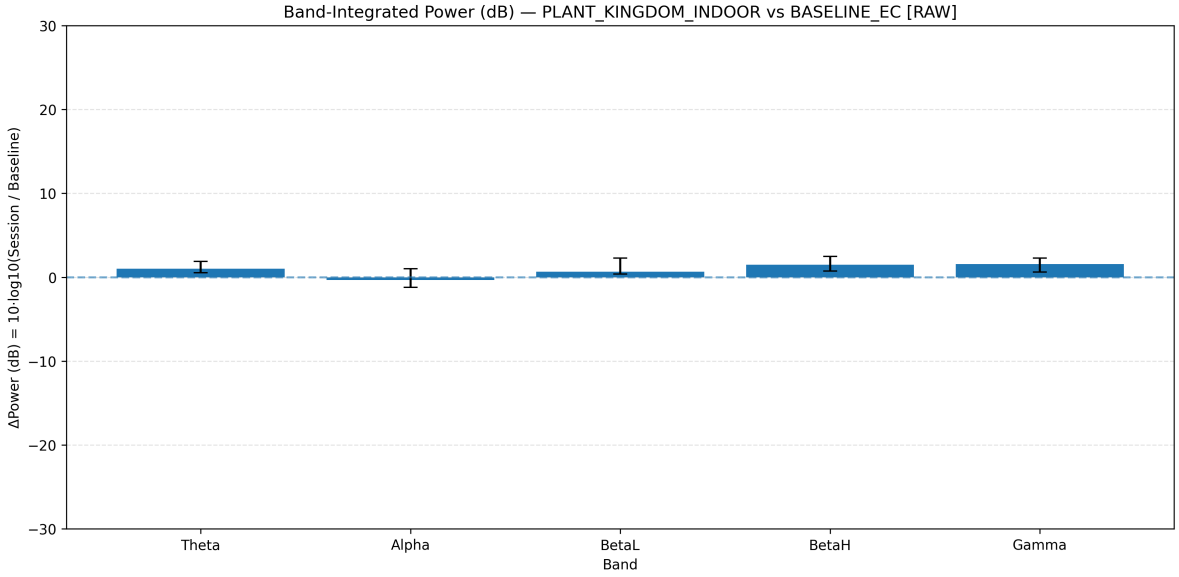

Figure 32: Baseline-normalised band-integrated power (dB; RAW): Plant Kingdom indoor vs baseline eyes-closed (EC).

Band-Integrated Power (dB) — PLANT KINGDOM OUTDOOR vs BASELINE EC [RAW]

This figure shows baseline-normalised band-integrated power for the Plant Kingdom outdoor session expressed in decibels relative to the eyes-closed (EC) baseline. Positive values indicate increases relative to baseline and negative values indicate reductions.

Theta remains near zero, indicating minimal change relative to baseline. Alpha shows a clear negative deviation, reflecting reduced alpha-band power across channels. In contrast, low beta and high beta both show positive shifts, with high beta exhibiting the larger increase. Gamma displays the strongest positive deviation, indicating elevated high-frequency power relative to baseline.

Error bars are small relative to the magnitude of these shifts, suggesting spatial consistency across channels. Overall, the outdoor condition is characterised by reduced alpha power alongside enhanced higher-frequency activity relative to baseline.

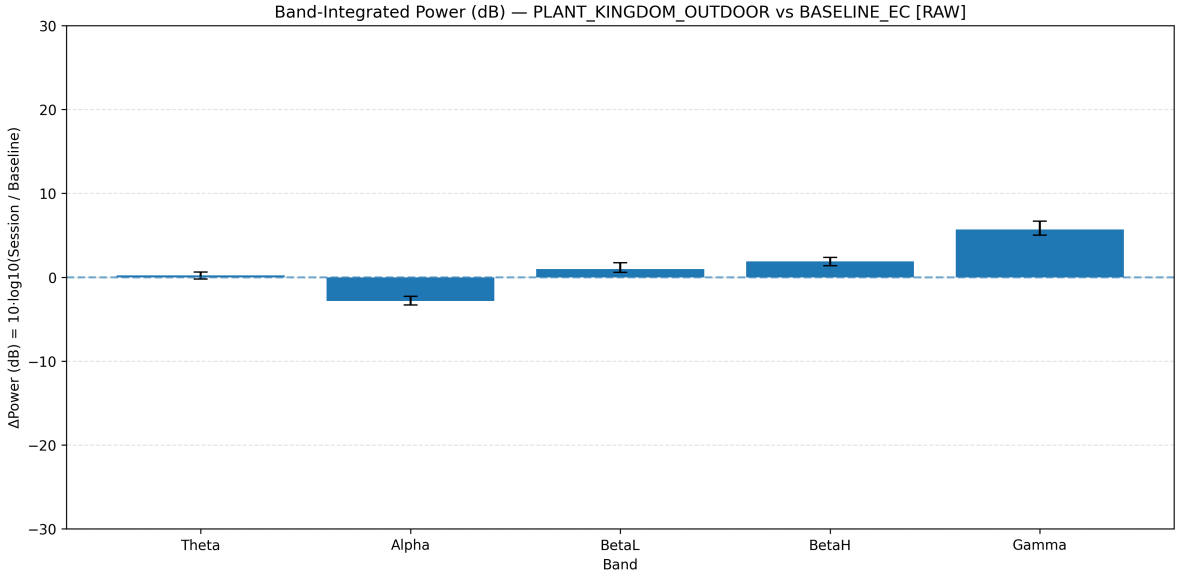

Figure 33: Baseline-normalised band-integrated power (dB; RAW): Plant Kingdom outdoor vs baseline eyes-closed (EC).

Relative PSD (dB) — PLANT KINGDOM INDOOR vs BASELINE EC [RAW]

This figure shows the frequency-resolved relative power spectral density (PSD) for the Plant Kingdom indoor session expressed in decibels relative to the eyes-closed (EC) baseline. Values represent the median change in PSD across channels.

Across much of the spectrum, the curve fluctuates around zero, indicating modest deviation from baseline. In the low-frequency range, small positive shifts are interspersed with narrow negative deflections, reflecting frequency-specific redistribution rather than broadband change. Within the alpha range, the curve remains near zero with localised reductions at specific frequencies. From beta into lower gamma frequencies, the profile trends slightly positive before gradually returning toward zero at higher frequencies.

Overall, the spectrum exhibits fine-grained, frequency-dependent modulation rather than a uniform shift across the band.

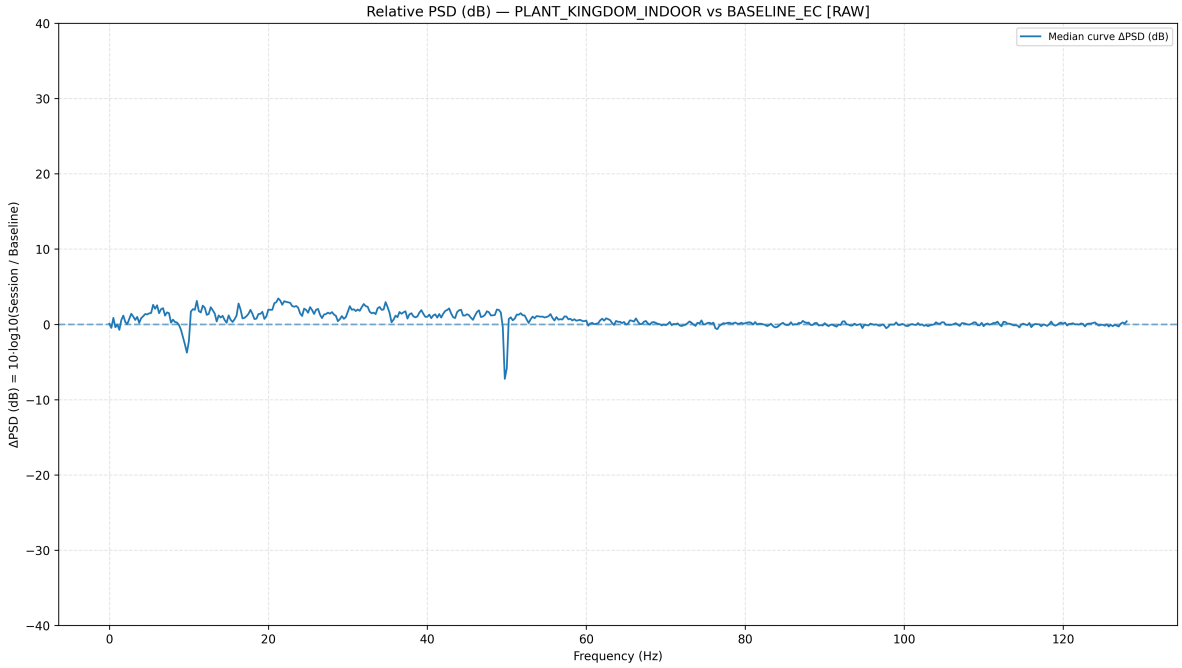

Figure 34: Relative PSD (dB; RAW): Plant Kingdom indoor vs baseline eyes-closed (EC), median across channels.

Relative PSD (dB) — PLANT KINGDOM OUTDOOR vs BASELINE EC [RAW]

This figure shows the frequency-resolved relative power spectral density (PSD) for the Plant Kingdom outdoor session expressed in decibels relative to the eyes-closed (EC) baseline. Values represent the median change in PSD across channels.

At the lowest frequencies, the spectrum shows positive deviations relative to baseline, followed by a pronounced negative trough within the alpha range, indicating reduced power at specific alpha frequencies. Beyond alpha, the curve rises into sustained positive values across beta and lower gamma frequencies and remains elevated across a broad portion of the spectrum. Localised peaks and troughs are visible throughout, indicating frequency-specific modulation rather than broadband change. At higher frequencies, the curve declines gradually but remains above zero, consistent with elevated high-frequency power relative to baseline.

Relative to the indoor condition, deviations are larger in magnitude and show clearer band-structured differences across the spectrum.

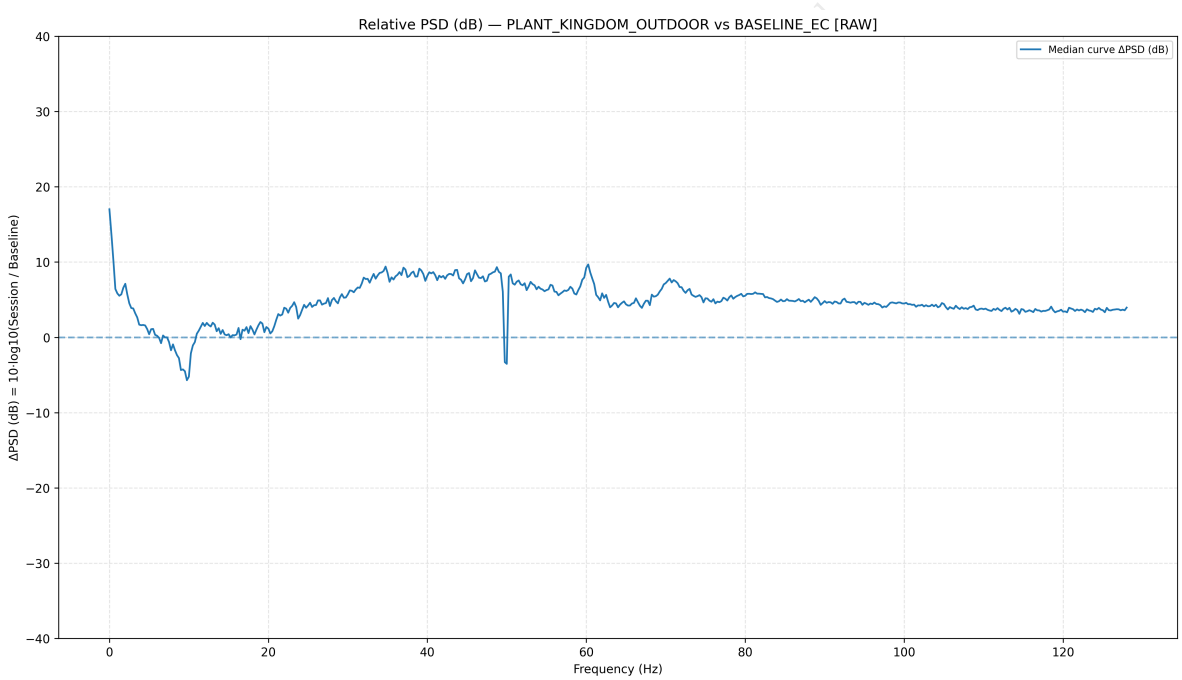

Figure 35: Relative PSD (dB; RAW): Plant Kingdom outdoor vs baseline eyes-closed (EC), median across channels.

Shannon Entropy (Windowed, Band-Limited)

This section examines the temporal structure of band-limited EEG activity using Shannon entropy computed in sliding windows over band-power (POW) streams. Whereas power measures reflect signal magnitude, entropy quantifies dispersion within the distribution of band-power values over time. Higher values indicate greater variability in band-power states within a window, and lower values indicate more constrained dynamics.

Entropy is computed separately for canonical frequency bands (Theta, Alpha, BetaL, BetaH, Gamma) and aggregated over predefined cortical regions using the native band-power sampling cadence (8 Hz). The windowed formulation permits time-resolved assessment of variability, allowing evaluation of stability, transitions, and within-session fluctuations rather than relying on single summary values.

All entropy estimates are derived from within-window probability distributions of band-power values rather than from raw EEG amplitudes. The measures therefore reflect variability in band-power envelopes over time rather than waveform-level irregularity.

Where baseline comparisons are included, entropy time series are evaluated relative to eyes-closed (EC) or eyes-open (EO) reference segments. These comparisons provide contextual reference points without imposing normative interpretation. Emphasis throughout is placed on temporal structure, regional variation, and persistence of entropy states within each session.

Figures in this section present entropy as time-resolved traces, regional summaries, and condition contrasts. Interpretation is restricted to descriptive characterisation of variability in band-limited activity over time.

Windowed Shannon Entropy — BASELINE EC — Theta

This figure shows windowed Shannon entropy of theta-band power during the eyes-closed (EC) baseline, computed using a 10-s window with 5-s stride and normalised to the [0–1] range. Traces are shown separately for cortical regions (central, frontal, occipital, parietal, temporal).

Across most regions, theta entropy remains high and temporally stable, with values clustered toward the upper portion of the range. Central and frontal regions show modest fluctuations but remain within a narrow band, indicating stable organisation of theta-band power. Occipital and parietal regions exhibit similar temporal profiles with slightly lower absolute values.

The temporal region shows a brief, localised reduction in entropy within a narrow time interval followed by rapid return to baseline levels. This excursion indicates a transient increase in regularity within temporal theta-band power rather than sustained instability.

Overall, baseline theta entropy is stable across regions with limited transient deviations. This profile provides the reference scale for subsequent condition and difference plots.

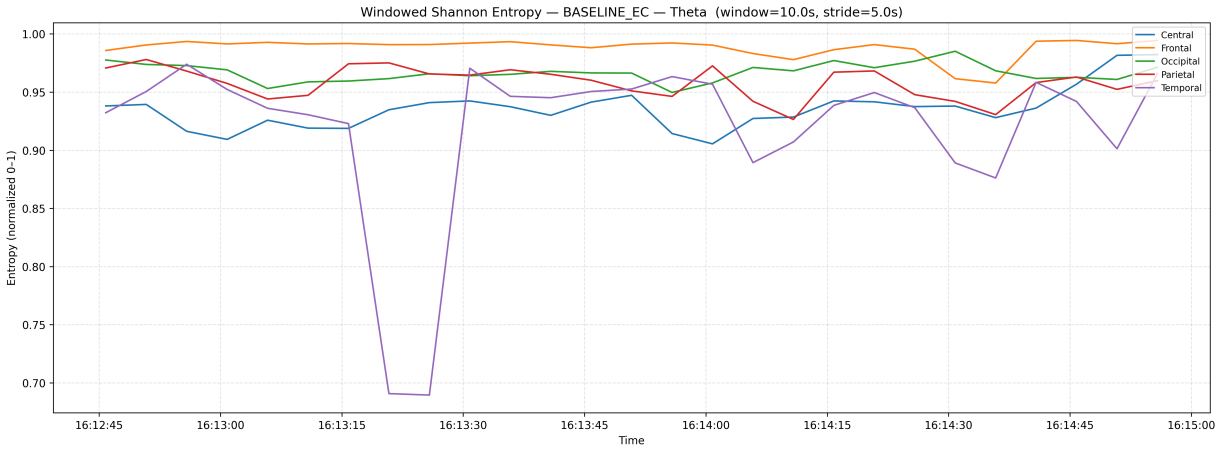

Figure 36: Windowed Shannon entropy (Theta band): baseline eyes-closed (EC).

Δ Windowed Shannon Entropy vs Baseline Median — PLANT KINGDOM INDOOR — Theta

This figure shows change in theta-band entropy relative to the baseline median, plotted as Δ entropy over time for the indoor Plant Kingdom condition. The dashed horizontal line indicates the baseline median for each region; positive values denote increased entropy relative to baseline and negative values denote reductions.

The central region shows consistently positive Δ entropy across the session with smooth temporal variation, indicating sustained elevation in theta-band variability relative to baseline. Occipital and parietal regions exhibit smaller positive deviations with greater temporal fluctuation and occasional crossings of the baseline reference.

The temporal region shows pronounced negative excursions, including structured troughs that persist across multiple windows. These reductions are larger in magnitude than fluctuations observed in other regions and indicate periods of increased regularity in temporal theta-band power relative to baseline. The recurrence of these troughs suggests a stable regional feature rather than an isolated event.

The frontal region remains near baseline with small bidirectional deviations, indicating minimal change in frontal theta entropy relative to baseline variability.

Overall, the indoor condition shows clear regional differentiation in theta entropy relative to baseline, with sustained central increases and marked temporal reductions.

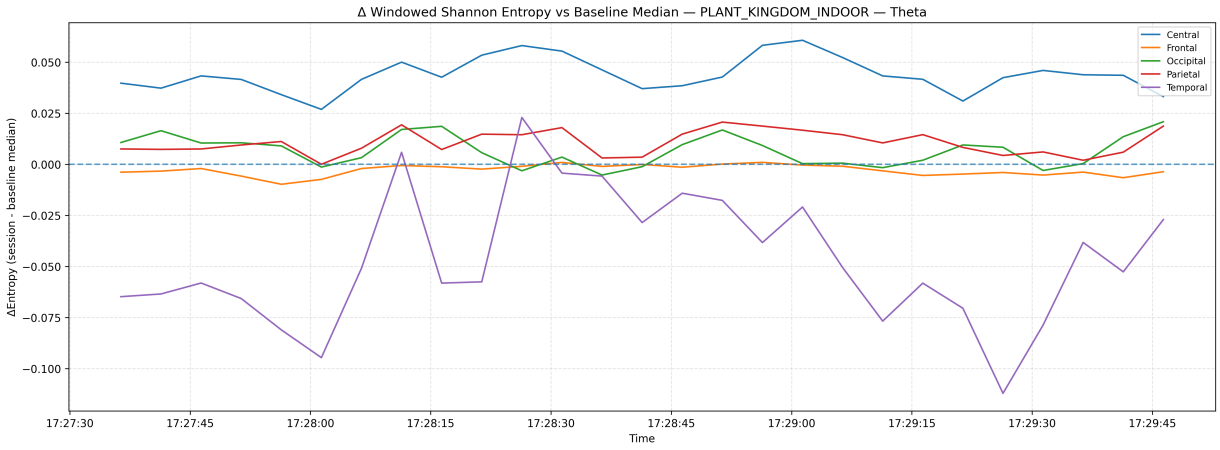

Figure 37: Δ windowed Shannon entropy vs baseline median (Theta band): Plant Kingdom indoor session.

Δ Windowed Shannon Entropy vs Baseline Median — PLANT KINGDOM OUTDOOR — Theta

This figure shows change in theta-band entropy relative to the baseline median for the outdoor Plant Kingdom condition. The zero line denotes the baseline median for each region; positive values indicate increased entropy and negative values indicate reductions relative to baseline.

The central region shows predominantly positive Δ entropy with greater temporal modulation than observed indoors. Deviations are broader and less uniform, indicating dynamic variation rather than a constant offset from baseline.

Occipital and parietal regions display sustained positive deviations across multiple windows, indicating elevated posterior theta entropy relative to baseline. These increases are smoother than those observed indoors, suggesting gradual modulation rather than abrupt shifts.

The temporal region exhibits pronounced negative excursions at multiple time points, interleaved with brief returns toward baseline. Relative to the indoor condition, reductions are more temporally distributed rather than concentrated within a single dominant trough.

The frontal region remains near baseline with small bidirectional fluctuations, indicating minimal departure from resting theta entropy.

Overall, both indoor and outdoor conditions alter theta entropy relative to baseline, but differ in temporal structure and regional expression, particularly in the distribution and persistence of temporal-region reductions.

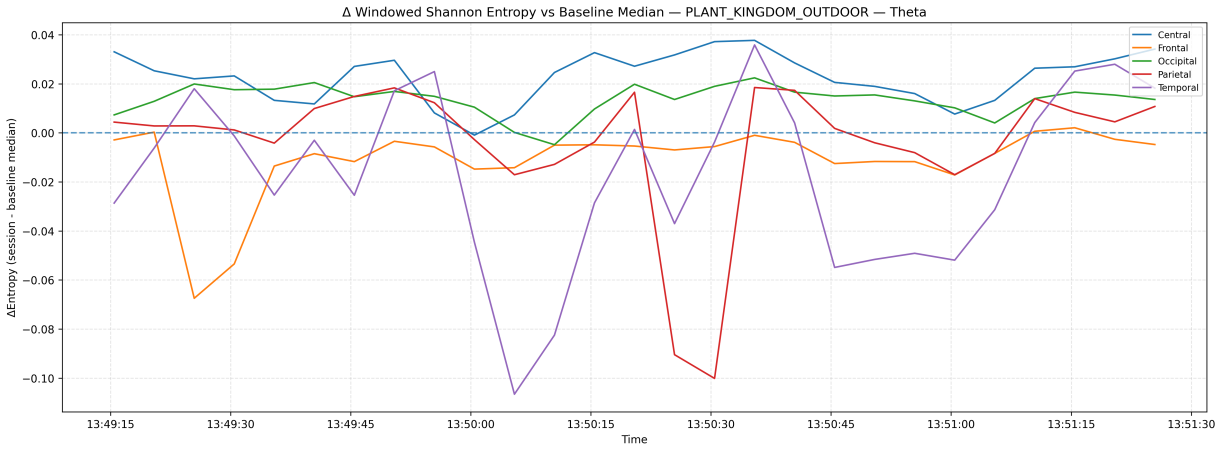

Figure 38: Δ windowed Shannon entropy vs baseline median (Theta band): Plant Kingdom outdoor session.

Windowed Shannon Entropy — BASELINE EC — Alpha

This figure shows windowed Shannon entropy of alpha-band power during the eyes-closed (EC) baseline, computed using a 10-s window with 5-s stride and normalised to the [0–1] range. Traces are shown for cortical regions (central, frontal, occipital, parietal, temporal).

Across regions, alpha entropy remains high and tightly clustered near the upper portion of the range. The frontal region shows the highest and most stable values with minimal temporal variation. Occipital and parietal regions exhibit slightly lower values with modest modulation but remain within a narrow band. The central region shows small fluctuations without sustained departures from baseline levels.

The temporal region exhibits the largest transient reductions in entropy, followed by rapid recovery to baseline values. These events indicate brief increases in regularity within temporal alpha-band power rather than sustained instability.

Overall, baseline alpha entropy is stable across regions with limited large-amplitude excursions and clear regional stratification. This profile provides the reference scale for interpreting subsequent condition-related changes in alpha entropy.

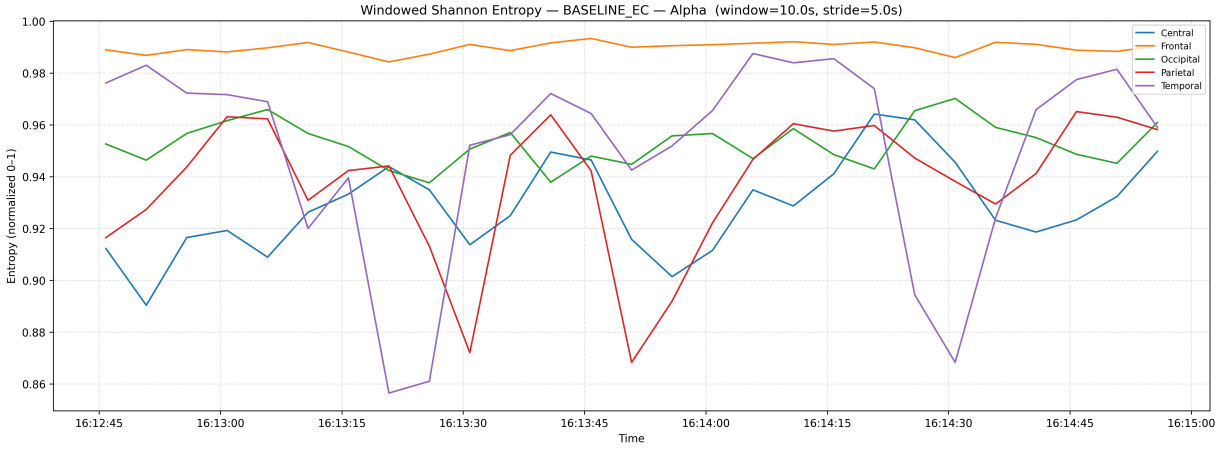

Figure 39: Windowed Shannon entropy (Alpha band): baseline eyes-closed (EC).

Δ Windowed Shannon Entropy vs Baseline Median — PLANT KINGDOM INDOOR — Alpha

This figure shows the change in alpha-band entropy relative to the baseline median for the indoor Plant Kingdom condition. Positive values indicate increased entropy relative to baseline, and negative values indicate reductions.

The central region exhibits a sustained positive Δ entropy across the session with smooth temporal variation, indicating persistent elevation in alpha entropy relative to baseline. The magnitude and stability of this increase exceed those observed for theta.

The occipital region shows consistently negative Δ entropy across most windows, indicating reduced variability and increased regularity in posterior alpha power. The temporal region exhibits larger negative excursions, including extended troughs across multiple windows, reflecting substantial reductions in alpha entropy relative to baseline.

The parietal region fluctuates around baseline with alternating positive and negative deviations. The frontal region remains tightly clustered near zero with minimal departure from baseline entropy.

Overall, the indoor condition shows regionally differentiated alpha entropy modulation, characterised by central increases alongside posterior and temporal reductions, with relatively stable frontal behaviour.

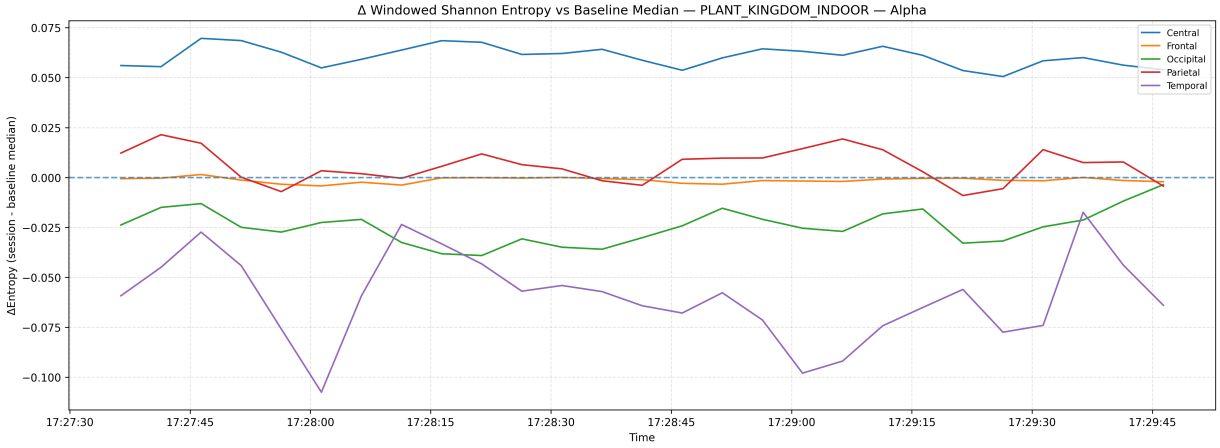

Figure 40: Δ windowed Shannon entropy vs baseline median (Alpha band): Plant Kingdom indoor session.

Δ Windowed Shannon Entropy vs Baseline Median — PLANT KINGDOM OUTDOOR — Alpha

This figure presents the change in alpha-band entropy relative to baseline for the outdoor Plant Kingdom condition. The same baseline reference and scaling as the indoor condition are used, enabling direct comparison of entropy changes.

The central region shows positive Δ entropy with greater temporal structure than in the indoor condition. Peaks and troughs are more pronounced, suggesting increased variability in alpha entropy evolution rather than a uniform shift from baseline.

Occipital and parietal regions exhibit alternating positive and negative deviations, with several periods of positive Δ entropy, contrasting with the predominantly negative occipital pattern observed indoors. These fluctuations indicate more dynamic modulation of posterior alpha entropy in the outdoor condition.

The temporal region shows large negative Δ entropy, including deep and sustained troughs, indicating repeated reductions in alpha entropy relative to baseline. The timing and structure of these troughs differ from the indoor condition, suggesting different temporal organisation of entropy modulation rather than simple amplitude scaling.

The frontal region remains close to baseline throughout, indicating minimal change in frontal alpha entropy relative to baseline under both indoor and outdoor conditions.

Overall, outdoor modulation of alpha entropy is more temporally heterogeneous than indoors, with less persistent suppression in posterior regions and more distributed fluctuations across regions.

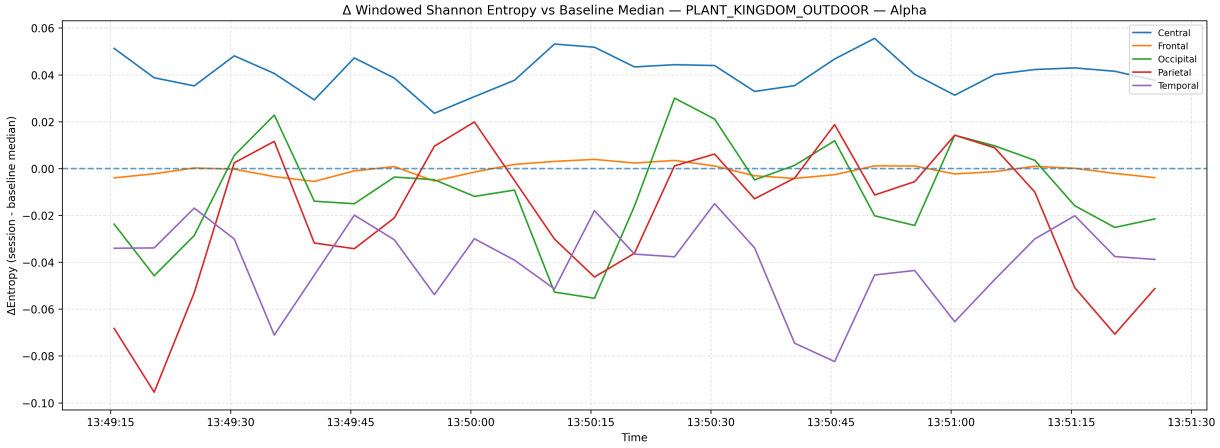

Figure 41: Δ windowed Shannon entropy vs baseline median (Alpha band): Plant Kingdom outdoor session.

Windowed Shannon Entropy — BASELINE EC — BetaL

This figure shows windowed Shannon entropy of low-beta (BetaL) band power during the eyes-closed (EC) baseline, normalised and plotted for each cortical region. The figure provides a reference for baseline organisation and temporal stability of BetaL activity.

Across the central, frontal, occipital, and parietal regions, BetaL entropy remains consistently high with only modest fluctuations over time. The frontal region shows the highest and most stable entropy, indicating a uniformly distributed BetaL power envelope during rest. Occipital and parietal regions track closely with minor undulations, suggesting stable regional organisation without significant shifts.

The central region shows slightly greater variability than the frontal region but remains within a narrow range, with no abrupt transitions. In contrast, the temporal region exhibits a pronounced transient drop in entropy, indicating a brief episode of increased regularity or constraint in temporal BetaL activity before returning to baseline levels.

Overall, baseline BetaL entropy is highly stable across regions, with occasional region-specific deviations, establishing BetaL as a band with strong baseline regularity.

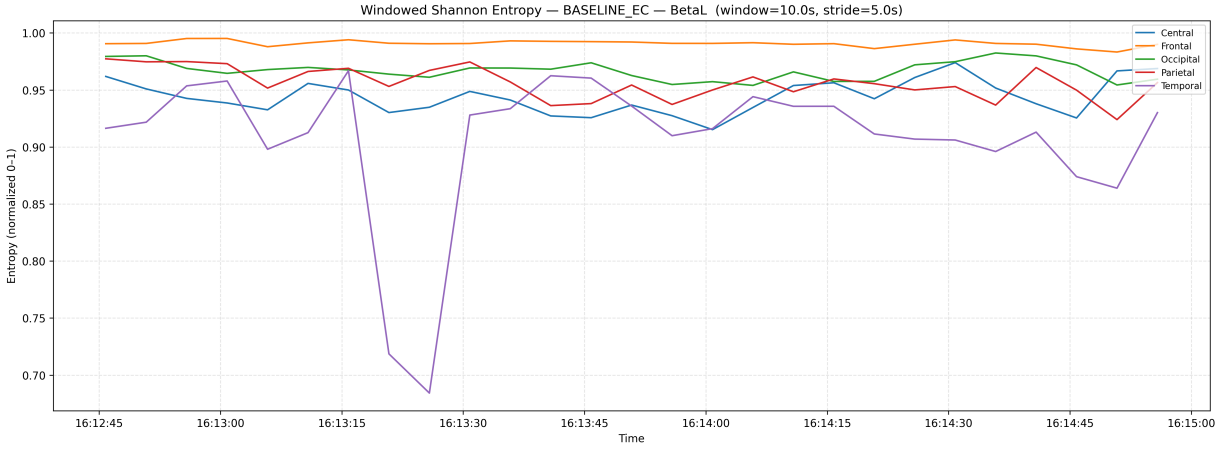

Figure 42: Windowed Shannon entropy (BetaL band): baseline eyes-closed (EC).

Δ Windowed Shannon Entropy vs Baseline Median — PLANT KINGDOM INDOOR — BetaL

This figure shows changes in BetaL entropy relative to the baseline median during the indoor Plant Kingdom condition. Positive values indicate increased entropy relative to baseline, while negative values indicate reduced entropy.

The central region shows sustained positive Δ entropy, remaining above baseline for most of the session. The magnitude of this increase is larger and more persistent than observed for theta or alpha, indicating a sustained elevation in BetaL entropy.

The parietal region also shows positive Δ entropy, though with smaller amplitude and greater temporal variability. These fluctuations remain predominantly above baseline, suggesting increased dispersion of BetaL power in posterior regions.

In contrast, the occipital region shows sustained negative Δ entropy, indicating reduced BetaL entropy relative to baseline. This suggests increased regularity in occipital BetaL activity under indoor conditions.

The temporal region exhibits large negative excursions, with deep troughs persisting across multiple windows. These reductions are larger than in other regions, indicating pronounced temporal suppression of BetaL entropy.

The frontal region remains near baseline with minimal deviations, indicating little change in frontal BetaL entropy during the indoor session.

This figure highlights strong anterior-posterior and temporal dissociation in BetaL entropy modulation, with central increases coexisting with occipital and temporal reductions.

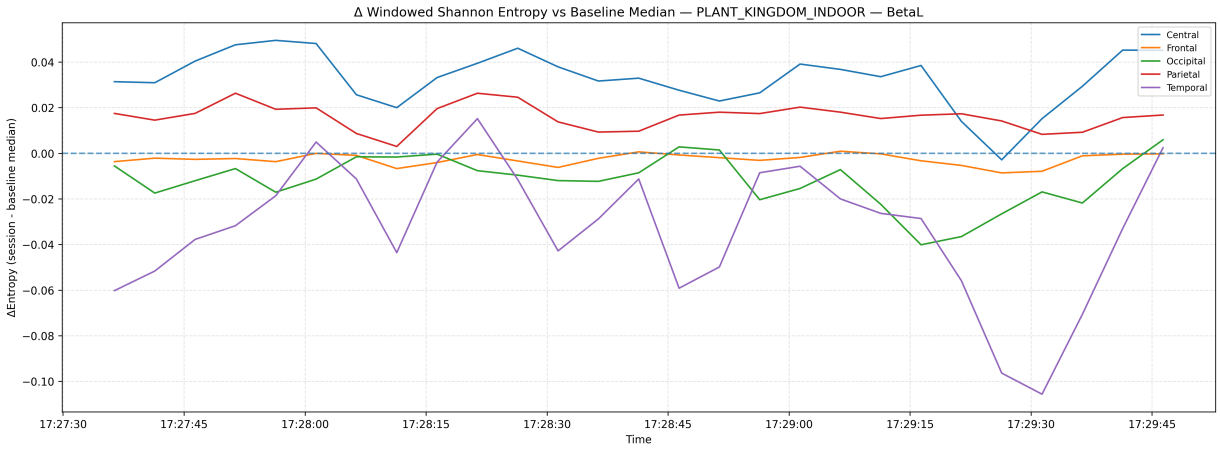

Figure 43: Δ windowed Shannon entropy vs baseline median (BetaL band): Plant Kingdom indoor session.

Δ Windowed Shannon Entropy vs Baseline Median — PLANT KINGDOM OUTDOOR — BetaL

This figure shows Δ BetaL entropy relative to baseline for the outdoor Plant Kingdom condition, using the same baseline reference and scaling as in the indoor condition.

The central region shows positive Δ entropy, with greater temporal structure than in the indoor condition. Peaks and troughs are more pronounced, with several brief crossings toward baseline, indicating increased variability rather than a uniform shift.

The occipital region alternates between small positive and negative deviations, contrasting with the predominantly negative pattern observed indoors. This suggests more dynamic modulation of occipital BetaL entropy outdoors, with less sustained constraint.

The parietal region shows moderate positive deviations interspersed with brief negative excursions, indicating fluctuating entropy rather than sustained elevation or suppression. The frontal region remains near baseline with small-amplitude variations, indicating minimal modulation.

The temporal region continues to show negative Δ entropy, including a deep trough early in the session followed by partial recovery. These reductions are more temporally localised than indoors, suggesting less sustained suppression of BetaL entropy.

Overall, this figure shows that while BetaL entropy is elevated centrally in both environments, the spatial distribution and temporal persistence of entropy reductions differ between indoor and outdoor conditions.

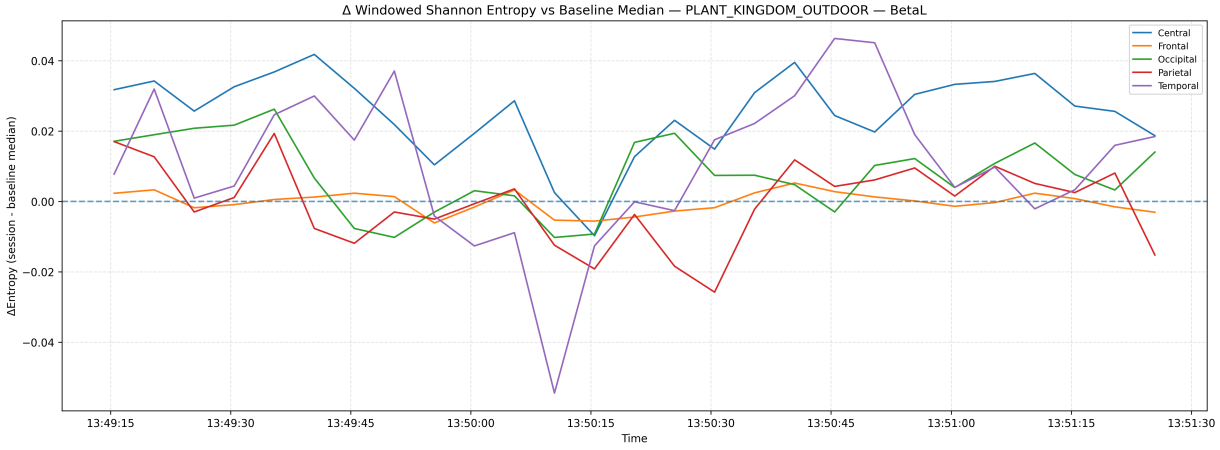

Figure 44: Δ windowed Shannon entropy vs baseline median (BetaL band): Plant Kingdom outdoor session.

Windowed Shannon Entropy — BASELINE EC — BetaH

This figure shows windowed Shannon entropy of high-beta (BetaH) band power during the eyes-closed (EC) baseline, computed with a 10-second window and 5-second stride. Entropy values are normalised and plotted separately for each cortical region, establishing the baseline organisation and intrinsic variability of BetaH activity.

Across central, frontal, occipital, and parietal regions, BetaH entropy is consistently high and stable, with only small-amplitude fluctuations. The frontal region shows the highest entropy with minimal temporal variation, indicating a uniformly distributed BetaH power envelope during rest. Occipital and parietal regions show slightly lower but tightly constrained entropy, maintaining stable regional separation without abrupt changes.

The central region displays modest undulations but remains within a narrow range, suggesting stable but dynamically modulated BetaH organisation. In contrast, the temporal region exhibits a large, transient entropy collapse, with a sharp drop followed by gradual recovery. This event is temporally localised and region-specific, indicating a brief episode of increased regularity in temporal BetaH power rather than global instability.

Baseline BetaH entropy is characterised by high stability and strong regional stratification, similar to BetaL, reinforcing its role as a stable reference for detecting relative entropy changes under different conditions.

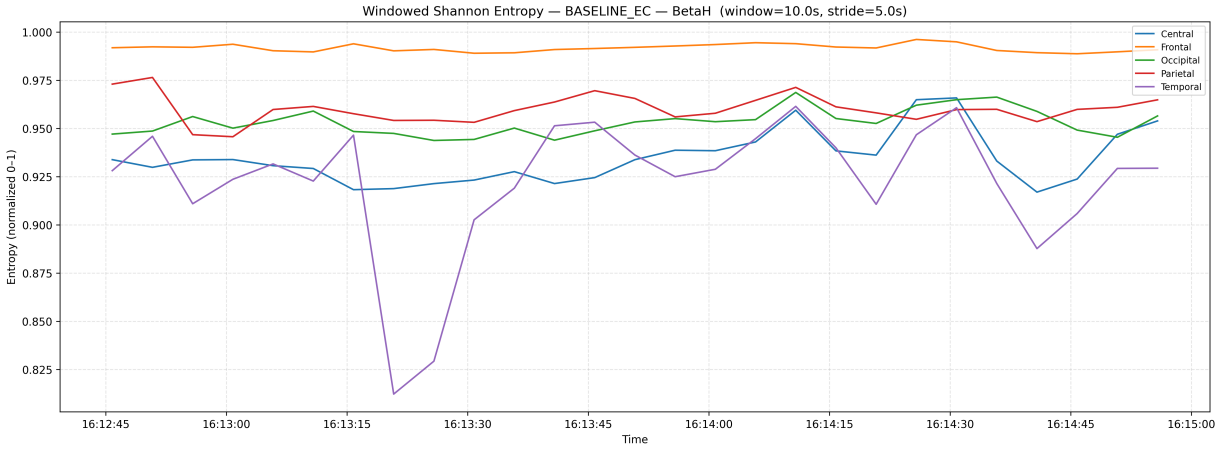

Figure 45: Windowed Shannon entropy (BetaH band): baseline eyes-closed (EC).

Δ Windowed Shannon Entropy vs Baseline Median — PLANT KINGDOM INDOOR — BetaH

This figure shows changes in BetaH entropy relative to the baseline median during the indoor Plant Kingdom condition. Positive values indicate increased entropy relative to baseline, while negative values indicate reduced entropy.

The central region shows a clear and sustained positive Δ entropy, remaining elevated throughout the session. The magnitude of this increase is comparable to, and at times exceeds, that observed for BetaL, indicating a robust increase in the variability of central BetaH power under indoor conditions.

The parietal region shows moderate positive Δ entropy with smooth temporal evolution and occasional brief returns toward baseline, suggesting increased entropy that is less dominant than in the central region. The occipital region shows consistent negative Δ entropy, indicating sustained reductions in BetaH entropy and increased regularity of posterior high-beta activity indoors.

The temporal region exhibits large negative Δ entropy excursions, with deep and repeated troughs persisting across multiple windows. These reductions are larger in magnitude than those in occipital or parietal regions, indicating pronounced temporal suppression of BetaH entropy relative to baseline. The frontal region remains near baseline with minimal deviation, indicating limited frontal modulation of BetaH entropy.

This figure highlights a strong central-temporal dissociation in BetaH entropy modulation indoors, with central increases coexisting alongside marked temporal reductions.

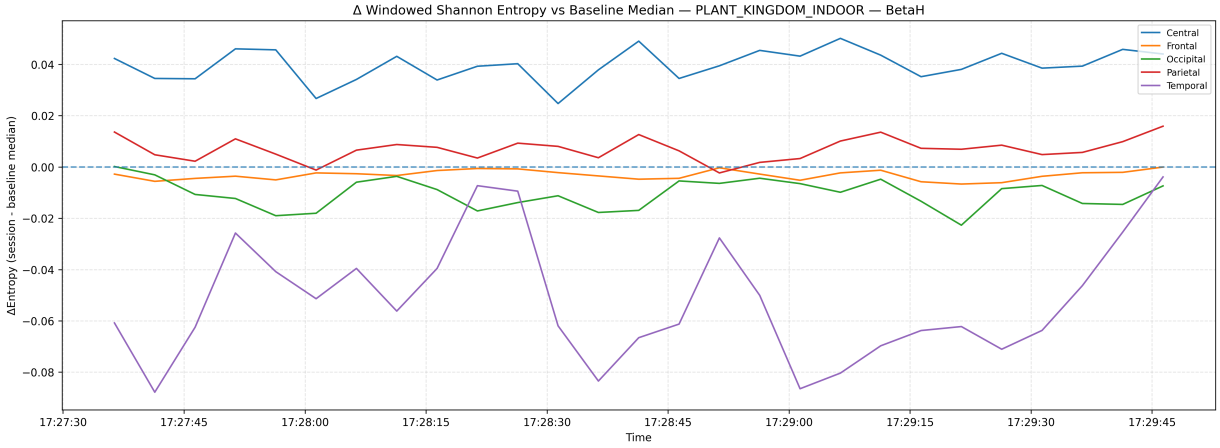

Figure 46: Δ windowed Shannon entropy vs baseline median (BetaH band): Plant Kingdom indoor session.

Δ Windowed Shannon Entropy vs Baseline Median — PLANT KINGDOM OUTDOOR — BetaH

This figure shows Δ BetaH entropy relative to baseline for the outdoor Plant Kingdom condition, using the same baseline reference and scaling as the indoor condition.

The central region shows positive Δ entropy with more pronounced temporal structure than indoors. Periods of elevated entropy are interspersed with brief reductions toward baseline, indicating increased variability rather than sustained shifts.

Occipital and parietal regions show predominantly positive Δ entropy, especially during the early and mid portions of the session, suggesting greater dispersion of BetaH power outdoors compared to baseline. These increases are more spatially distributed than indoors, with fewer sustained negative deviations.

The temporal region exhibits alternating positive and negative Δ entropy, with a notable negative excursion late in the session. These reductions are less sustained and more temporally fragmented compared to the indoor condition, indicating intermittent modulation rather than persistent suppression of temporal BetaH entropy.

The frontal region remains close to baseline with minimal modulation.

This figure shows that outdoor modulation of BetaH entropy is more spatially distributed and temporally heterogeneous than indoors, with less sustained suppression and broader engagement of posterior regions.

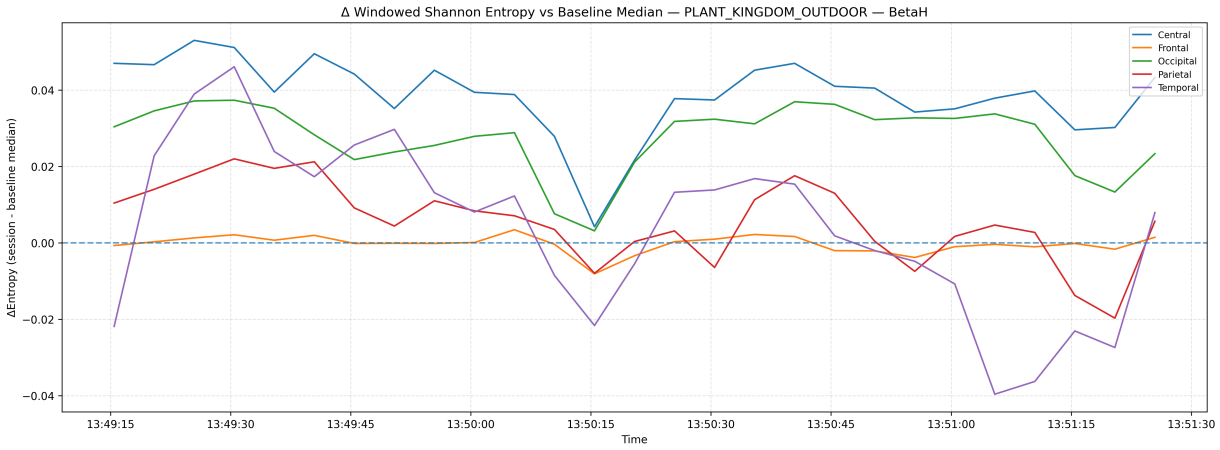

Figure 47: Δ windowed Shannon entropy vs baseline median (BetaH band): Plant Kingdom outdoor session.

Windowed Shannon Entropy — BASELINE EC — Gamma

This figure shows windowed Shannon entropy of gamma-band power during the eyes-closed (EC) baseline, computed using a 10-second window with a 5-second stride. Entropy values are normalised and plotted for each cortical region, providing a reference for baseline organisation and stability of high-frequency activity.

Across central, frontal, occipital, and parietal regions, gamma entropy remains consistently high with only small, smooth fluctuations over time. The frontal region shows the highest and most stable entropy, indicating a broadly distributed and temporally consistent gamma power envelope during baseline rest. Occipital and parietal regions show similarly stable patterns with minimal variance.

The central region shows modest fluctuations but remains within a narrow entropy range, indicating stable yet dynamically modulated gamma organisation. In contrast, the temporal region shows a pronounced transient drop in entropy, with a sharp decline followed by recovery to baseline levels. This event is temporally isolated and region-specific, indicating brief increased regularity in temporal gamma activity rather than global baseline instability.

Baseline gamma entropy mirrors the structure seen in beta bands, with high entropy, strong regional stratification, and occasional temporal-specific reductions.

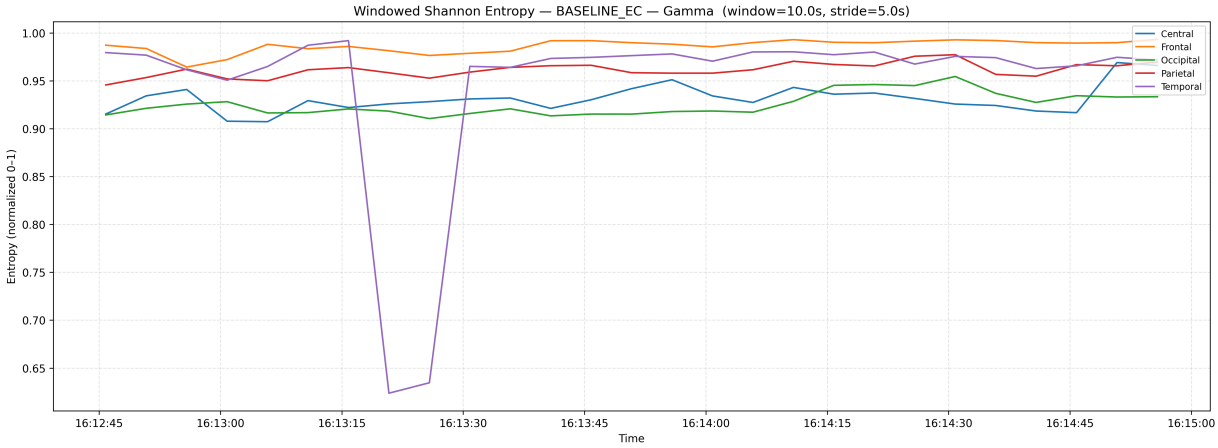

Figure 48: Windowed Shannon entropy (Gamma band): baseline eyes-closed (EC).

Δ Windowed Shannon Entropy vs Baseline Median — PLANT KINGDOM INDOOR — Gamma

This figure shows changes in gamma entropy relative to the baseline median during the indoor Plant Kingdom condition. Positive values indicate increased entropy relative to baseline, and negative values indicate reduced entropy.

The occipital region shows consistently elevated positive Δ entropy throughout the session, indicating sustained increase in dispersion or variability of occipital gamma power under indoor conditions. The central region also shows robust positive Δ entropy, with moderate temporal variability but persistent elevation above baseline.

The parietal region exhibits moderate positive Δ entropy, remaining elevated but with smaller amplitude than central and occipital regions. These changes are smooth and temporally stable, suggesting sustained but regionally constrained modulation.

In contrast, the frontal region remains close to baseline, with small negative deviations fluctuating around zero, indicating minimal frontal gamma entropy modulation. The temporal region exhibits predominantly negative Δ entropy, including a deeper excursion mid-session, with reductions sustained across multiple windows. These reductions suggest increased regularity or constraint in temporal gamma activity relative to baseline.

This figure highlights a clear posterior-temporal dissociation in indoor gamma entropy modulation, with strong occipital and central increases alongside temporal reductions.

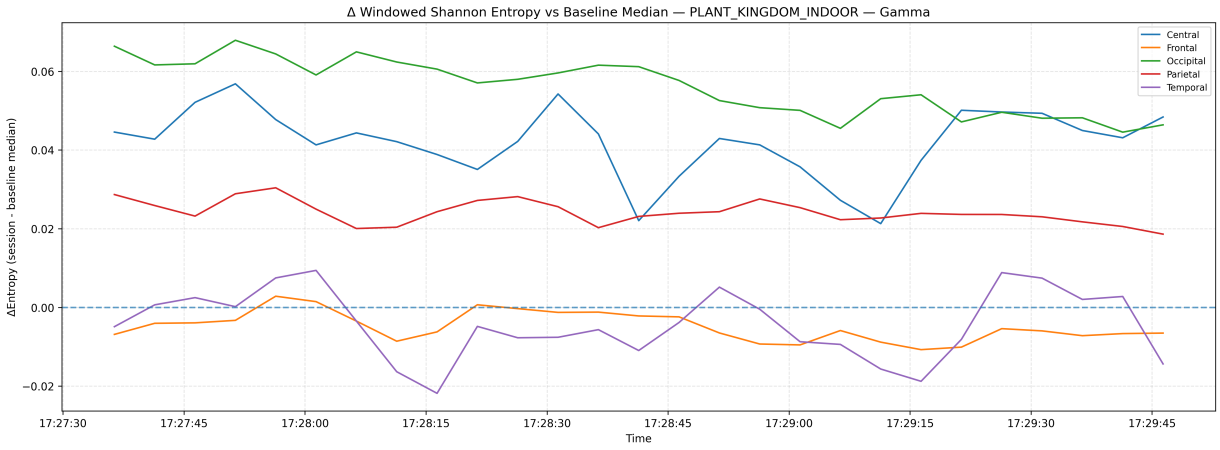

Figure 49: Δ windowed Shannon entropy vs baseline median (Gamma band): Plant Kingdom indoor session.

Δ Windowed Shannon Entropy vs Baseline Median — PLANT KINGDOM OUTDOOR — Gamma

This figure shows Δ Gamma entropy relative to baseline for the outdoor Plant Kingdom condition, using the same baseline reference and scaling as the indoor condition.

The occipital region shows sustained positive Δ entropy across nearly the entire session. Compared to the indoor condition, this elevation is more uniform, with fewer fluctuations and no extended returns toward baseline.

The central region also shows persistent positive Δ entropy, with greater temporal structure than occipital regions. Peaks and troughs remain consistently above baseline, indicating sustained elevation rather than transient modulation.

The parietal region shows small positive Δ entropy, remaining close to baseline with brief increases and minimal variability. The frontal region remains near baseline, with negligible deviation from baseline gamma entropy outdoors.

The temporal region shows large, sustained negative Δ entropy, with a deep trough early in the session followed by partial recovery. These reductions are larger and more persistent than those observed indoors, indicating stronger and more sustained suppression of gamma entropy in the outdoor condition.

This figure shows that outdoor gamma entropy modulation is spatially differentiated, with strong posterior elevation and pronounced temporal suppression.

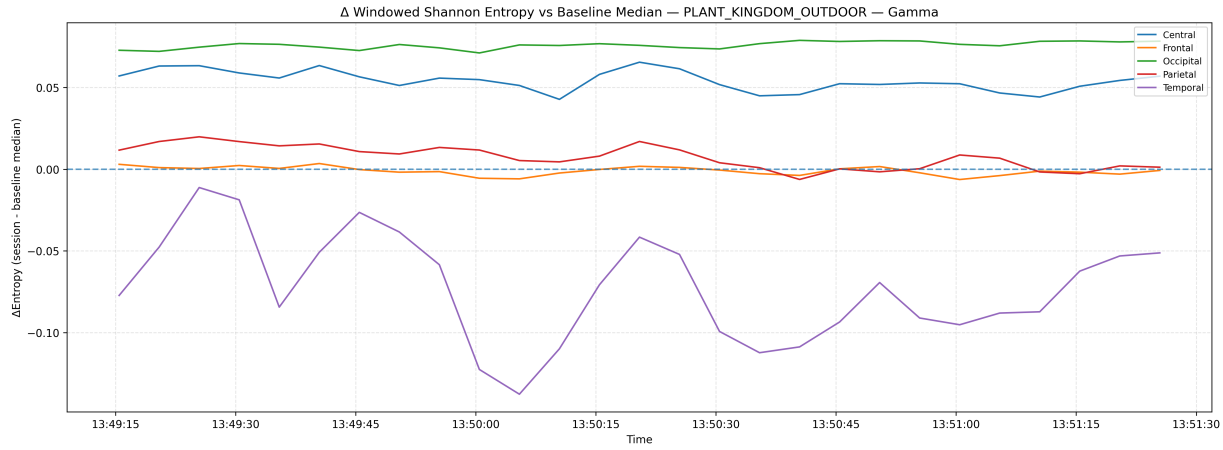

Figure 50: Δ windowed Shannon entropy vs baseline median (Gamma band): Plant Kingdom outdoor session.

Cross-Frequency Coupling (PAC and Phase–Amplitude)

This section examines cross-frequency coupling (CFC) within the EEG band-power envelope domain, focusing on phase–amplitude coupling (PAC) between slower and faster oscillatory bands. Rather than analyzing raw EEG phase relationships, this script operates on Emotiv POW streams sampled at 8 Hz, treating band-limited power envelopes as continuous signals for stable phase and amplitude extraction.

The core question addressed is whether the phase of slower rhythms (e.g., Theta or Alpha) modulates the amplitude of faster rhythms (e.g., BetaH or Gamma), and how this coupling strength varies across experimental conditions and cortical regions. This approach assesses coupling structure at the mesoscale level, less sensitive to transient raw-signal artefacts, while remaining temporally aligned to the task window.

Phase–amplitude coupling is quantified using the Tort Modulation Index (MI), computed by extracting the instantaneous phase of the slow-band envelope and the amplitude of the fast-band envelope via the Hilbert transform. Amplitude distributions across discretised phase bins are then evaluated for deviation from uniformity. Higher MI values indicate stronger coupling, while values near zero indicate weak or absent coupling.

Coupling is computed at the regional level, aggregating across anatomically defined electrode groups (frontal, temporal, central, parietal, occipital) to reduce noise and ensure spatial consistency. Minimum channel and sample thresholds are enforced to ensure stable estimates of coupling.

For each session, absolute PAC values are reported alongside baseline-referenced differences, allowing both raw coupling strength and deviation from resting baseline to be examined. Baseline anchoring is performed against the eyes-closed condition unless specified. Importantly, the diagonal structure of coupling is not assumed; only explicitly defined slow→fast band pairings are evaluated, and missing data are carried through as NaNs.

Figures in this section characterise where and to what degree cross-frequency coordination emerges during the task window. Interpretation is based on coupling magnitude, regional distribution, and relative change, rather than mechanistic or causal explanations. This section serves as a descriptive mapping of coupling structure under different conditions, forming a basis for later integration with spectral, entropy, and state-space analyses.

Some figures may later be candidates for manuscript inclusion, particularly those showing regional differentiation or consistent baseline-referenced effects. At this stage, all outputs are retained for internal understanding and comparison.

PAC (MI) — PLANT KINGDOM INDOOR — Alpha→BetaH

This figure shows phase–amplitude coupling strength, quantified using the Tort Modulation Index (MI), between the phase of the Alpha band-power envelope and the amplitude of the high-beta (BetaH) band-power envelope during the indoor Plant Kingdom condition. Higher MI values indicate stronger modulation of BetaH amplitude by Alpha phase.

Across regions, Alpha→BetaH coupling is present at moderate and similar magnitudes, with MI values clustering in a narrow range. The temporal region shows the highest coupling, slightly exceeding the other regions. Frontal, central, parietal, and occipital regions display comparable MI values, suggesting broadly distributed coupling rather than a sharply localized effect.

The small spread across regions indicates that Alpha-phase modulation of high-beta amplitude is a stable, global feature of the indoor condition, rather than being dominated by a specific cortical area. This figure may later be a candidate for inclusion if regional uniformity versus specificity becomes a key comparison across conditions.

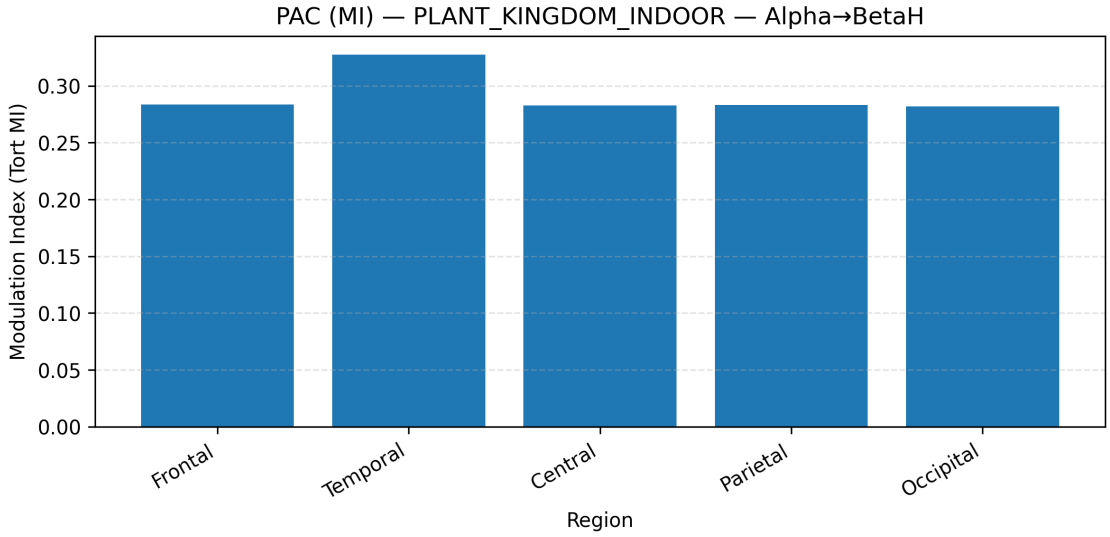

Figure 51: Absolute PAC (MI): Plant Kingdom indoor session, Alpha→BetaH.

PAC (MI) — PLANT KINGDOM INDOOR — Theta→Gamma

This figure shows phase–amplitude coupling between the phase of the Theta band-power envelope and the amplitude of the Gamma band-power envelope during the indoor Plant Kingdom condition. As in the previous chart, MI values are summarised by region.

Theta→Gamma coupling is consistently elevated across most regions, with frontal and parietal regions showing the highest MI values. Temporal and occipital regions show slightly lower values but remain within a similar range, while the central region shows the lowest coupling, though still clearly above zero.

This pattern suggests that Theta-phase modulation of Gamma amplitude is robust during the indoor condition, with modest regional differentiation. Frontal and parietal regions contribute more strongly, while the overall magnitude and consistency of MI values indicate a well-formed cross-frequency structure.

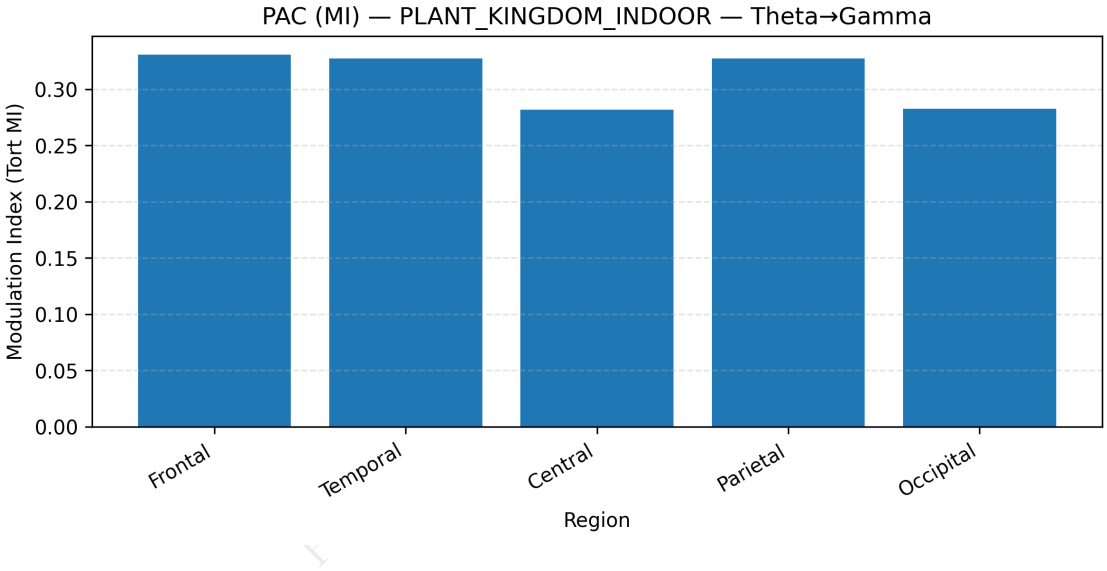

Figure 52: Absolute PAC (MI): Plant Kingdom indoor session, Theta→Gamma.

PAC (MI) — PLANT KINGDOM OUTDOOR — Alpha→BetaH

This figure shows absolute Alpha→BetaH phase–amplitude coupling during the outdoor Plant Kingdom condition, summarised at the regional level. Compared to the indoor condition, the regional pattern remains broadly similar, but with some redistribution of coupling strength.

The temporal region exhibits the strongest Alpha→BetaH coupling, standing clearly above the other regions. Frontal, central, and parietal regions cluster at intermediate MI values, while the occipital region shows noticeably lower coupling strength relative to the rest.

This pattern suggests that, outdoors, Alpha-phase modulation of high-beta amplitude remains strongest in temporal regions, with reduced involvement of posterior visual areas. The clearer occipital drop-off indicates a shift toward more anterior and lateral coupling structures. This figure may serve as a useful reference when contrasting indoor and outdoor spatial distributions.

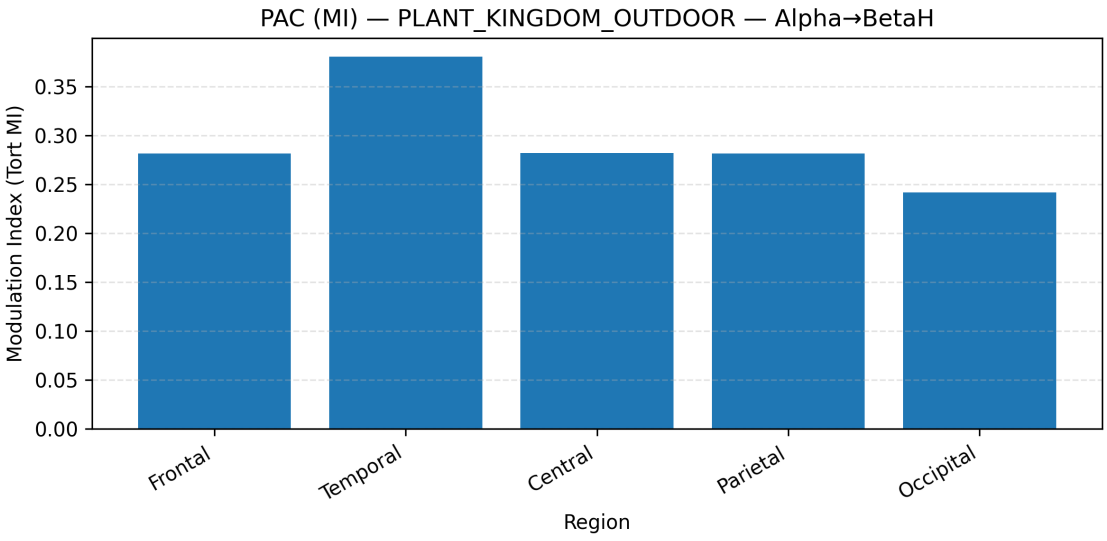

Figure 53: Absolute PAC (MI): Plant Kingdom outdoor session, Alpha→BetaH.

PAC (MI) — PLANT KINGDOM OUTDOOR — Theta→Gamma

This figure shows Theta→Gamma phase–amplitude coupling during the outdoor Plant Kingdom condition. MI values are presented by region, allowing inspection of slow–fast coupling distribution across the environment.

The frontal region exhibits the highest Theta→Gamma coupling, standing above all other regions. Temporal, central, parietal, and occipital regions form a tight cluster at slightly lower MI values, indicating broadly similar coupling strength across these areas.

The dominance of frontal coupling suggests that, outdoors, Theta-phase modulation of Gamma amplitude is most strongly expressed anteriorly, with less regional differentiation elsewhere. The compact spread among non-frontal regions indicates stable but less spatially specialised coupling outside the frontal cortex. This figure may be a candidate for inclusion if frontal dominance of Theta→Gamma coupling becomes a consistent condition-dependent feature.

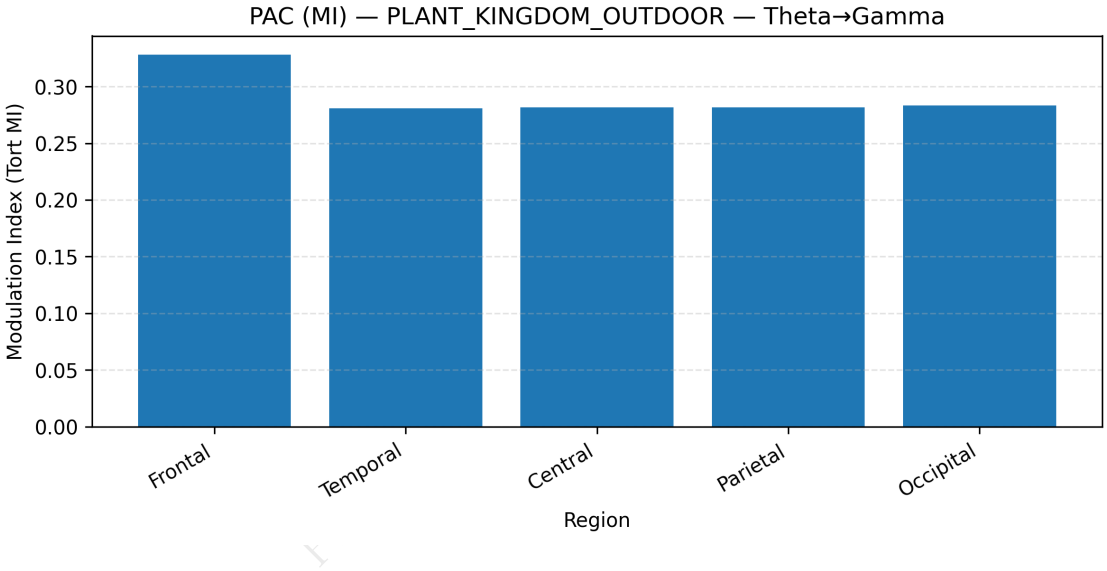

Figure 54: Absolute PAC (MI): Plant Kingdom outdoor session, Theta→Gamma.

ΔPAC vs Baseline — PLANT KINGDOM INDOOR — Alpha→BetaH

This figure shows the change in Alpha→BetaH phase–amplitude coupling relative to baseline, expressed as Δ Modulation Index (ΔMI), during the indoor Plant Kingdom session. Positive values indicate increased coupling compared to baseline, while values near zero indicate little or no change.

Frontal and parietal regions show the largest positive deviations from baseline, indicating a clear increase in Alpha-phase modulation of high-beta amplitude in these areas during the indoor condition. The occipital region also shows a positive shift, though smaller in magnitude. The temporal region exhibits a modest increase, while the central region remains close to baseline, with minimal change.

This pattern suggests that the indoor condition selectively enhances Alpha→BetaH coupling in frontal and posterior associative regions, rather than producing a uniform increase across the cortex. The near-zero change in the central region highlights spatial specificity rather than global coupling inflation.

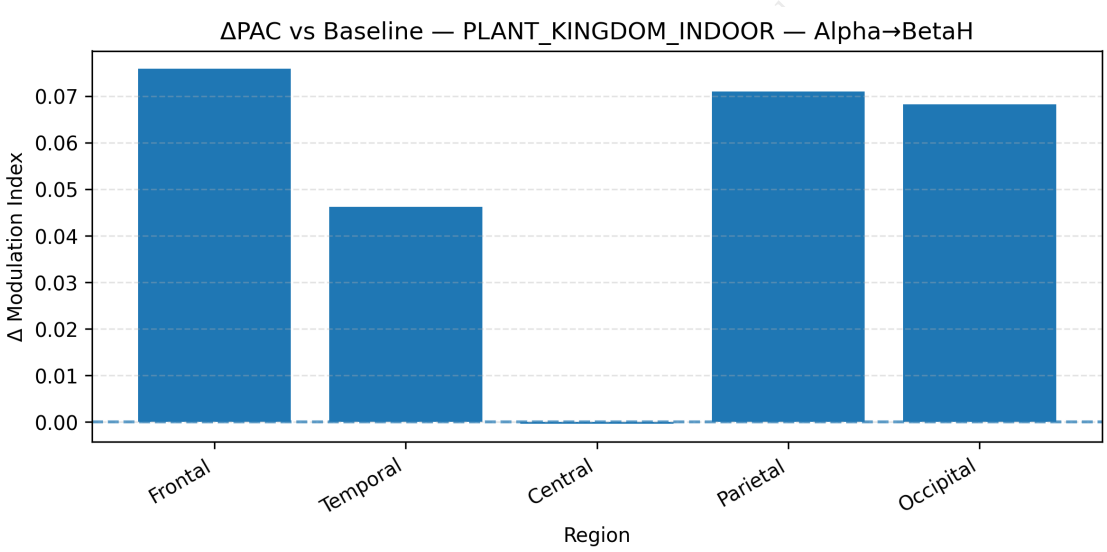

Figure 55: ΔPAC vs baseline (ΔMI): Plant Kingdom indoor session, Alpha→BetaH.

ΔPAC vs Baseline — PLANT KINGDOM INDOOR — Theta→Gamma

This figure shows baseline-referenced changes in Theta→Gamma phase–amplitude coupling during the indoor Plant Kingdom condition. ΔMI values indicate the extent of deviation from the resting baseline on a regional basis.

Frontal, temporal, and parietal regions show clear positive increases relative to baseline, with frontal and parietal regions exhibiting the largest deviations. The central region remains near zero, indicating minimal change from baseline coupling levels. The occipital region shows only a small positive shift, substantially lower than other regions.

This pattern suggests that indoor Theta→Gamma coupling increases are concentrated in frontal and associative regions, with limited posterior visual involvement and minimal change centrally. The regional enhancement indicates structured modulation rather than broad elevation in cross-frequency coupling.

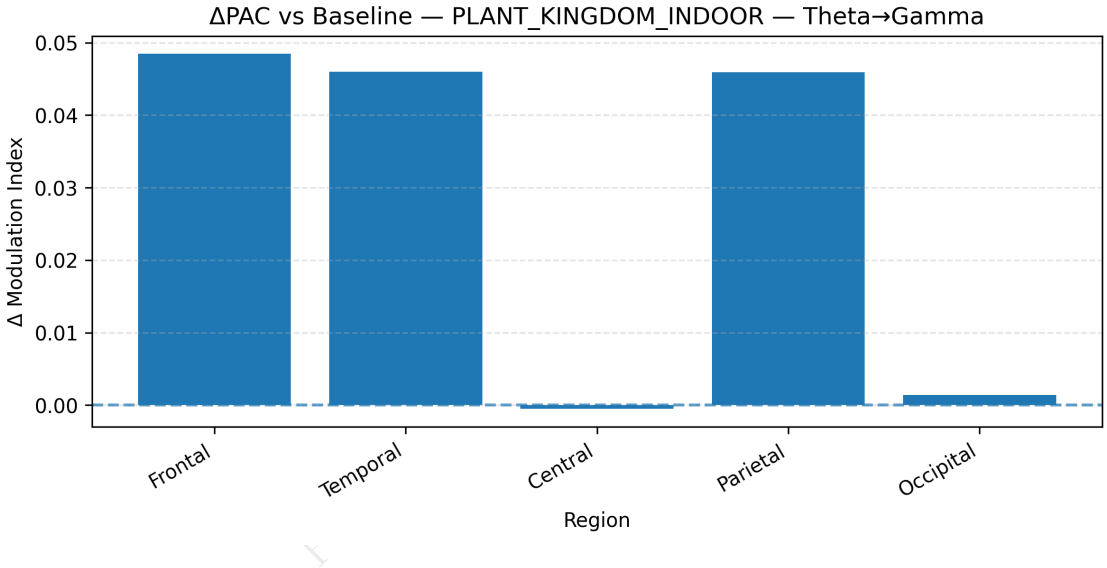

Figure 56: ΔPAC vs baseline (ΔMI): Plant Kingdom indoor session, Theta→Gamma.

ΔPAC vs Baseline — PLANT KINGDOM OUTDOOR — Alpha→BetaH

This figure shows ΔPAC values for Alpha→BetaH coupling during the outdoor Plant Kingdom condition. Compared to baseline, several regions show pronounced increases, while others show weaker changes.

The temporal region exhibits the largest positive deviation, standing clearly above all other regions. Frontal and parietal regions also show substantial increases, while the occipital region exhibits a smaller but still positive change. As in previous figures, the central region remains near baseline, indicating minimal modulation.

This pattern suggests that outdoor exposure is associated with strong enhancement of Alpha→BetaH coupling in temporal regions, with moderate increases in frontal and parietal areas. The near-baseline central region indicates that coupling changes are spatially selective, not globally distributed.

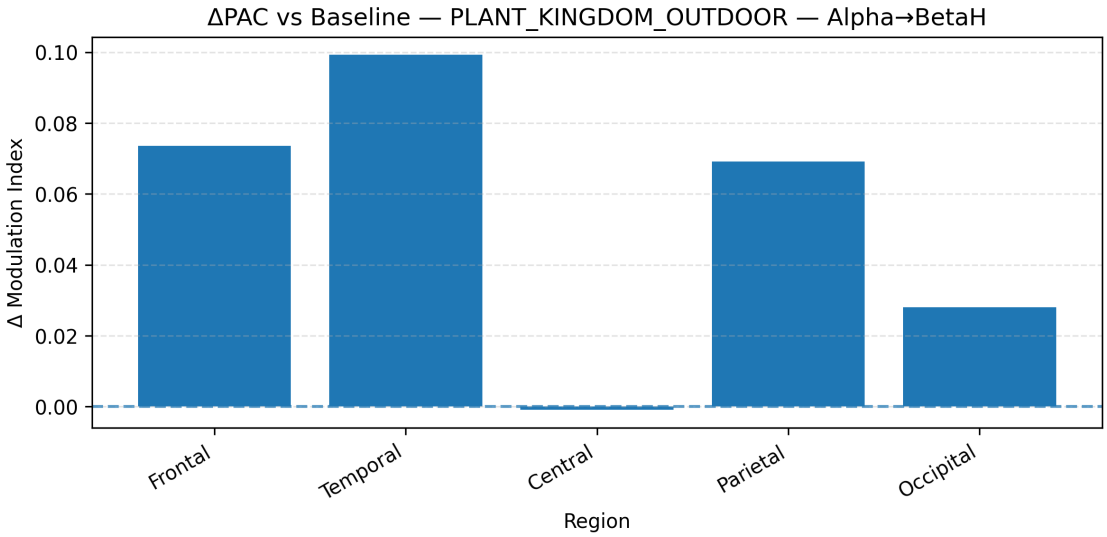

Figure 57: ΔPAC vs baseline (ΔMI): Plant Kingdom outdoor session, Alpha→BetaH.

ΔPAC vs Baseline — PLANT KINGDOM OUTDOOR — Theta→Gamma

This figure shows baseline-referenced changes in Theta→Gamma coupling during the outdoor Plant Kingdom condition. In contrast to other ΔPAC figures, the pattern here is highly focal.

The frontal region exhibits a clear positive increase relative to baseline, while all other regions remain near zero or show negligible changes. Temporal, central, and parietal regions show no meaningful deviations, and occipital coupling shows only a very small positive shift.

This pattern suggests that outdoor Theta→Gamma coupling changes are largely confined to the frontal cortex, with minimal engagement in other regions. The sharp regional contrast indicates a highly localized modulation pattern rather than a broadly distributed coupling response.

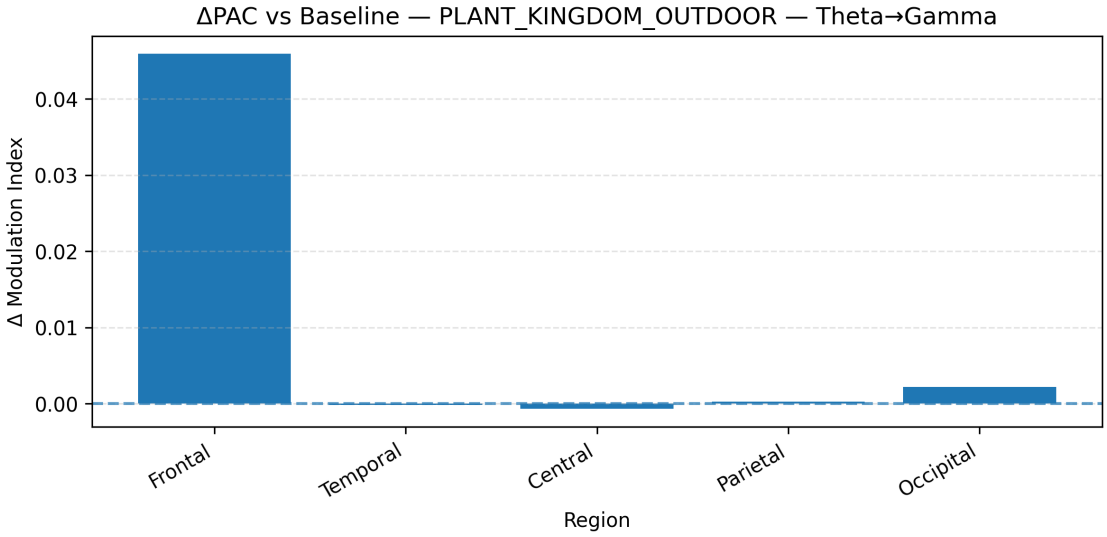

Figure 58: ΔPAC vs baseline (ΔMI): Plant Kingdom outdoor session, Theta→Gamma.

Temporal Stability and Persistence Index — Introduction

This section examines the temporal stability of EEG metrics by quantifying how long specific signal properties persist over time, rather than their instantaneous values. While previous analyses focused on power, spectral composition, or spatial structure, the Temporal Stability and Persistence Index shifts attention to time-dependent behaviour: how slowly or rapidly key measures evolve, how long they remain above or below reference levels, and how predictable their trajectories are throughout the session.

The core idea is that meaningful neural states are defined not just by amplitude or spatial patterns, but by their durational coherence. A state that briefly appears and collapses may reflect noise, while a state that persists indicates sustained organisation. Thus, time is treated as an active dimension of structure rather than a passive axis.

Operationally, the analysis uses band-limited, region-aggregated time series from earlier scripts, such as Shannon entropy and theta–alpha ratio (TAR). These measures are assessed using complementary notions of persistence: autocorrelation-based metrics estimate decay times, capturing how long a signal remains similar to its recent past, and dwell-time measures quantify how long the signal stays above or below a baseline median (from eyes-closed or eyes-open resting data). Together, these metrics capture both the smoothness of temporal evolution and the tendency of the system to remain in particular regimes.

Persistence metrics are computed using robust, time-aware methods that account for irregular sampling, missing values, and short time series. Medians are used over means, and minimum sample thresholds are enforced to ensure reliable estimates. The aim is not to force a single definition of "stability," but to reveal different facets of temporal behaviour for comparison across bands, regions, and conditions.

The figures in this section do not determine whether a session is "more" or "less" stable in an abstract sense. Rather, they show how stability manifests: whether signals decay slowly or rapidly, whether they dwell symmetrically around baseline or remain biased, and whether these temporal properties differ across neural features. These patterns provide the empirical basis for later interpretation, without assuming their functional or experiential significance.

PLANT KINGDOM INDOOR — Entropy Persistence τ (1/e) [seconds]

This heatmap shows the autocorrelation persistence time (τ) of Shannon entropy time series for the indoor Plant Kingdom session. τ is defined as the time it takes for the normalised autocorrelation function to decay to $1/e$. Values are reported in seconds and are organised by cortical region (rows) and frequency band (columns). Larger values indicate slower entropy fluctuations, reflecting greater temporal stability, while smaller values indicate faster decorrelation and more rapid entropy changes.

Across most regions and bands, persistence times cluster between 3 and 10 seconds, suggesting broadly comparable entropy dynamics across much of the cortex. A notable exception is the occipital gamma band, which shows an elevated persistence value (˜36 s), indicating unusually slow entropy dynamics. This suggests that entropy in this specific region–band combination remains correlated over much longer time scales compared to other areas. In contrast, high-beta bands in several regions exhibit shorter persistence values, implying faster temporal turnover of entropy.

Spatially, no strong anterior–posterior gradient is evident across most bands, with central, frontal, parietal, and temporal regions exhibiting similar τ values. The occipital gamma cell stands out as an outlier rather than part of a global pattern. This figure is primarily useful for identifying region–band outliers in entropy stability, rather than demonstrating uniform shifts across the cortex. It may be a candidate for later inclusion if the occipital gamma persistence remains distinctive across conditions.

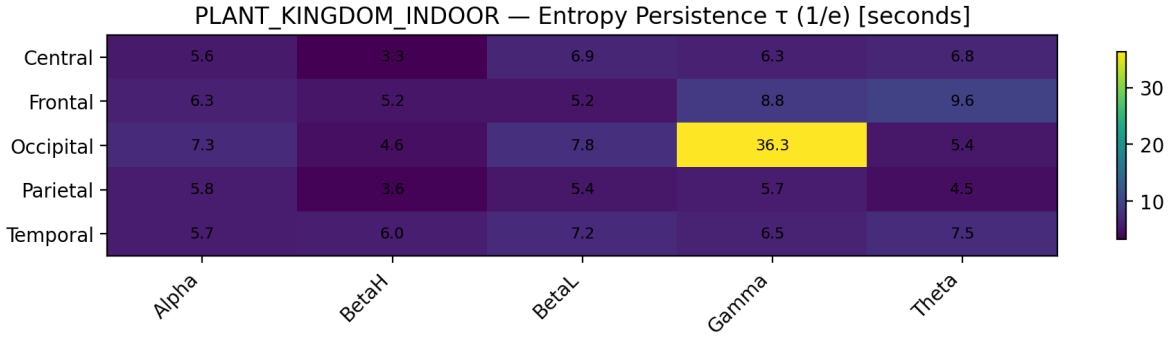

Figure 59: Plant Kingdom indoor: entropy autocorrelation persistence time τ (1/e), in seconds.

PLANT KINGDOM INDOOR — Entropy Mean Dwell ABOVE anchor [seconds] (baseline median)

This heatmap shows the mean dwell time that entropy values remain above a baseline-derived anchor, defined as the median entropy measured during the selected baseline condition. Values represent the average duration (in seconds) of continuous periods where entropy exceeds this anchor, organised by region and frequency band.

Several cells reach the maximum dwell duration of 135 seconds, indicating that in these cases, entropy remains above baseline for nearly the entire analysed segment, with few or no transitions back below the anchor. This behaviour is particularly evident in central regions across multiple bands, as well as in parietal BetaL, Gamma, and Theta, and occipital Gamma. These high values reflect sustained elevations rather than intermittent excursions above baseline.

In contrast, frontal regions show consistently short dwell times (around 5-8 seconds), indicating frequent crossings of the baseline median and more dynamic entropy fluctuations. Temporal regions also show shorter dwell durations, with modest exceptions in Gamma. The strong contrast between long dwell times in central/parietal areas and short dwell times in frontal areas suggests regional differences in how persistently entropy departs from baseline indoors.

It is important to note that long dwell times do not imply high entropy, only sustained deviation relative to baseline. This figure is particularly useful for identifying regions where entropy dynamics remain above baseline for extended periods.

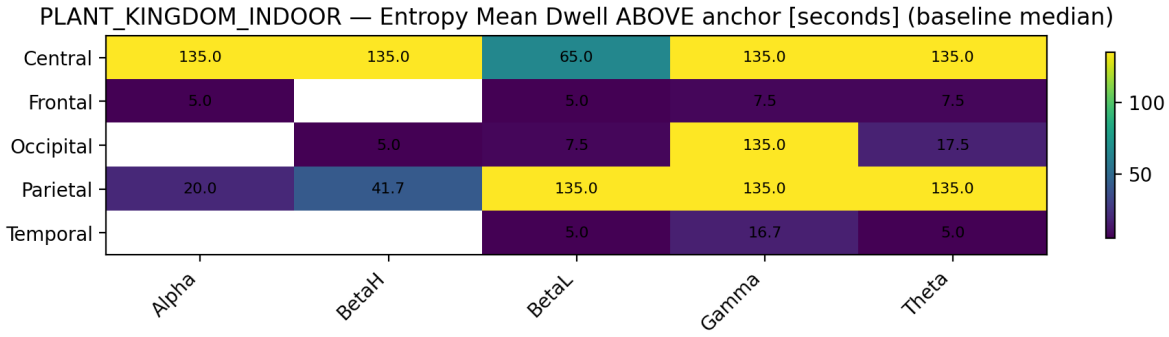

Figure 60: Plant Kingdom indoor: entropy mean dwell time above baseline-median anchor, in seconds.

PLANT KINGDOM INDOOR — TAR Persistence τ (1/e) [seconds]

This heatmap shows the autocorrelation persistence time of the theta–alpha ratio (TAR) time series, computed at a global level rather than regionally. Two representations are shown: TAR and log-transformed TAR (logTAR). Values indicate how long TAR remains correlated with its recent past before decaying to $1/e$.

Both TAR and logTAR exhibit nearly identical persistence values of approximately 0.6 seconds, indicating rapid temporal decorrelation. This suggests that, indoors, global TAR fluctuates quickly, with limited temporal memory, regardless of whether the ratio is considered in linear or logarithmic space. The similarity between TAR and logTAR indicates that the persistence estimate is not strongly influenced by the distributional scaling of the metric.

The short persistence time contrasts with the multi-second entropy persistence values seen in the previous figure, highlighting that ratio-based measures evolve much faster than entropy-based measures. This figure establishes a baseline expectation for TAR dynamics indoors and serves primarily as a reference for comparison with other conditions.

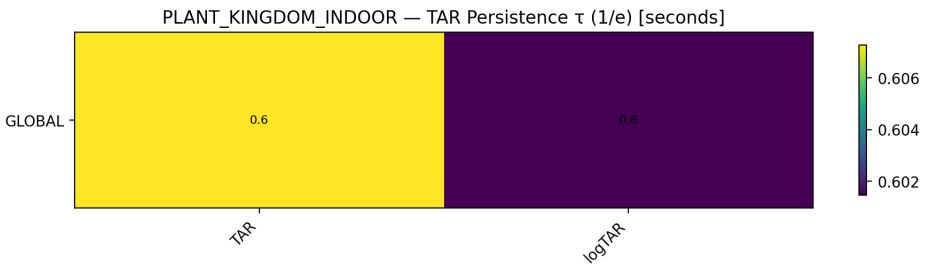

Figure 61: Plant Kingdom indoor: TAR and logTAR autocorrelation persistence time τ (1/e), in seconds.

PLANT KINGDOM INDOOR — TAR Mean Dwell ABOVE anchor [seconds] (baseline median)

This heatmap reports the mean dwell time above baseline for the global TAR and logTAR time series. The baseline anchor is defined as the median, and values indicate the average duration of continuous periods above that level.

Both TAR and logTAR show very short mean dwell times of approximately 2.4 seconds, indicating frequent baseline crossings. This suggests that global TAR fluctuates symmetrically around baseline, rather than remaining biased toward prolonged above-baseline or below-baseline regimes. The near-identical dwell times for TAR and logTAR indicate that the transformation does not materially alter the temporal structure of baseline crossings.

In combination with the short autocorrelation persistence, this figure reinforces the interpretation that TAR is a rapidly varying, dynamically balanced metric indoors, lacking the long-lived regimes observed in entropy for certain region–band combinations. While visually simple, this figure is important for anchoring expectations about TAR behaviour before examining other environments or conditions.

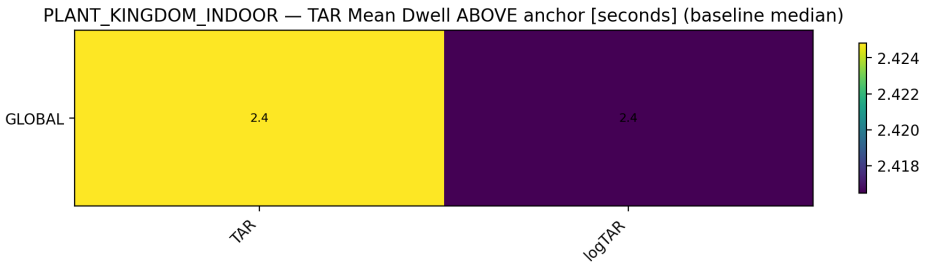

Figure 62: Plant Kingdom indoor: TAR and logTAR mean dwell time above baseline-median anchor, in seconds.

PLANT KINGDOM OUTDOOR — Entropy Persistence τ (1/e) [seconds]

This heatmap shows the autocorrelation persistence time (τ) of Shannon entropy during the outdoor Plant Kingdom session, measured as the time required for the autocorrelation function to decay to $1/e$. Values are expressed in seconds and organised by cortical region and frequency band, with higher values indicating more slowly evolving entropy dynamics.

Across most regions and bands, persistence times fall in the range of approximately 5–10 seconds, indicating moderately stable entropy fluctuations outdoors. Unlike the indoor condition, persistence values are more evenly distributed across regions, with fewer extreme outliers. One notable exception is the parietal gamma band, which shows a substantially elevated persistence value (14.6 s), indicating slower decay of entropy fluctuations in this region–band combination.

Temporal regions show relatively high persistence in BetaH and BetaL bands, suggesting sustained entropy structure in these frequencies. In contrast, alpha-band persistence is consistently lower across regions, indicating faster temporal variability in alpha-related entropy outdoors. Overall, the spatial pattern suggests distributed, region-specific persistence, rather than a single dominant cortical locus.

This figure is useful for characterising how entropy stability is organised across the cortex in the outdoor environment, highlighting parietal gamma as a region–band combination with particularly slow entropy dynamics.

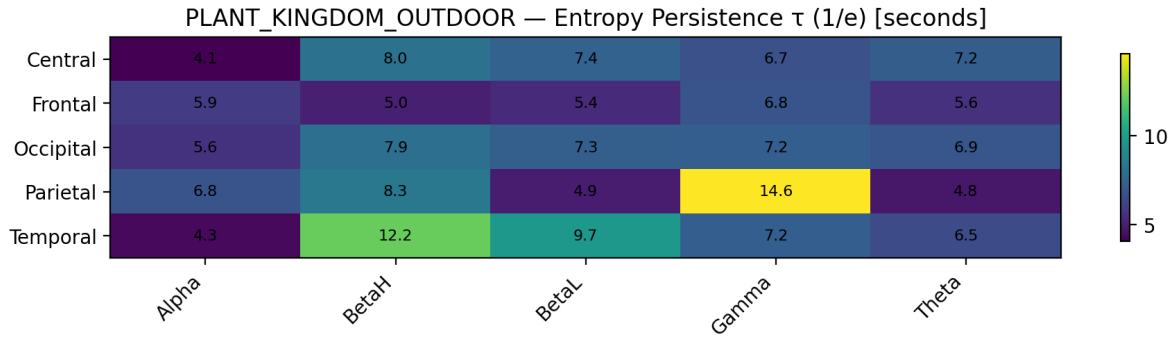

Figure 63: Plant Kingdom outdoor: entropy autocorrelation persistence time τ (1/e), in seconds.

PLANT KINGDOM OUTDOOR — Entropy Mean Dwell ABOVE anchor [seconds] (baseline median)

This heatmap reports the mean dwell time that entropy remains above the baseline median, measured in seconds and organised by region and frequency band. Longer dwell times indicate sustained periods where entropy remains elevated relative to baseline, while shorter values reflect frequent crossings of the anchor.

Several region–band combinations reach the maximum dwell duration of 135 seconds, notably in central Alpha, BetaH, and Gamma, as well as occipital BetaH and Gamma. These values indicate prolonged epochs in which entropy remains consistently above baseline, with minimal reversion. In contrast to the indoor condition, dwell times outdoors show greater regional differentiation, with frontal and parietal regions generally exhibiting shorter dwell durations.

Temporal regions show moderate dwell times in Beta bands, while Alpha and Gamma dwell values are missing or reduced in some cases, reflecting either insufficient above-baseline segments or more balanced fluctuations around the anchor. Theta-band dwell times are generally intermediate, suggesting neither strong bias nor rapid oscillation relative to baseline.

Overall, this figure reveals a mixture of sustained above-baseline entropy regimes in specific region–band pairs, alongside more dynamically balanced behaviour elsewhere. It is particularly informative for identifying where outdoor entropy dynamics are persistently elevated rather than intermittently fluctuating.

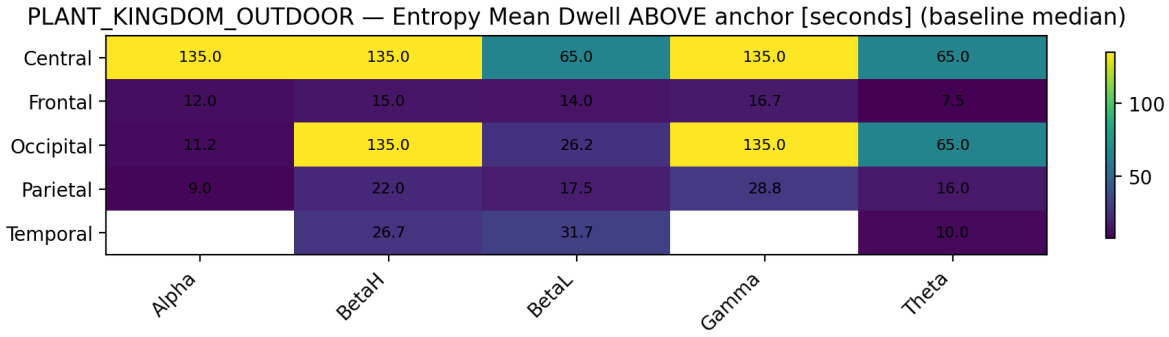

Figure 64: Plant Kingdom outdoor: entropy mean dwell time above baseline-median anchor, in seconds.

PLANT KINGDOM OUTDOOR — TAR Persistence τ (1/e) [seconds]

This figure shows the autocorrelation persistence time of the global theta–alpha ratio (TAR) and its logarithmic transform (logTAR) during the outdoor session. Values reflect how long TAR remains temporally correlated before decorrelating to $1/e$.

Persistence times are short for both measures, around 0.6–0.7 seconds, indicating rapid temporal variability in TAR. The log-transformed TAR shows slightly longer persistence than the linear TAR, suggesting marginal smoothing of temporal fluctuations when expressed in logarithmic space. However, both measures remain firmly within a sub-second persistence regime.

These results indicate that, outdoors, global TAR continues to behave as a fast-changing metric, with little temporal inertia. The short persistence suggests that TAR is sensitive to moment-to-moment fluctuations rather than sustained state occupancy. This figure provides a compact summary of TAR temporal dynamics and serves as a useful reference for comparisons with other conditions.

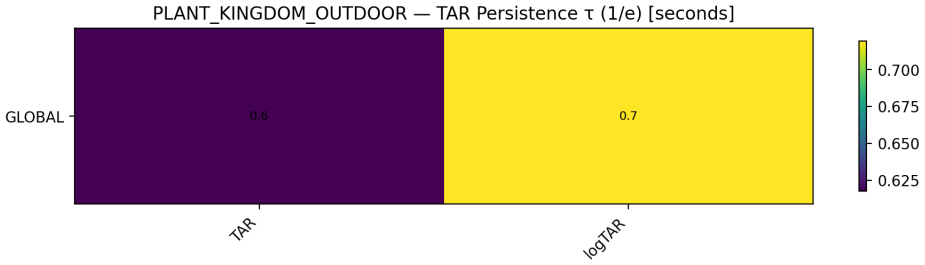

Figure 65: Plant Kingdom outdoor: TAR and logTAR autocorrelation persistence time τ (1/e), in seconds.

PLANT KINGDOM OUTDOOR — TAR Mean Dwell ABOVE anchor [seconds] (baseline median)

This heatmap reports the mean dwell time above the baseline median for global TAR and logTAR during the outdoor session. Values indicate the average duration of continuous periods where TAR exceeds the baseline-derived anchor.

Both TAR and logTAR show mean dwell times of approximately 3.7 seconds, indicating relatively brief but slightly longer above-baseline episodes compared to indoor values. Despite this increase, dwell durations remain short overall, reflecting frequent crossings of the baseline median and a lack of prolonged bias toward elevated TAR states.

The similarity between TAR and logTAR dwell times indicates that the transformation does not substantially alter the temporal structure of baseline crossings. Together with the short persistence times, this figure reinforces the interpretation that TAR dynamics outdoors are fast, transient, and centrally balanced around baseline, rather than organised into long-lived regimes.

This figure is primarily valuable as a temporal characterisation reference and would be most informative when placed alongside entropy-based persistence and dwell metrics.

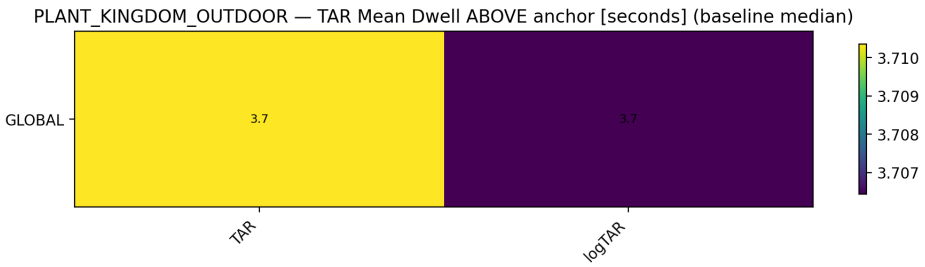

Figure 66: Plant Kingdom outdoor: TAR and logTAR mean dwell time above baseline-median anchor, in seconds.

Notes on interpreting persistence values

The numerical values shown in the figures correspond to time-based persistence measures expressed in seconds. For autocorrelation-based metrics (τ, reported as $1/e$ decay time), the value represents the characteristic time scale over which the signal remains statistically similar to its immediate past. Larger τ values indicate slower temporal evolution, suggesting that once the signal enters a particular configuration, it changes gradually. Smaller τ values indicate faster decorrelation, where the signal loses memory of its recent state more quickly and fluctuates on shorter time scales.

For dwell-time metrics, the values represent the average duration during which the signal remains above a defined reference level, typically the baseline median derived from resting data. Longer dwell times indicate sustained occupancy of an above-baseline regime, while shorter dwell times indicate frequent crossings of the reference level, reflecting more dynamically balanced behaviour. Dwell times approaching the full analysis window indicate prolonged bias rather than intermittent excursions.

Importantly, these values are not measures of magnitude or intensity. A large persistence or dwell value does not imply "more" activity, higher power, or greater entropy; it indicates a more stable or long-lived temporal structure. Conversely, low values do not imply weak signals, but rather faster temporal turnover. All values should be interpreted as describing how long a given signal property persists, not how strong it is at any given moment.

Reorganisation Velocity (State-Space Flux)

This section examines the rate at which the brain's band-channel power configuration reorganises over time, treating the multiband EEG state as a trajectory through a high-dimensional state space rather than a set of independent signals. Instead of quantifying the strength of activity within a specific band or region, this analysis focuses on how quickly and continuously the overall configuration of band-limited power changes from one moment to the next.

At each time point, the EEG state is represented as a single vector formed by concatenating band-power values across all channels and frequency bands (Theta, Alpha, BetaL, BetaH, Gamma). The evolution of this vector over time defines a path through state space. Reorganisation velocity, or state-space flux, is computed as the frame-to-frame distance between successive state vectors, yielding a time-resolved measure of how much the system reorganises per unit of time.

This approach captures global dynamical behaviour that static power summaries or slow temporal averages cannot reveal. Periods of low flux correspond to relatively stable configurations, where band-channel relationships persist over time, while periods of high flux indicate rapid reconfiguration, where the system transitions quickly between different states. Importantly, this metric is agnostic to the direction of change and focuses solely on the magnitude of reorganisation.

Flux is computed using the native Emotiv band-power cadence (nominally 8 Hz), with time steps estimated directly from available timestamps. The primary flux metric uses the ℓ_2 (Euclidean) distance between successive state vectors, providing an intuitive measure of absolute movement through state space. An optional cosine-distance variant is also computed to characterise changes in configuration independent of overall magnitude, offering complementary views of reorganisation dynamics.

To support interpretation at multiple scales, the script produces both global flux measures (using the full band $\times$ channel state vector) and decomposed views, including band-wise flux, regional flux (where channels are collapsed into anatomical regions), and regime-style representations linking flux to concurrent entropy measures. These analyses aim to reveal whether reorganisation is uniform across the system or driven preferentially by specific frequency bands or spatial groupings.

All flux values are reported in units normalised by time (per second), enabling direct comparisons across sessions and baselines. Baseline (eyes-closed) datasets are processed identically, providing a reference distribution for visually and descriptively comparing session-specific reorganisation rates.

The figures in this section characterise the tempo of neural state changes rather than their content. Each chart is interpreted independently, focusing on temporal structure, variability, and stability within that specific representation, without assuming causal mechanisms or functional interpretations at this stage.

State-Space Flux (L2) — BASELINE EC

This figure shows the time-resolved L2 state-space flux during the baseline eyes-closed (EC) condition. Each point represents the Euclidean distance between successive band × channel power-state vectors, quantifying the extent of change in the overall EEG configuration from one time step to the next. Higher values indicate more rapid reorganisation of the multiband spatial state, while lower values suggest greater stability.

Throughout most of the recording, flux values remain within a low-to-moderate range, with frequent small fluctuations rather than extended periods of stability. This pattern suggests continuous but modest reorganisation, consistent with a baseline resting state where neural dynamics remain active but relatively constrained. The trace is punctuated by a small number of sharp, high-amplitude spikes that rise well above the surrounding activity. These spikes are brief and isolated, signifying transient episodes of unusually rapid state change, rather than sustained instability.

Outside of these spikes, the signal quickly returns to its typical range, indicating that the baseline system maintains temporal stability despite occasional large reconfigurations. The absence of long plateaus or drifting trends suggests that reorganisation velocity fluctuates around a stable operating regime, rather than progressively increasing or decreasing over time. This figure establishes a reference for the magnitude and variability of spontaneous state-space movement during a resting state, without task engagement or environmental modulation.

This plot is a strong candidate for inclusion as a baseline reference figure, as it provides a clear understanding of the characteristic flux range and temporal structure against which other experimental conditions can be compared.

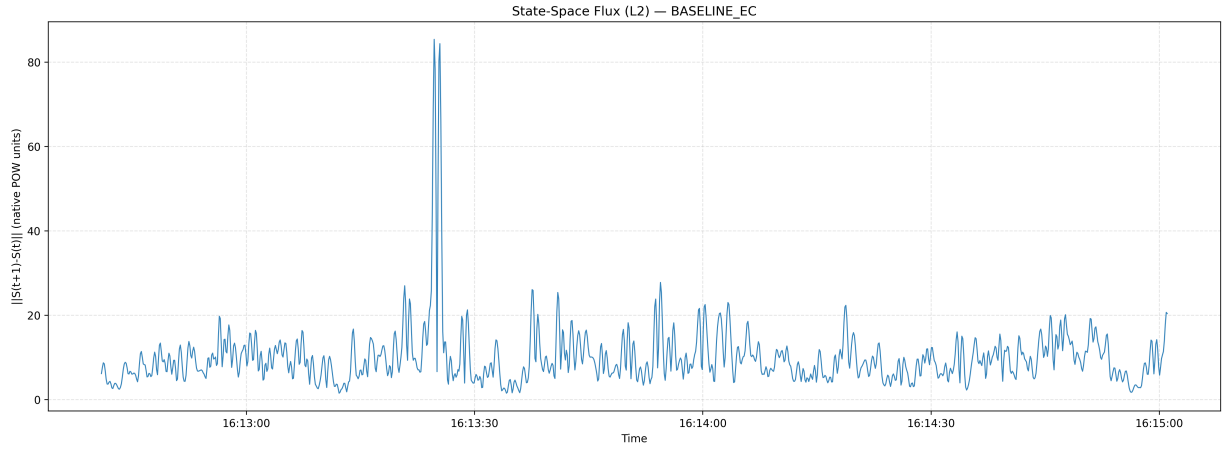

Figure 67: State-space flux (ℓ_2) time series: baseline eyes-closed (EC).

State-Space Flux (L2) — PLANT KINGDOM INDOOR

This figure displays the L2 state-space flux during the Plant Kingdom indoor session. As in the baseline plot, the trace represents the magnitude of frame-to-frame changes in the full band × channel power configuration, capturing the rate at which the neural state reorganises over time.

Compared to the baseline, the flux trace demonstrates a broader dynamic range, with more frequent excursions into higher values. While low-level fluctuations persist throughout the session, there are repeated bursts where flux rises sharply, often exceeding the baseline's typical operating range. These bursts are followed by periods of lower activity, suggesting episodic rather than sustained reorganisation.

The temporal structure is heterogeneous, with some intervals exhibiting clustered peaks occurring close together, while others display calmer segments. This pattern indicates that the system alternates between relatively stable configurations and phases of rapid reconfiguration. Unlike the baseline trace, these elevated events are recurrent across the session rather than isolated outliers.

Despite this increased variability, the signal does not show runaway behaviour or long-term drift. After high-flux episodes, values reliably return to mid-range levels, indicating that reorganisation remains contained. This figure highlights an increase in the tempo and variability of neural state change in the indoor Plant Kingdom condition, while maintaining overall temporal stability.

This plot is likely a key descriptive figure for documenting condition-specific modulation of reorganisation velocity.

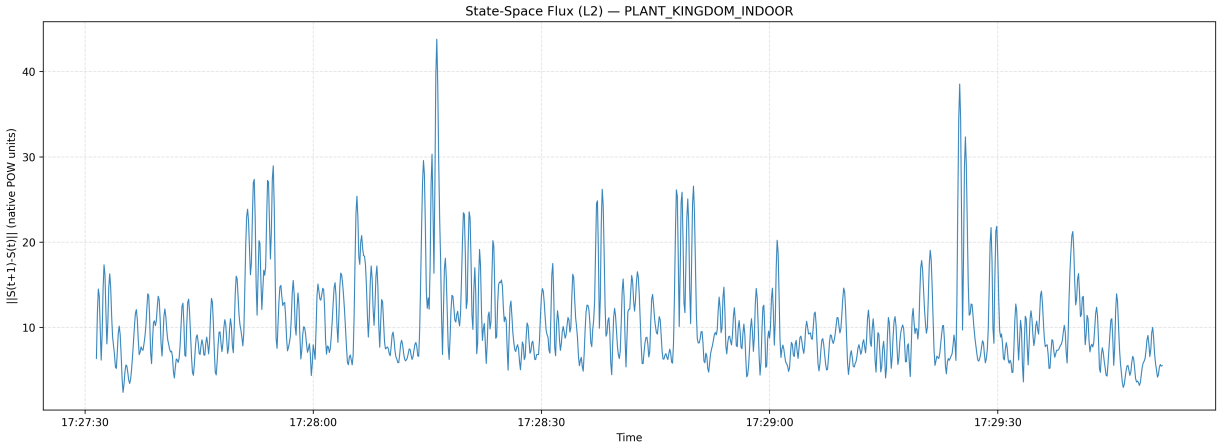

Figure 68: State-space flux (ℓ_2) time series: Plant Kingdom indoor session.

State-Space Flux (L2) — PLANT KINGDOM OUTDOOR

This figure shows the L2 state-space flux during the Plant Kingdom outdoor session. As with previous figures, the trace reflects the magnitude of successive changes in the global band × channel power-state vector, providing a direct measure of reorganisation velocity over time.

The outdoor flux trace is characterised by pronounced burst structure. While most of the signal occupies a low-to-moderate range, similar to other conditions, there are multiple large-amplitude spikes that clearly stand out from the surrounding activity. These high-flux events are among the largest observed across all conditions and occur at distinct moments in the recording, rather than being confined to a single segment.

Between bursts, the flux drops back to relatively low values, creating a strongly intermittent pattern. This alternation between quiescent periods and abrupt, high-magnitude reorganisation suggests a dynamic regime where the neural state remains stable for stretches of time before undergoing rapid, coordinated shifts. The contrast between baseline levels and peak amplitudes is particularly stark in this condition.

The absence of sustained elevated flux indicates that these events are transient, rather than reflecting continuous instability. Instead, the defining feature of this trace is the heavy-tailed nature of the reorganisation process, with rare but substantial state transitions embedded within otherwise moderate dynamics. This temporal structure is not apparent from summary statistics alone, which highlights the importance of examining flux in a time-resolved manner.

This figure is a strong candidate for inclusion, as it clearly illustrates condition-specific differences in both the magnitude and temporal patterning of neural reorganisation.

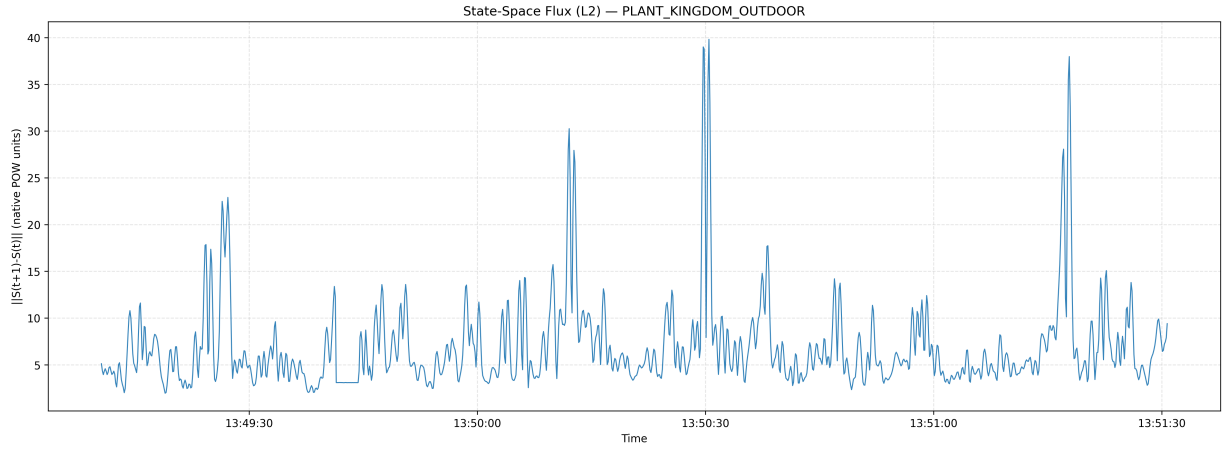

Figure 69: State-space flux (ℓ_2) time series: Plant Kingdom outdoor session.

Flux (L2) Distribution — PLANT KINGDOM OUTDOOR vs BASELINE EC

This figure shows the distribution of L2 state-space flux values for the Plant Kingdom outdoor session, compared directly to the baseline eyes-closed condition. Each distribution represents the frequency of observed frame-to-frame reorganisation magnitudes, computed as the Euclidean distance between successive band × channel power-state vectors. Unlike the time-series plots, which show when reorganisation occurs, this figure summarises how often different magnitudes of reorganisation are observed across the entire session.

The baseline distribution is concentrated within a relatively narrow range of low-to-moderate

flux values, forming a unimodal shape with a gradual rightward decay. While the baseline does exhibit a tail extending toward higher values, the majority of observations cluster tightly around the central region of the distribution, indicating that large reorganisation events are rare during eyes-closed resting conditions.

In contrast, the outdoor session distribution is noticeably broader and more right-skewed. While its central mass overlaps with the baseline range, the session exhibits an extended tail reaching substantially higher flux values. This suggests a greater prevalence of large-magnitude reorganisation events during the outdoor condition. The presence of non-negligible counts at high flux values reflects the burst-like events seen in the corresponding time-series plot, but here expressed as a statistical property of the entire session rather than isolated temporal episodes.

Importantly, the overlap between the two distributions at lower flux values demonstrates that the outdoor condition still spends considerable time in relatively stable regimes. The key difference lies not in the absence of low-flux states, but in the increased probability of entering high-flux regimes. This distributional shift highlights that reorganisation during the outdoor session is characterised by heavier tails, rather than a uniform elevation of flux across all time points.

This figure serves as a complementary summary to the flux time-series, translating the observed intermittency and burst structure into a distributional form. It is a strong candidate for inclusion, as it clearly illustrates how the statistical structure of reorganisation velocity differs from baseline without relying on temporal alignment or event timing.

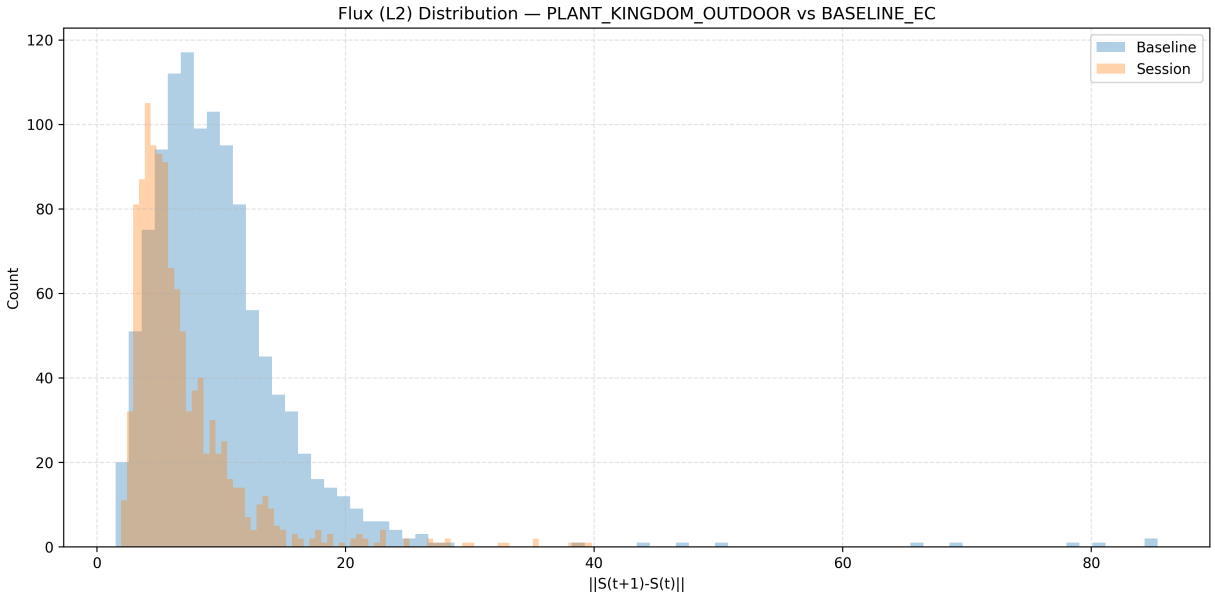

Figure 70: Distribution of state-space flux (ℓ_2): Plant Kingdom outdoor vs baseline eyes-closed (EC).

State-Space Flux (Cosine Distance) — BASELINE EC

This figure shows the time-resolved cosine-distance flux during the baseline eyes-closed condition. Each value represents one minus the cosine similarity between successive band × channel power-state vectors, capturing changes in the direction or configuration of the neural state independently of overall magnitude. Low values indicate that the relative pattern of activity across bands and channels remains stable from one time step to the next, while higher values suggest a reorientation of that pattern.

For most of the baseline recording, cosine-distance values remain very low, indicating strong moment-to-moment configurational continuity. The trace is dominated by small fluctuations clustered near zero, suggesting that although the system is continuously active, the relative relationships between bands and channels are largely stable over time.

Occasional sharp spikes are present, rising well above the surrounding values. These events are brief and isolated, indicating transient reconfigurations of the state pattern rather than prolonged shifts in configuration. Importantly, these spikes are not followed by sustained elevation, with the signal quickly returning to its low baseline range. This behaviour mirrors the baseline L2 flux trace by showing stability punctuated by rare, abrupt events, but here it is expressed specifically in terms of configurational change.

This figure serves as a useful reference for the degree of spontaneous pattern reorientation under resting conditions and provides a baseline for comparing configurational dynamics in other conditions.

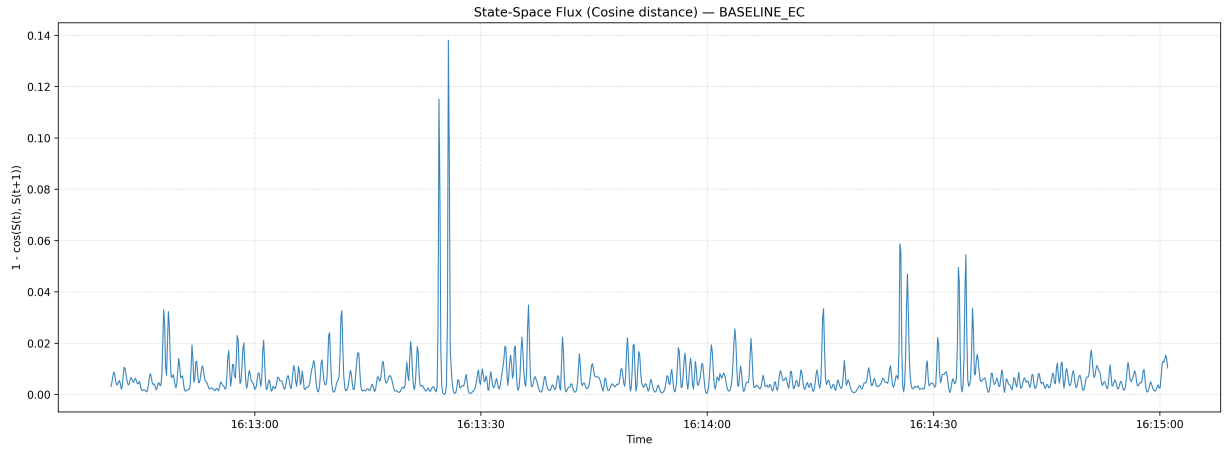

Figure 71: State-space flux (cosine distance) time series: baseline eyes-closed (EC).

State-Space Flux (Cosine Distance) — PLANT KINGDOM INDOOR

This figure presents the cosine-distance state-space flux during the Plant Kingdom indoor session. As with the baseline plot, this metric reflects changes in the orientation of the band × channel state vector, rather than its absolute magnitude.

Compared to baseline, the indoor trace exhibits more frequent and larger excursions away from zero. While the signal still spends much of its time in a low-distance regime, indicating periods of configurational stability, there are numerous spikes distributed throughout the session. These spikes reflect moments where the relative pattern of band- and channel-level activity shifts more substantially between successive time points.

The temporal structure of the trace is irregular, with no obvious periodicity or monotonic trend. Instead, episodes of increased configurational change appear intermittently, separated by intervals of relative stability. This pattern suggests that the indoor condition involves more frequent reorientation of the neural state configuration than baseline, without collapsing into a continuously unstable regime.

Despite the increased activity, cosine-distance values remain bounded within a narrow absolute range, indicating that even the largest configurational changes are transient, with the system frequently returning to a stable patterning. This figure complements the L2 flux results by showing that increased reorganisation in the indoor condition involves both changes in magnitude and repeated shifts in configuration.

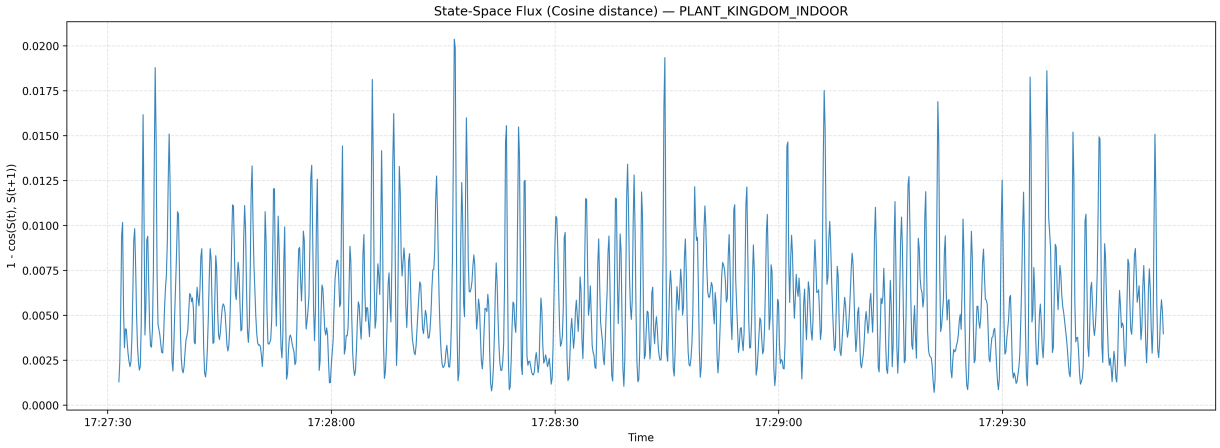

Figure 72: State-space flux (cosine distance) time series: Plant Kingdom indoor session.

State-Space Flux (Cosine Distance) — PLANT KINGDOM OUTDOOR

This figure shows the cosine-distance state-space flux during the Plant Kingdom outdoor session. The trace again captures changes in the orientation of the global band × channel state vector over time.

The outdoor condition displays a distinctly burst-like structure, with extended low-distance intervals punctuated by prominent spikes. These spikes reach higher values than those observed in the baseline and indoor conditions, indicating moments of pronounced configurational reorientation. As in the other conditions, these events are brief rather than sustained, and the signal quickly returns to lower values following each peak.

Between bursts, the cosine-distance values remain low and relatively stable, suggesting that the system frequently occupies persistent configurational states before transitioning abruptly to new ones. This intermittent structure closely parallels the burst dynamics seen in the L2 flux time-series but highlights that these events involve sharp changes in the pattern of activity, not merely increases in overall power differences.

This figure complements the L2 flux plot, demonstrating that large reorganisation events in the outdoor condition correspond to both magnitude-based and configuration-based changes. It provides additional detail on the nature of reorganisation without introducing new assumptions about its source or function.

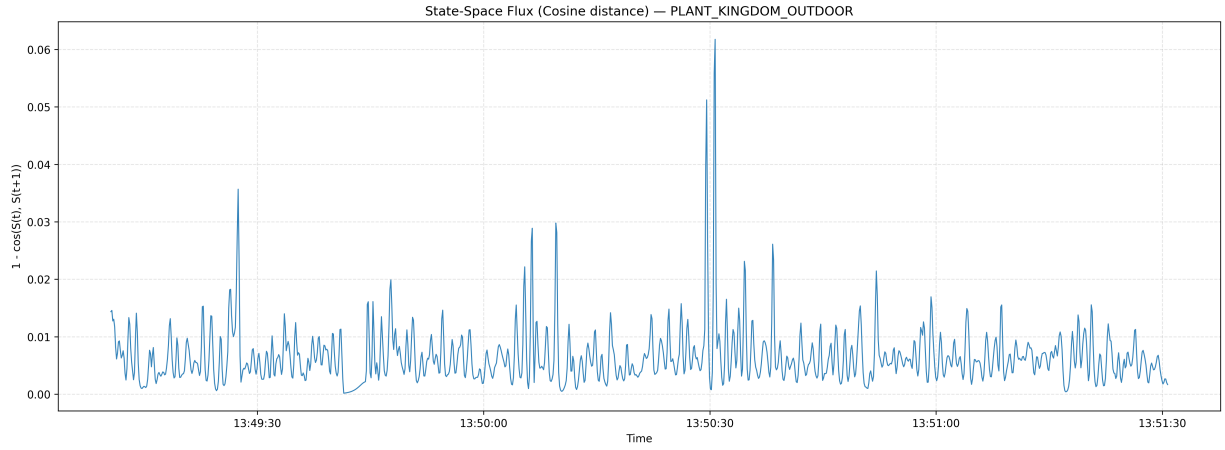

Figure 73: State-space flux (cosine distance) time series: Plant Kingdom outdoor session.

Bandwise Flux (L2) — PLANT KINGDOM OUTDOOR — Theta

This figure shows the time-resolved L2 state-space flux computed within the theta band for the Plant Kingdom outdoor session. At each time step, the metric represents the Euclidean distance between successive theta-band power vectors across all channels, isolating how much the theta component of the neural state reorganises over time.

For much of the session, theta-band flux remains low and relatively stable, indicating periods where the spatial distribution of theta power changes gradually from one moment to the next. Superimposed on this baseline are several pronounced bursts where theta flux rises sharply, reaching values substantially above the surrounding activity. These bursts are temporally sparse and clearly delineated, rather than forming a continuous elevated regime.

The most prominent peak occurs near the centre of the recording and coincides with the largest

theta-specific reorganisation observed in the session. This event stands out not only in magnitude but also in its abrupt onset and rapid decay, indicating a transient but substantial restructuring of theta-band activity across channels. Additional smaller bursts are distributed throughout the trace, suggesting repeated episodes of theta-driven reorganisation rather than a single isolated event.

Between these bursts, theta flux consistently returns to a low operating range, indicating that the system repeatedly settles back into relatively stable theta configurations. This pattern mirrors the intermittent structure seen in the global L2 flux time-series, but here reveals that a significant portion of those reorganisation events are driven by changes within the theta band itself.

This figure serves as a band-specific decomposition of the global reorganisation dynamics, showing that large-scale state transitions during the outdoor condition involve distinct, temporally localised restructuring of theta-band activity.

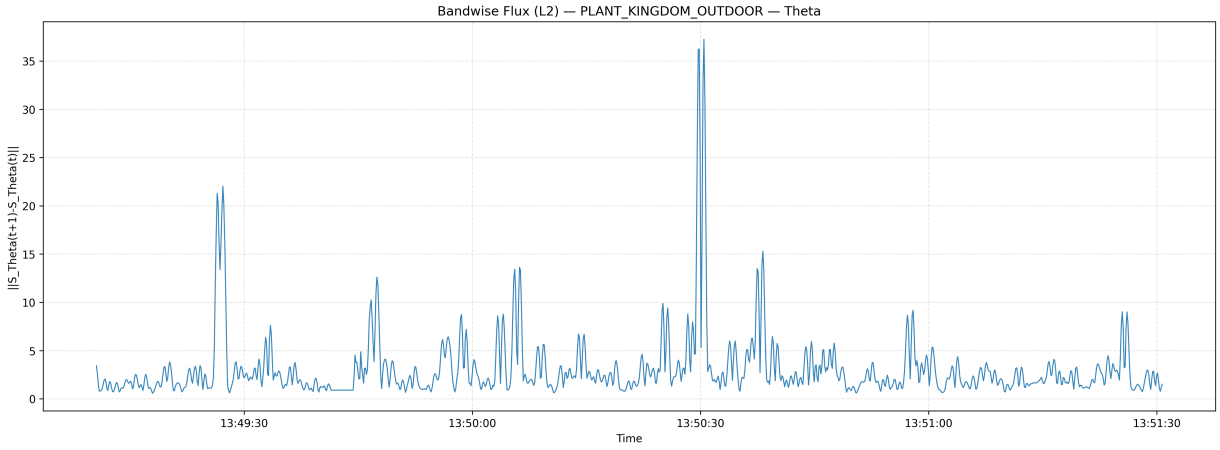

Figure 74: Bandwise state-space flux (ℓ_2): Plant Kingdom outdoor session (theta band).

Bandwise Flux (L2) — PLANT KINGDOM OUTDOOR — Alpha

This figure shows the time-resolved L2 state-space flux computed within the alpha band for the Plant Kingdom outdoor session. Each value represents the Euclidean distance between successive alpha-band power vectors across channels, isolating how the alpha-band spatial configuration reorganises over time.

Throughout much of the session, alpha-band flux remains within a low-to-moderate range, indicating relatively gradual changes in the distribution of alpha power across the scalp. Superimposed on this baseline are several prominent bursts in which alpha flux rises sharply, reaching magnitudes comparable to or exceeding those observed in the theta-band flux. These bursts are temporally localised and clearly separated from one another, rather than forming a sustained high-flux period.

Several of the largest alpha-specific peaks occur at times distinct from the dominant theta peaks, while others appear in closer temporal proximity. This pattern suggests that alpha-band reorganisation can occur independently or alongside theta-band changes, rather than simply mirroring theta dynamics. The alpha flux trace thus reflects its own contribution to overall state-space reorganisation, with distinct episodes of pronounced configurational change.

Between high-flux events, alpha activity consistently returns to a stable operating range, suggesting that alpha-band configurations are persistently re-established following transient reorganisation. The absence of prolonged elevation or drift indicates that alpha reconfiguration, like theta, is episodic rather than continuous.

This figure complements the theta-band flux plot by showing that reorganisation during the outdoor condition is not confined to a single low-frequency band. Instead, alpha-band dynamics contribute significantly and with structured timing to the overall state-space flux, highlighting the multi-band nature of the observed reorganisation events.

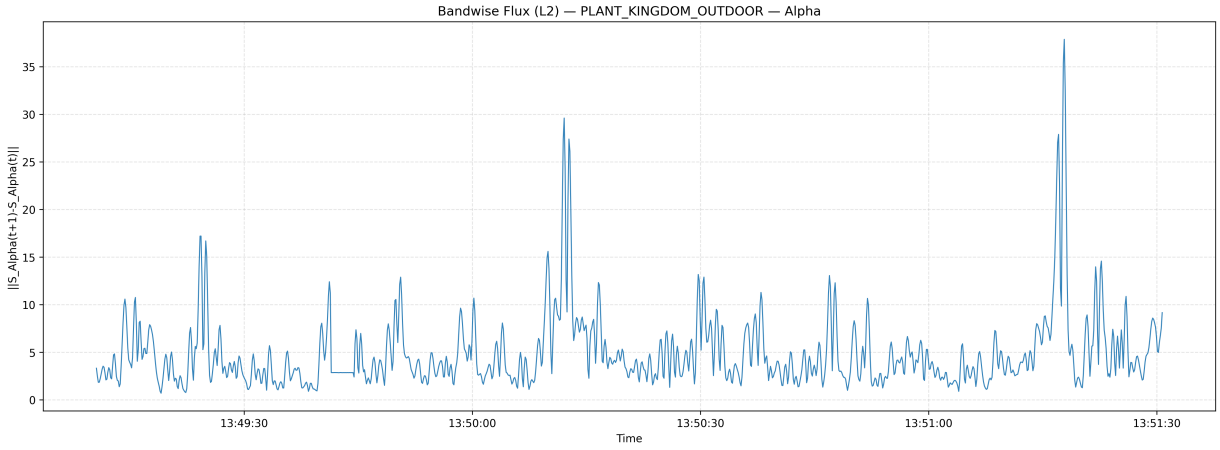

Figure 75: Bandwise state-space flux (ℓ_2): Plant Kingdom outdoor session (alpha band).

Bandwise Flux (L2) — PLANT KINGDOM INDOOR — Theta

This figure shows the time-resolved L2 state-space flux computed within the theta band for the Plant Kingdom indoor session. Each value represents the Euclidean distance between successive theta-band power vectors across channels, capturing how strongly the spatial distribution of theta activity reorganises from one moment to the next.

Throughout the session, theta-band flux remains within a relatively narrow operating range for extended periods, indicating sustained intervals of gradual, low-amplitude reorganisation. Superimposed on this baseline are a series of discrete peaks where theta flux increases sharply. These events are intermittent and temporally localised, rather than forming a sustained high-flux regime.

The largest theta-specific peaks are fewer and lower in magnitude compared to those observed in the outdoor condition, but they are still clearly distinguishable from the surrounding activity. Their abrupt onset and rapid decay suggest transient episodes of coordinated theta reconfiguration rather than slow drift or progressive instability. Between these events, theta flux consistently returns to low values, indicating the repeated re-establishment of stable theta configurations.

Overall, this trace reflects a dynamic in which theta-band organisation is largely stable indoors, punctuated by occasional, well-defined reorganisation events. The temporal pattern suggests that theta contributes to reorganisation in the indoor condition primarily through discrete transitions rather than continuous variability.

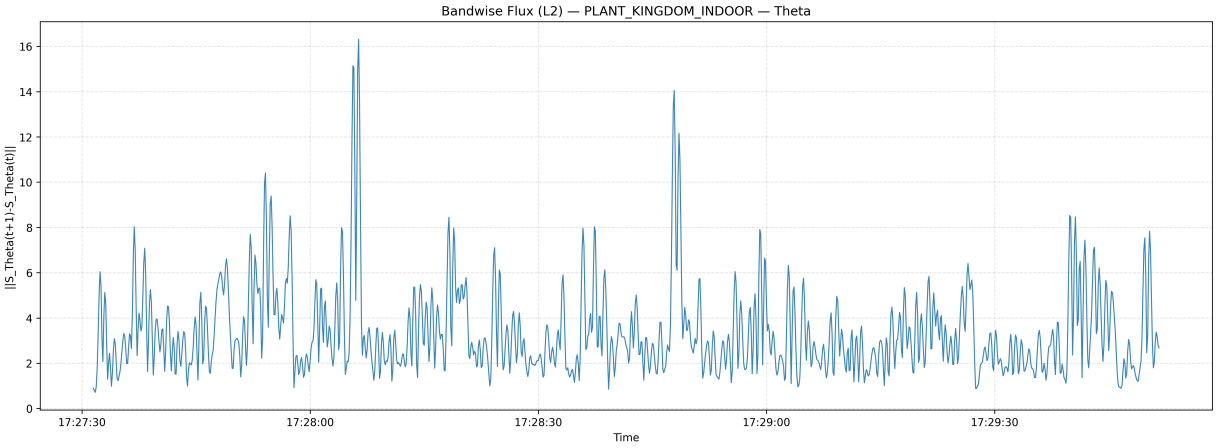

Figure 76: Bandwise state-space flux (ℓ_2): Plant Kingdom indoor session (theta band).

Bandwise Flux (L2) — PLANT KINGDOM INDOOR — Alpha

This figure shows the L2 state-space flux computed within the alpha band for the Plant Kingdom indoor session. The trace represents frame-to-frame changes in the spatial distribution of alpha-band power across channels, isolating alpha-specific contributions to overall state reorganisation.

Alpha-band flux exhibits greater overall variability than theta in this condition, with a higher baseline level and more frequent excursions from low values. Throughout the session, the trace alternates between moderate-amplitude fluctuations and pronounced peaks, indicating that alpha-band configurations reorganise more actively, even outside the largest events.

Several high-amplitude alpha-specific bursts are clearly visible, standing out from the surrounding activity. These peaks are transient but substantial, indicating moments of strong alpha-band reconfiguration across the scalp. Between these bursts, alpha flux remains elevated relative to theta, suggesting that alpha continuously contributes to ongoing reorganisation, not just during isolated transitions.

Despite this increased activity, the alpha flux trace does not display sustained runaway behaviour or long-term drift. After large peaks, values reliably return to a mid-range level, indicating bounded dynamics and the repeated re-stabilisation of alpha-band structure.

This figure illustrates that, within the indoor condition, alpha-band dynamics play a prominent role in shaping state-space reorganisation, contributing through frequent moderate adjustments as well as occasional high-magnitude reconfiguration events.

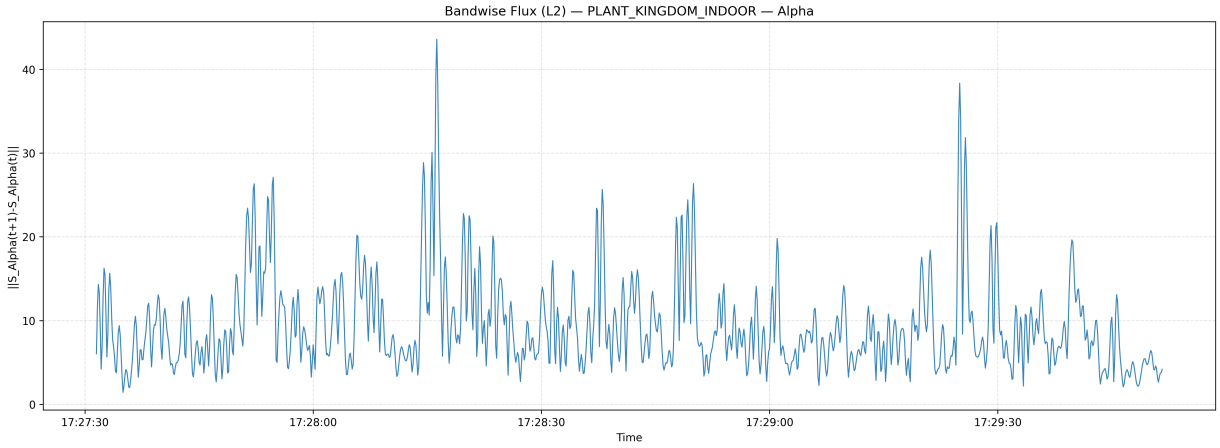

Figure 77: Bandwise state-space flux (ℓ_2): Plant Kingdom indoor session (alpha band).

Entropy × Regionalised Flux (Cosine) — BASELINE EC

This scatter plot shows the relationship between instantaneous signal entropy and regionalised state-space flux, where flux is quantified using cosine distance between successive regional state vectors. Each point corresponds to a single time step, with entropy on the x-axis and flux on the y-axis.

The distribution is strongly right-skewed in flux, with most points clustered at low flux values and a sparse set extending into higher-flux events. This indicates that during baseline eyes-closed conditions, the system spends most of its time undergoing small, incremental changes in state-space orientation, punctuated by occasional larger reorientations. These larger excursions are discrete events, not continuous.

Entropy values span a relatively narrow range, and there is no simple linear relationship between entropy and flux. Instead, higher-flux points are distributed across much of the entropy range, suggesting that in baseline conditions, large directional changes in regional state configuration can occur without requiring a large change in overall signal diversity.

Visually, the plot reveals a regime structure: a dense low-flux "background" with a sparse high-flux tail. This makes the figure useful for characterising burst-like reorganisation events in an otherwise stable regime. This plot is a strong candidate for later inclusion, as it clearly demonstrates non-Gaussian flux behaviour and the separation between typical and extreme state transitions.

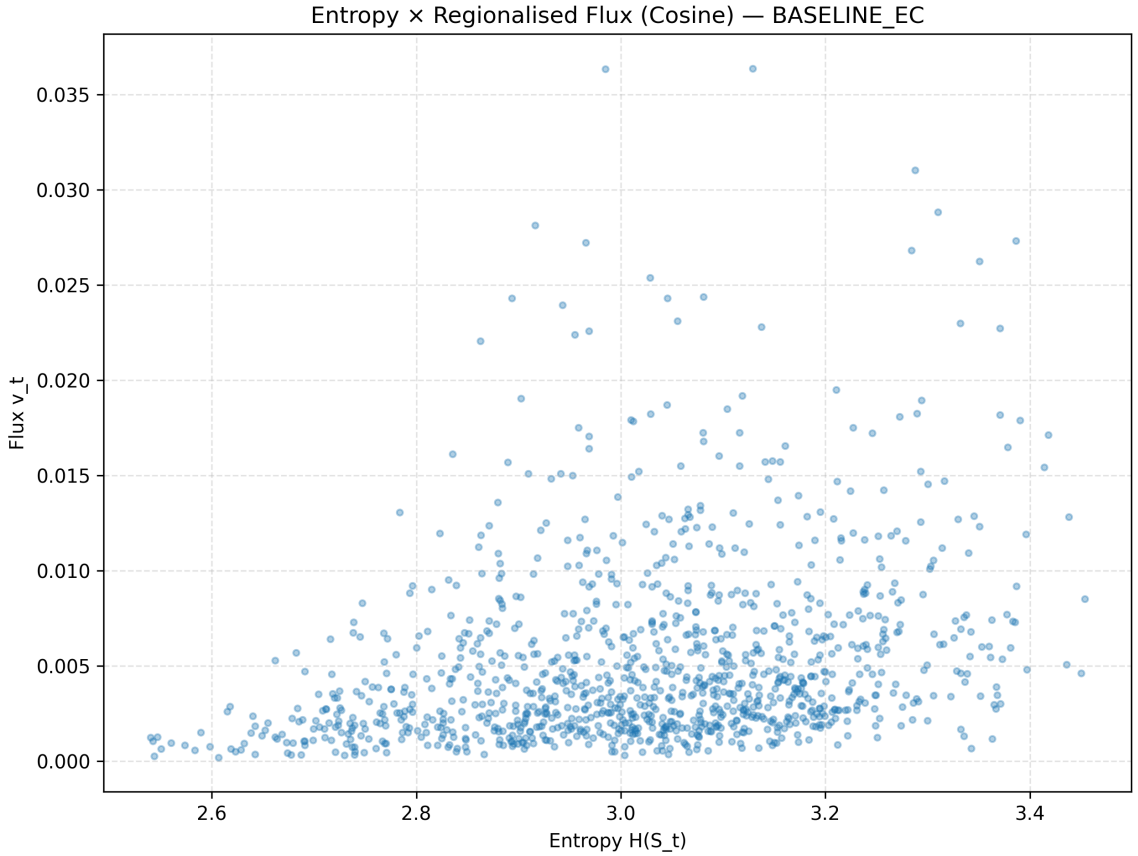

Figure 78: Baseline eyes-closed (EC): entropy vs regionalised flux (cosine distance).

Entropy × Regionalised Flux (L2) — BASELINE EC

This scatter plot shows the same entropy–flux relationship as the previous figure, but here flux is quantified using the L2 (Euclidean) norm of changes in regional state vectors rather than cosine distance. As before, each point represents a single time step.

Compared to the cosine-based plot, the flux axis spans a much wider numerical range, reflecting sensitivity to absolute magnitude changes rather than purely directional shifts. The point cloud is broader and more vertically dispersed, with many moderate-to-high flux values appearing across the entropy range.

A notable pattern in this figure is the downward trend in the upper envelope of flux as entropy increases. Higher entropy values tend to be associated with lower L2 flux, whereas the largest L2 flux events are more common at lower to mid-entropy levels. This implies that when the signal is already highly diverse, state transitions tend to be more incremental in magnitude, whereas larger absolute shifts occur when entropy is more constrained.

Unlike the cosine version, the L2 plot emphasises amplitude-driven reorganisation, capturing how much the regional configuration changes rather than how sharply it reorients. The absence of a tight clustering around a single trajectory further suggests that a simple monotonic relationship does not apply, pointing instead to multiple operating regimes within baseline activity.

This figure provides a complementary view to the cosine plot, distinguishing between directional reconfiguration and magnitude-based restructuring. Whether this plot is included later will likely depend on whether both metrics are necessary to explicitly make that distinction.

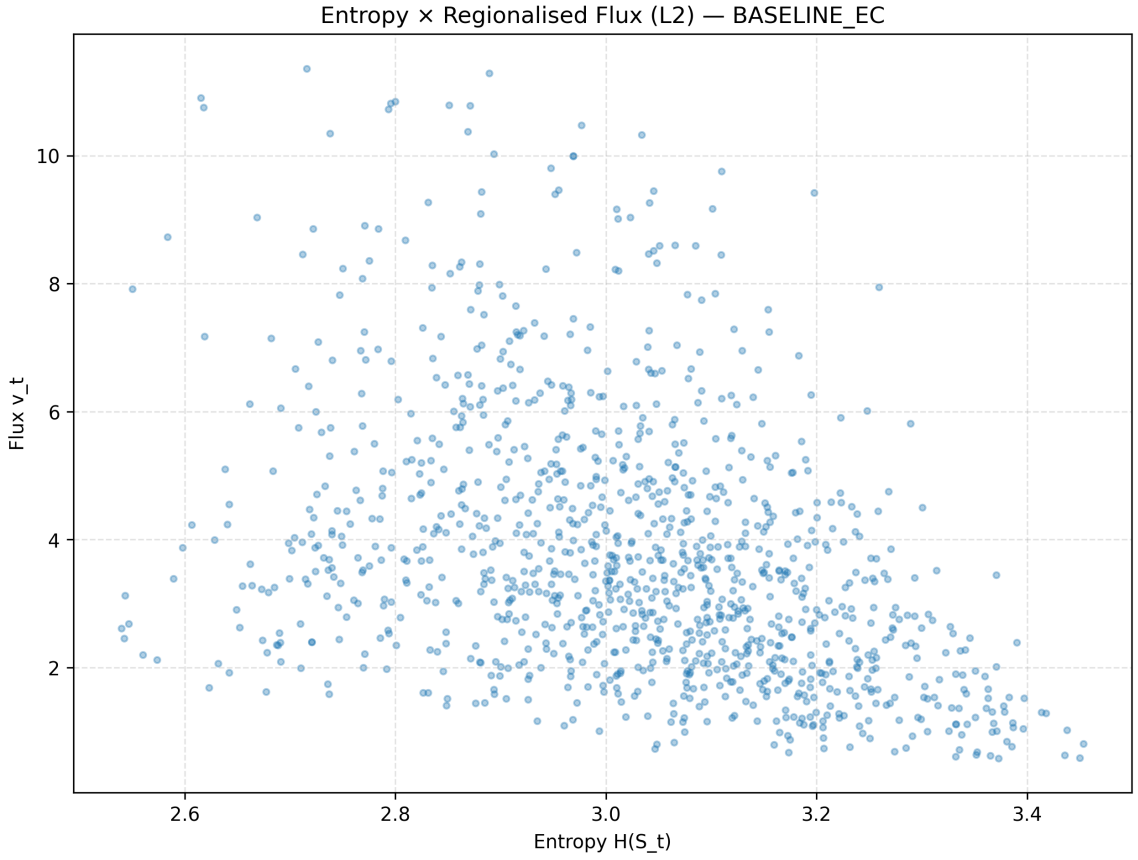

Figure 79: Baseline eyes-closed (EC): entropy vs regionalised flux (ℓ_2).

Entropy × Regionalised Flux (Cosine) — PLANT KINGDOM INDOOR

This scatter plot shows the relationship between regionalised state entropy at time t and the directional change of that state between consecutive time points, measured using cosine distance. Each point corresponds to a single time step, where the horizontal position reflects the entropy of the regional state vector and the vertical position reflects how much the orientation of that vector changes from one moment to the next.

The distribution is strongly concentrated in a narrow band of entropy values, primarily between approximately 3.0 and 3.2. Within this entropy range, most points cluster at relatively low cosine flux values, indicating that when the system occupies these entropy levels, the direction of the regional state tends to change only modestly from one step to the next. This suggests that these entropy values correspond to relatively stable configurations in state-space, where regional relationships are preserved over time.

At the same time, the plot shows a vertical spread within this dominant entropy band. Occasional points rise to higher cosine flux values, indicating brief moments where the direction of the state vector shifts more substantially, even though overall entropy remains similar. These events appear as upward excursions rather than forming a separate cluster, implying transient reorientations rather than sustained alternative regimes.

At lower entropy values, the point density decreases noticeably. These lower-entropy states show more variability in cosine flux but occur less frequently overall. The absence of a strong monotonic relationship between entropy and cosine flux indicates that higher entropy does not necessarily imply greater directional instability. Instead, entropy and directional change appear partially decoupled: the system can maintain similar entropy levels while undergoing either small or occasionally larger directional transitions.

This figure is useful for illustrating how state orientation stability varies across entropy levels during the indoor Plant Kingdom session and may be a candidate for inclusion if the goal is to show regime structure without relying on amplitude-based measures.

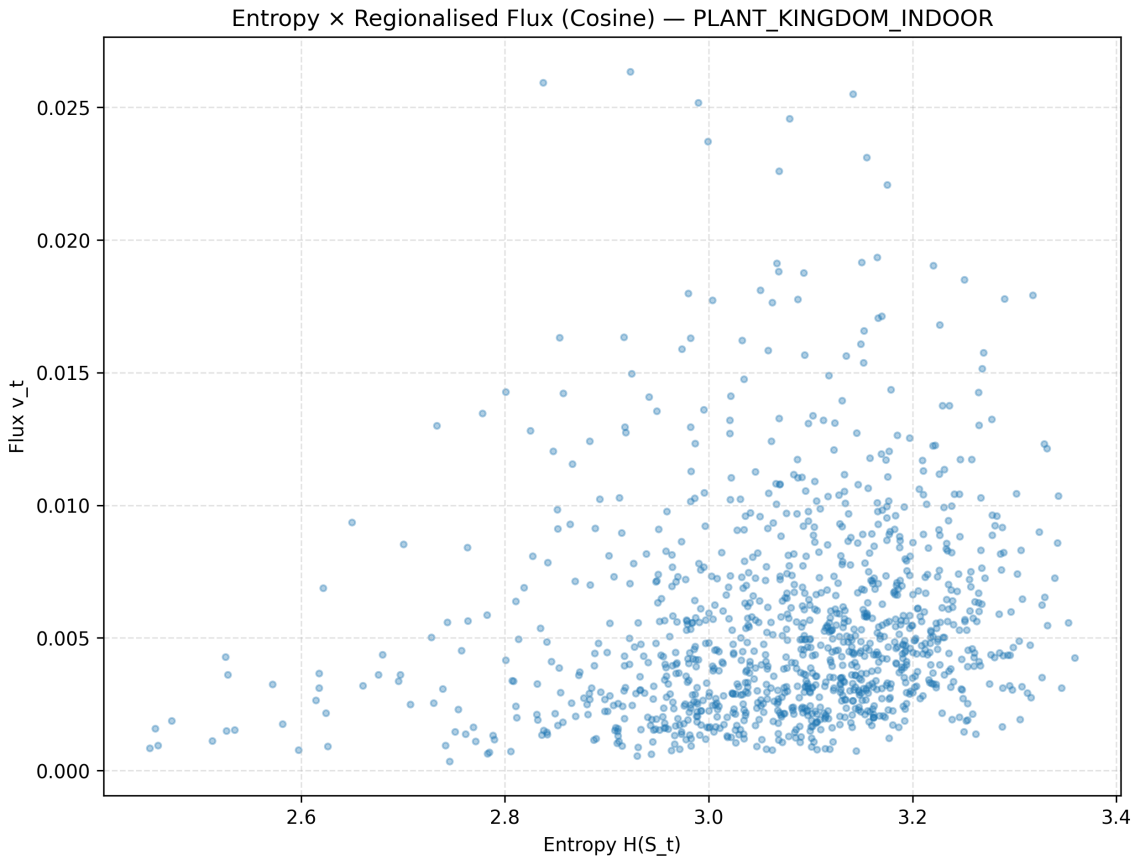

Figure 80: Plant Kingdom indoor: entropy vs regionalised flux (cosine distance).

Entropy × Regionalised Flux (L2) — PLANT KINGDOM INDOOR

This scatter plot shows the relationship between regionalised state entropy and magnitude-based state change, measured as the ℓ_2 norm of the difference between successive regional state vectors. Unlike the cosine version, this plot reflects how much the size of the state change varies, regardless of direction.

The point cloud again shows a dense concentration at entropy values between roughly 3.0 and 3.2, but the vertical structure differs markedly from the cosine case. Within this dominant entropy range, ℓ_2 flux spans a wide range of values, from relatively small changes to very large excursions. This indicates that even when entropy remains within a narrow band, the magnitude of reorganisation across regions can vary substantially.

A clear wedge-like structure is visible: higher ℓ_2 flux values are more prevalent at lower-to-mid entropy values, while higher entropy states tend to cluster at lower ℓ_2 flux. This suggests that large-magnitude state transitions are more likely when the system is in relatively more ordered (lower entropy) configurations, whereas higher-entropy states tend to evolve through smaller incremental changes.

The presence of several high-flux outliers at moderate entropy values indicates episodic, large-scale reorganisation events rather than continuous instability. These points do not form a separate cluster, reinforcing the interpretation that they represent transient departures from otherwise stable trajectories rather than a distinct regime.

Compared to the cosine plot, this figure makes clear that the magnitude and direction of state change behave differently. The system can undergo large ℓ_2 changes without correspondingly large directional shifts, and vice versa. This plot is particularly valuable for demonstrating how entropy constrains the scale of reorganisation rather than its orientation, and is likely a strong candidate for inclusion if illustrating state-space flux dynamics in a concrete, quantitative way.

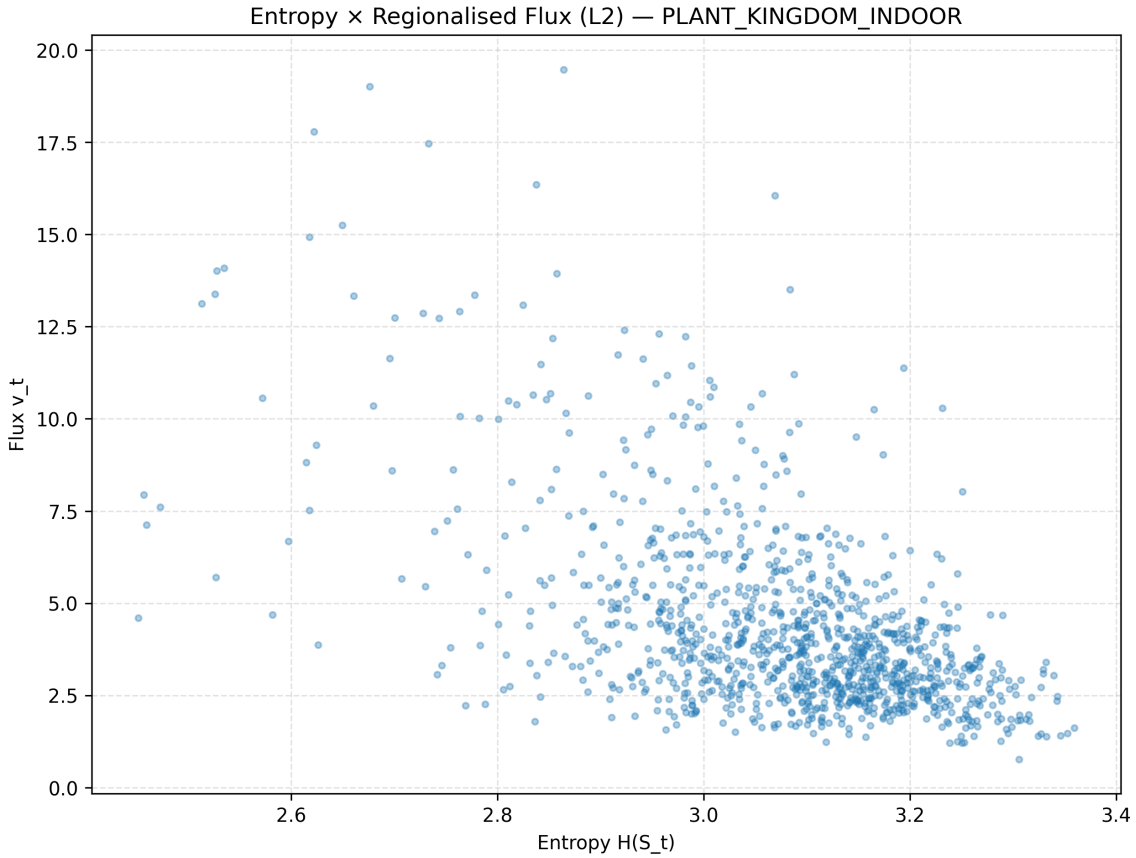

Figure 81: Plant Kingdom indoor: entropy vs regionalised flux (ℓ_2).

Entropy × Regionalised Flux (Cosine) — PLANT KINGDOM OUTDOOR

This scatter plot shows the relationship between regionalised state entropy at time t and the cosine-based state-space flux between consecutive time points during the outdoor Plant Kingdom session. Each point corresponds to a single time step, with entropy on the horizontal axis and cosine flux on the vertical axis, where higher values indicate a larger directional change in the regional state configuration from one moment to the next.

The distribution is dominated by a dense cluster at higher entropy values, concentrated roughly between 3.2 and 3.45 on the entropy axis. Within this region, most flux values remain relatively low, forming a tight band close to the lower portion of the y-axis. This indicates that even when the regional state is highly distributed and information-rich, transitions between successive states are typically directionally conservative, with only small angular deviations in state space.

A smaller number of points extend upward into higher cosine flux values, forming a sparse tail above the main cluster. These events represent moments where relatively large directional reconfigurations occur despite entropy remaining high. The absence of a strong monotonic trend suggests that higher entropy does not systematically require higher directional flux; instead, the system appears capable of maintaining stable trajectories within a high-entropy regime, punctuated by occasional reorientation events.

The overall shape of the distribution suggests a regime where outdoor conditions support sustained high entropy with comparatively smooth directional evolution, rather than frequent abrupt state reconfigurations. This figure may later be a candidate for inclusion if illustrating directional stability within high-entropy environmental states becomes important.

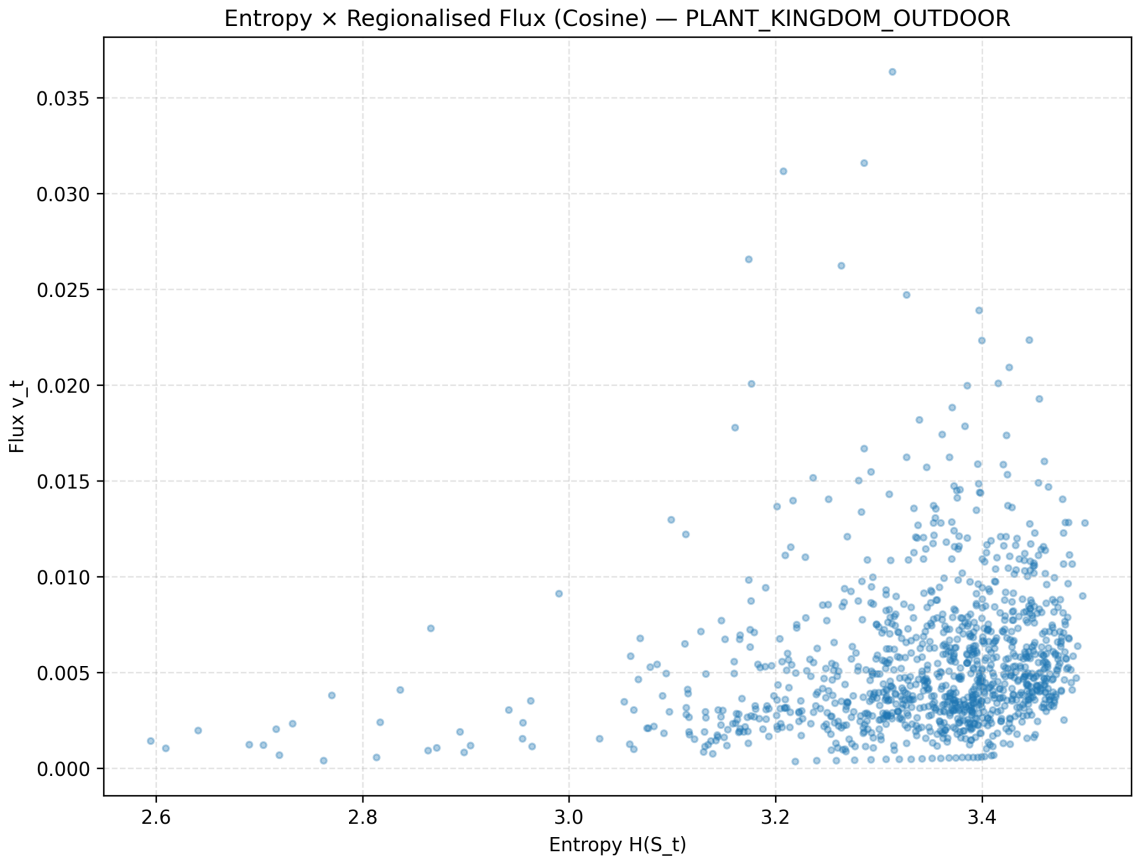

Figure 82: Plant Kingdom outdoor: entropy vs regionalised flux (cosine distance).

Entropy × Regionalised Flux (L2) — PLANT KINGDOM OUTDOOR

This plot presents the same entropy values on the horizontal axis, but replaces cosine flux with the ℓ_2-norm of the difference between successive regional state vectors. Here, flux magnitude reflects the absolute size of the state-space displacement rather than its directional change, providing a complementary view of temporal reorganisation.

As in the cosine-based plot, the data are dominated by a dense cluster at higher entropy values, again primarily between approximately 3.2 and 3.45. Within this cluster, L2 flux values are relatively low and tightly grouped, indicating that most transitions involve modest absolute changes in regional activity patterns even when entropy is high.

Notably, the L2 representation reveals a clearer vertical spread than the cosine version, with a more visible tail extending to higher flux magnitudes. These higher-magnitude points are sparse but present across a range of entropy values, including within the high-entropy cluster. This indicates that while directional changes may remain small, some transitions involve substantial amplitude redistribution across regions.

The distribution does not show a simple linear relationship between entropy and L2 flux. Instead, high entropy supports both low- and moderate-magnitude transitions, with larger flux events occurring intermittently rather than continuously. This pattern suggests that outdoor conditions allow the system to occupy a high-entropy state space while occasionally undergoing sizeable reorganisations in regional activation strength.

This figure may later be useful for illustrating how absolute reorganisation magnitude behaves independently of entropy during naturalistic outdoor engagement, particularly when contrasted with cosine-based measures that emphasise directional continuity.

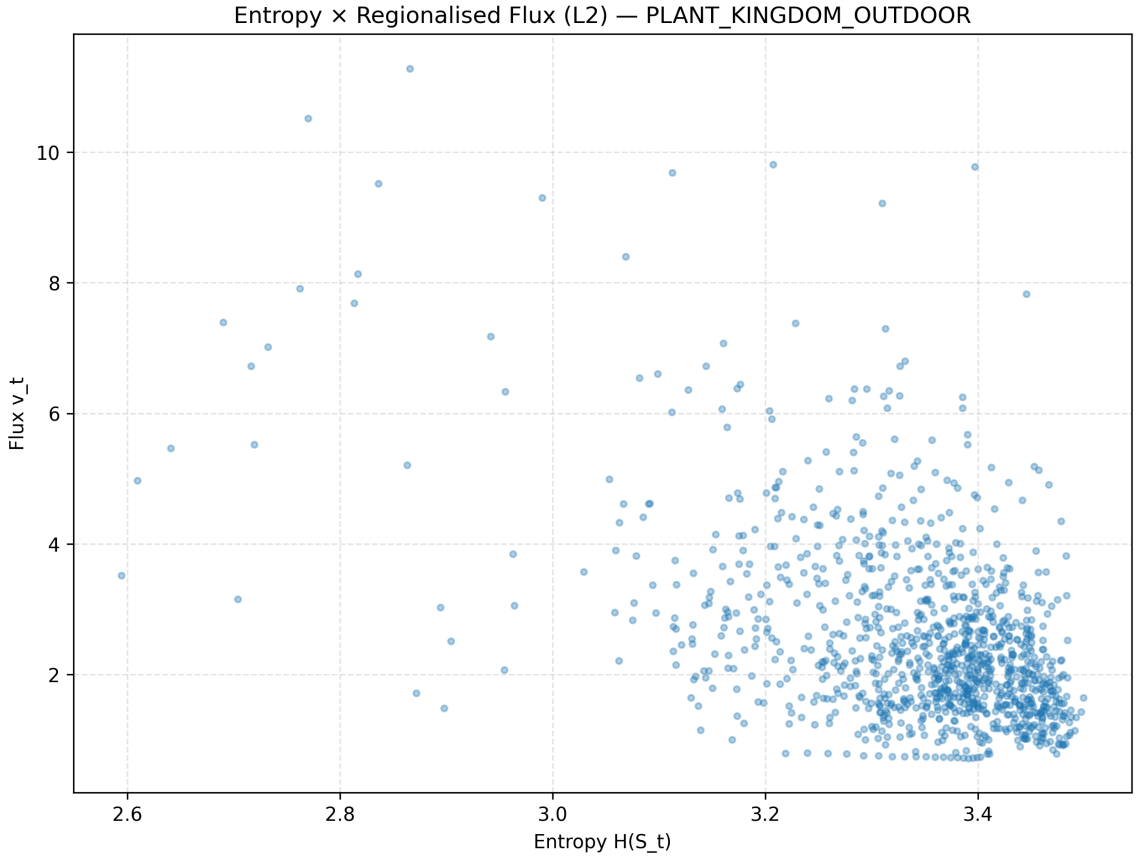

Figure 83: Plant Kingdom outdoor: entropy vs regionalised flux (ℓ_2).

Entropy × Flux (Cosine) — BASELINE EC (scatter)

This scatter plot shows the relationship between instantaneous signal entropy and cosine-based flux during the baseline eyes-closed condition. The dominant structure is a dense, low-flux band concentrated at moderate-to-high entropy values (roughly mid-4s), indicating that most baseline states combine relatively high signal diversity with very small directional changes between successive states. As entropy increases within this dominant band, flux remains tightly constrained near zero, suggesting that higher entropy at baseline does not imply greater moment-to-moment reconfiguration, but rather stable, richly structured activity. A small number of isolated points appear at much higher flux values across a wider entropy range; these are sparse and discontinuous, indicating transient departures rather than a secondary regime.

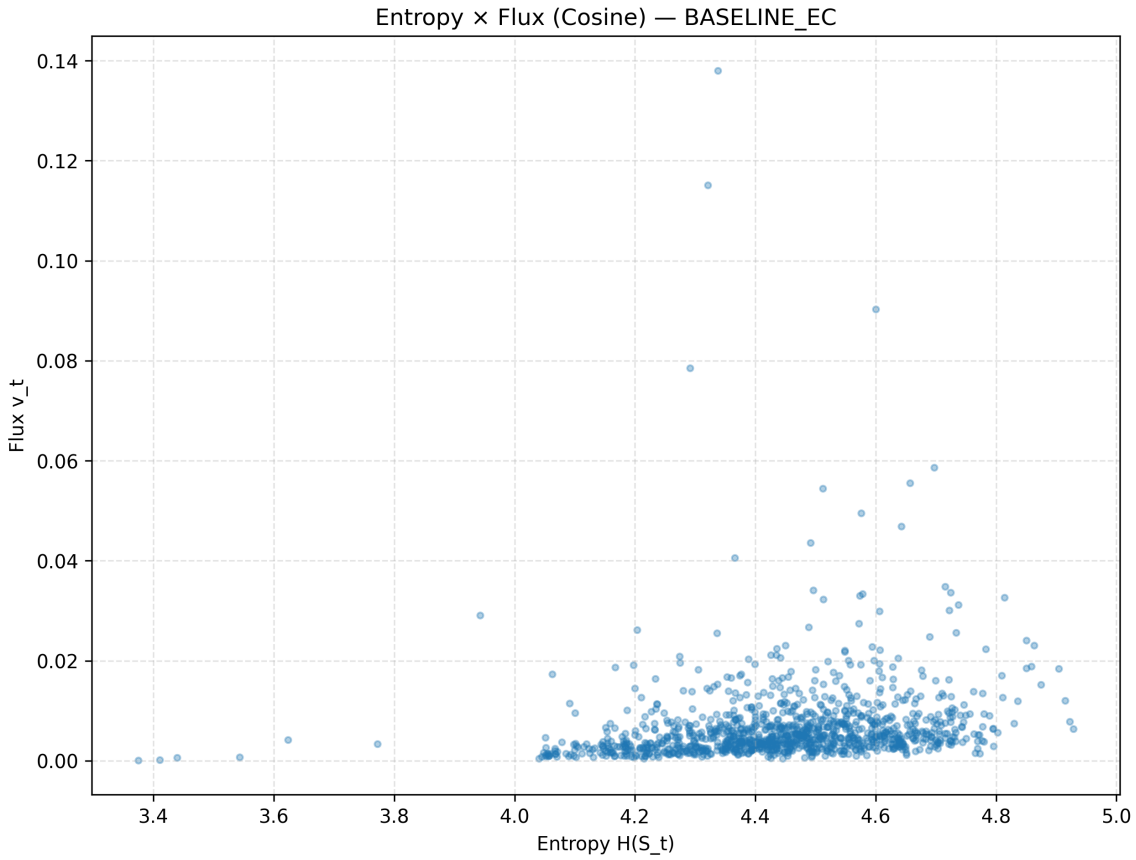

Figure 84: Baseline eyes-closed (EC): entropy vs flux (cosine distance), scatter.

Entropy × Flux (Cosine) — BASELINE EC (hexbin)

The hexbin representation of the same data clarifies the density structure obscured by overplotting in the scatter plot. The highest-density region forms a compact ridge centered at moderate-to-high entropy with near-zero flux, confirming that this state dominates the baseline distribution. Density drops off sharply away from this ridge, and the high-flux points visible in the scatter plot correspond to isolated, low-count bins rather than coherent clusters. This reinforces the interpretation that baseline eyes-closed activity is characterized by entropy-rich but directionally stable dynamics, with flux excursions being rare and weakly structured.

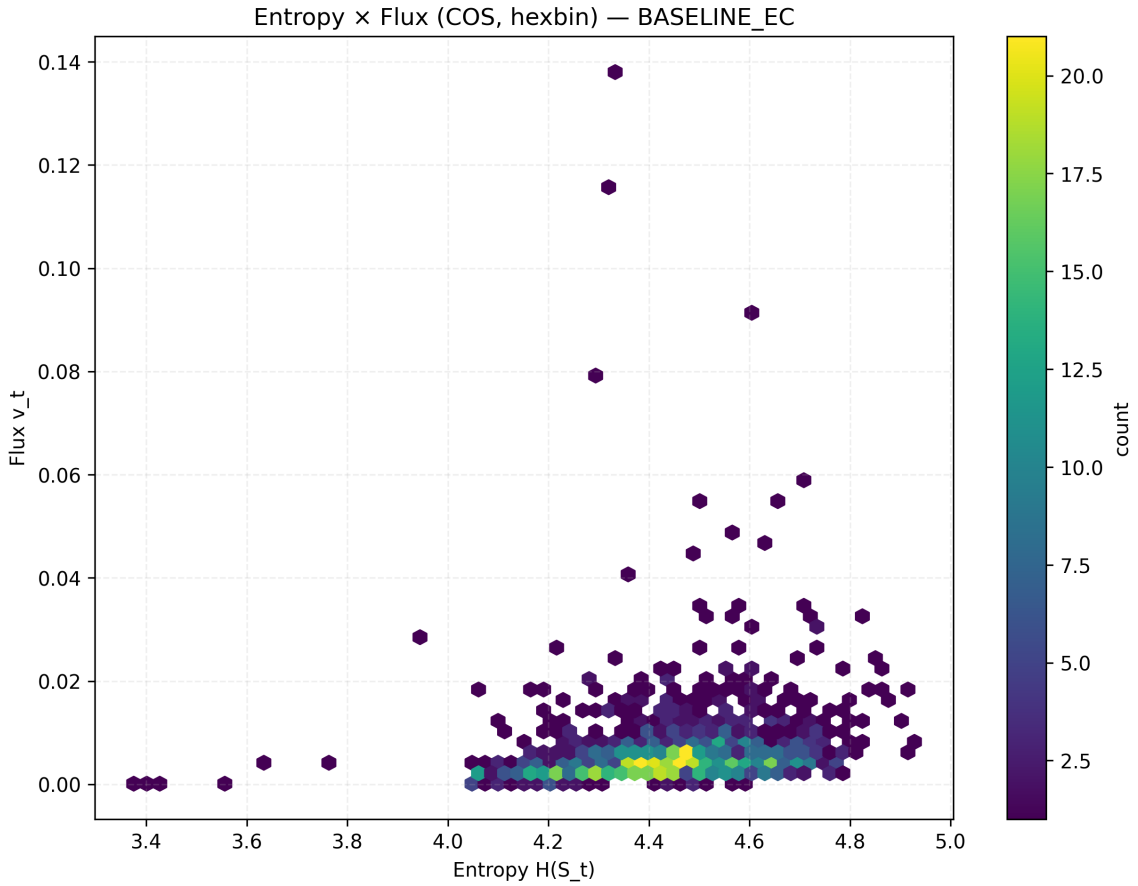

Figure 85: Baseline eyes-closed (EC): entropy vs flux (cosine distance), hexbin.

Entropy × Flux (L2) — BASELINE EC (scatter)

Using the L2 metric, the same entropy values are associated with a much broader numerical flux range, but the underlying structure remains similar. The majority of observations again form a dense cloud at moderate-to-high entropy with comparatively low L2 flux values, indicating small overall magnitude changes between successive regional states. As entropy increases, there is a visible tendency for L2 flux to remain constrained or even decrease slightly, rather than spreading upward. A few extreme outliers appear at very large L2 flux values, scattered across lower and mid entropy, suggesting occasional large-magnitude transitions that are not entropy-dependent and do not form a stable pattern.

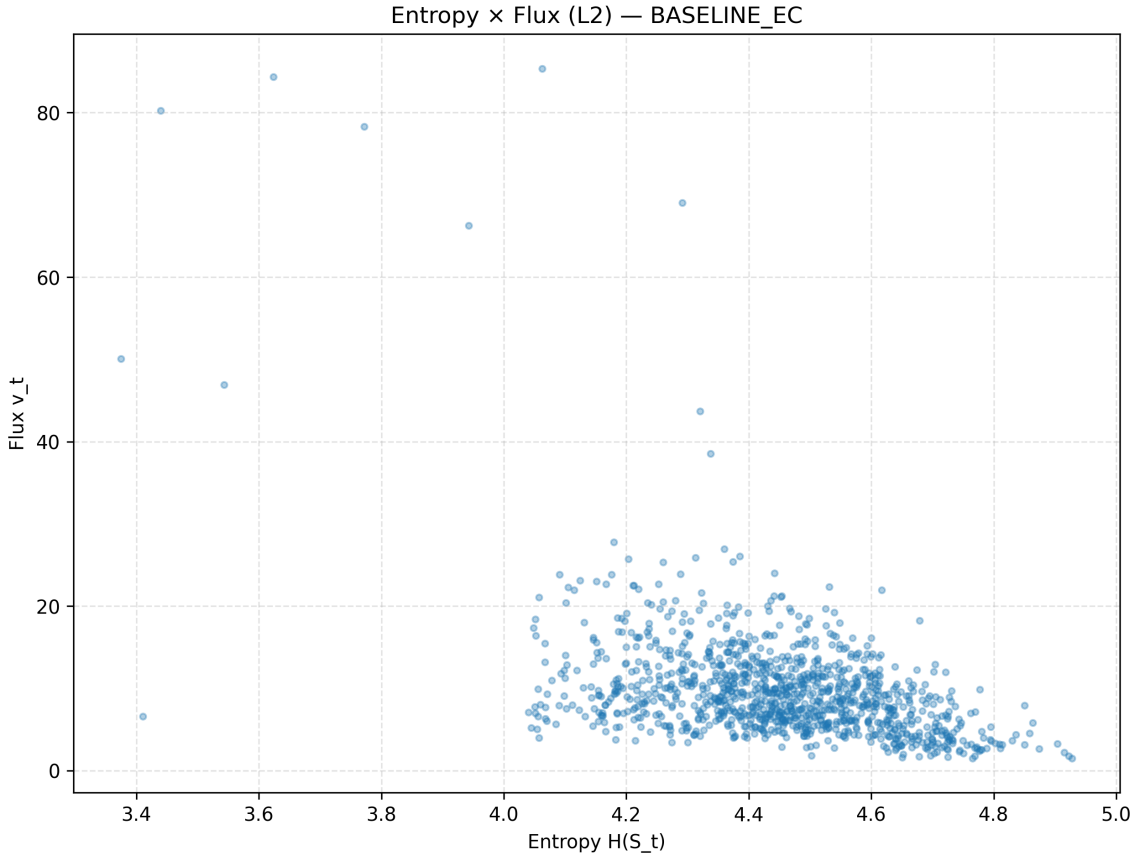

Figure 86: Baseline eyes-closed (EC): entropy vs flux (ℓ_2), scatter.

Entropy × Flux (L2) — BASELINE EC (hexbin)

The L2 hexbin plot makes the dominant baseline regime explicit. The highest-count bins occupy a compact region at moderate-to-high entropy and low-to-moderate flux, forming a slanted density core rather than a vertical spread. This indicates that even when flux is measured as absolute magnitude rather than directional similarity, baseline activity remains tightly organised around low transition energy. The extreme L2 values observed in the scatter plot fall into isolated, low-count bins and do not contribute meaningfully to the distribution's structure.

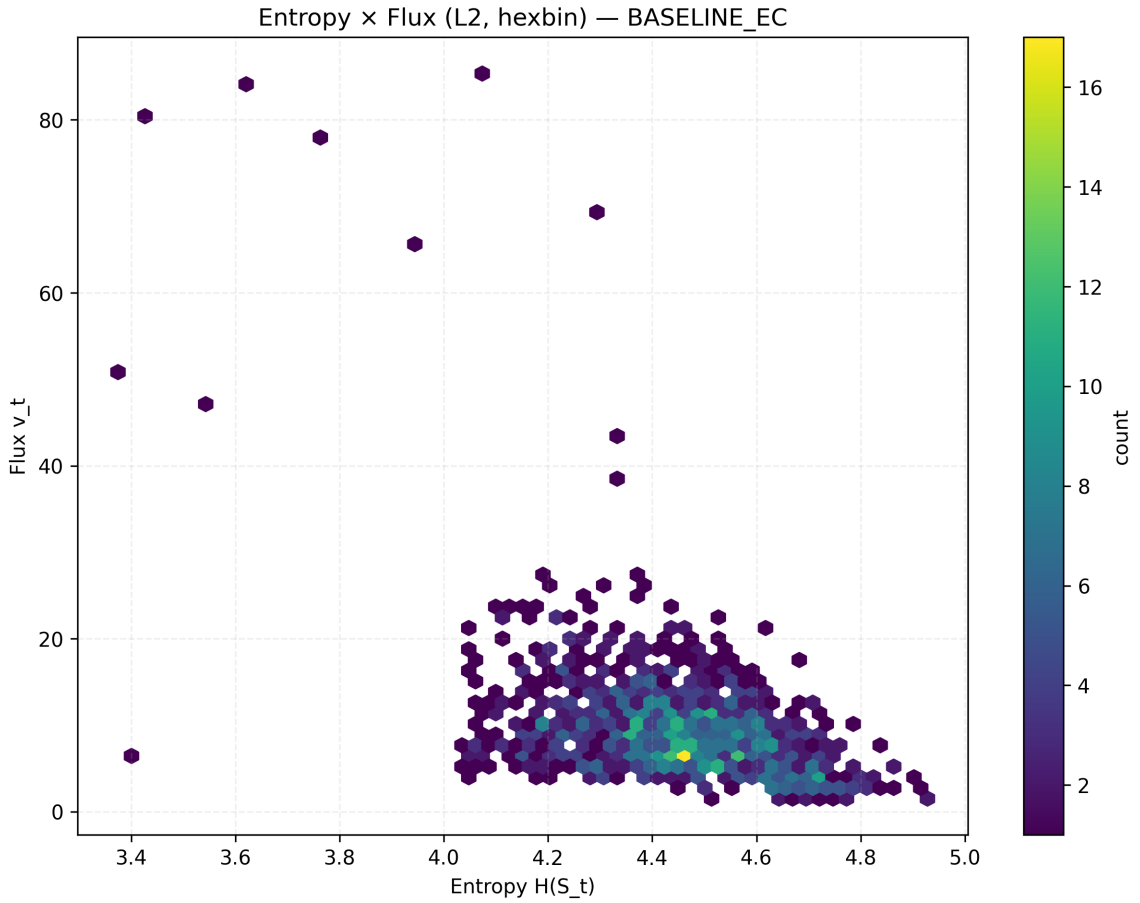

Figure 87: Baseline eyes-closed (EC): entropy vs flux (ℓ_2), hexbin.

Entropy × Flux (Cosine) — PLANT KINGDOM INDOOR

This scatter plot shows the relationship between instantaneous entropy $H(S_t)$ and cosine-based flux for the indoor Plant Kingdom session. The point cloud is concentrated in a diagonal band spanning approximately entropy 4.3–4.7, with flux values mostly below 0.01. Within this dominant region, flux increases gradually with entropy, forming a weak but consistent positive association. At lower entropy values (< 4.2), points become sparse, and flux magnitudes drop markedly, indicating reduced reorganisation activity in lower-entropy states. A small number of higher-flux outliers extend upward beyond the main cloud, suggesting brief reorganisation bursts that are not sustained across entropy levels. Overall, the distribution indicates that most indoor activity occupies a narrow, stable entropy-flux regime with occasional transient excursions.

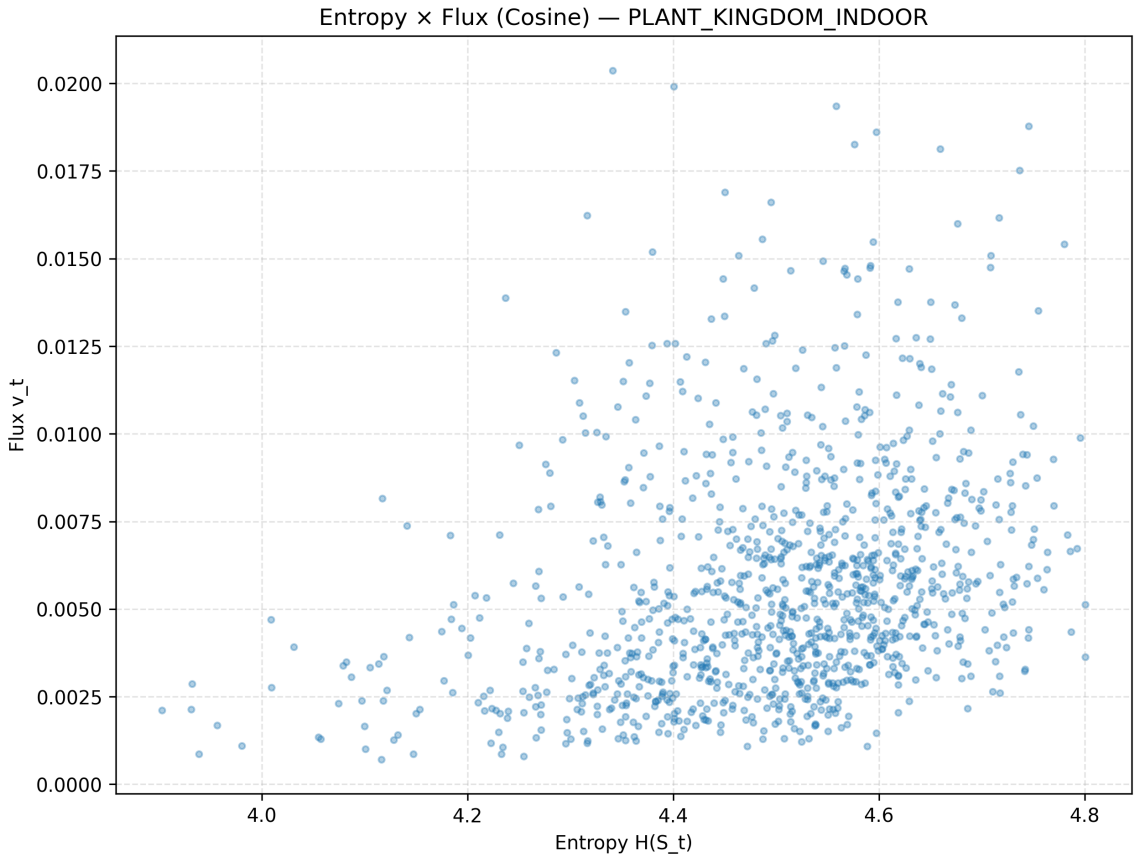

Figure 88: Plant Kingdom indoor: entropy vs flux (cosine distance), scatter.

Entropy × Flux (Cosine, hexbin) — PLANT KINGDOM INDOOR

The hexbin representation of cosine flux highlights the density structure underlying the scatter plot. The highest-density bins form a compact core centred around entropy values of roughly 4.4–4.6 and flux values around 0.003–0.006. This core indicates that the majority of samples repeatedly occupy a specific entropy–flux operating region rather than being broadly distributed. Density falls off rapidly above this core, and higher-flux bins appear sparsely populated, reinforcing that large cosine-flux events are rare. The hexbin view clarifies that the apparent spread in the scatter plot is driven more by low-density tails than by multiple dense regimes. This suggests a dominant indoor organisational state with limited variability in cosine-based reorientation.

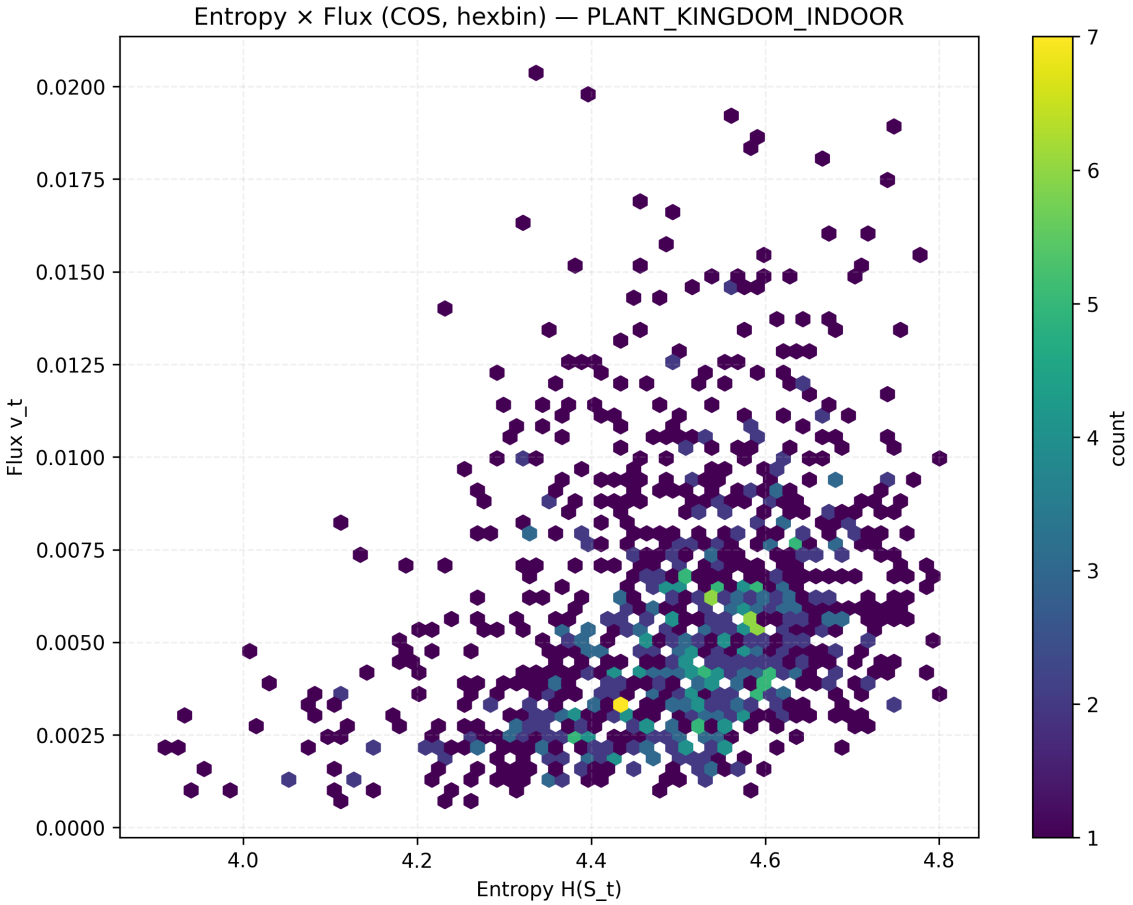

Figure 89: Plant Kingdom indoor: entropy vs flux (cosine distance), hexbin.

Entropy × Flux (L2) — PLANT KINGDOM INDOOR

In the L2-based flux scatter plot, the structure differs markedly in scale while preserving a similar entropy range. Most points cluster between entropy values of 4.4–4.7, with flux values concentrated roughly between 5 and 15. Unlike the cosine metric, the L2 flux shows a broader vertical spread, with numerous moderate-to-high flux values coexisting at similar entropy levels. There is a visible downward trend at the upper entropy end, where higher entropy corresponds to slightly reduced L2 flux, suggesting increased stability at peak entropy. Several high-flux outliers extend above 30, indicating episodic large-magnitude reorganisations that are not mirrored in the cosine representation. This pattern implies that magnitude-based reorganisation varies substantially even when directional alignment remains relatively stable.

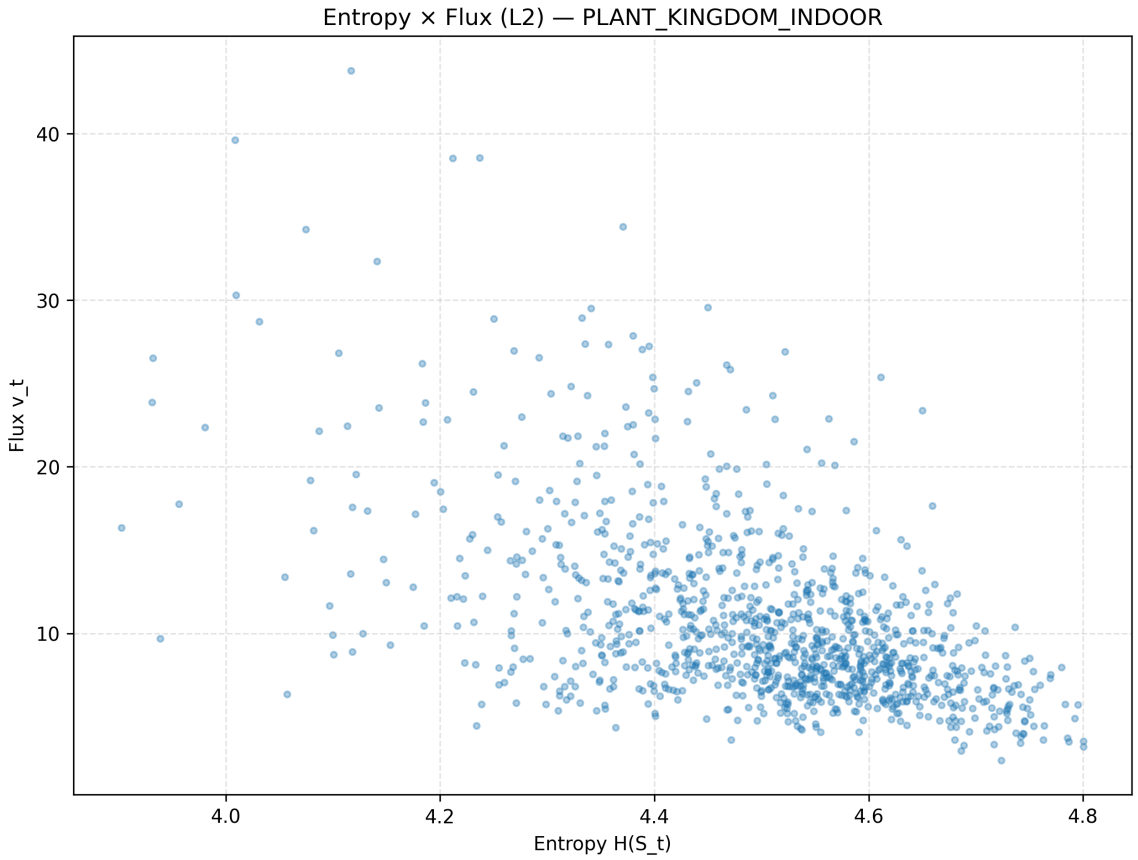

Figure 90: Plant Kingdom indoor: entropy vs flux (ℓ_2), scatter.

Entropy × Flux (L2, hexbin) — PLANT KINGDOM INDOOR

The hexbin plot for L2 flux reveals a dense ridge spanning entropy values of approximately 4.4–4.6 and flux values around 6–10. This ridge represents the dominant operating regime for indoor L2-based reorganisation. Above this ridge, bins thin out rapidly, showing that high-magnitude flux events are infrequent and dispersed rather than forming a secondary stable regime. The density gradient slopes downward with increasing entropy, reinforcing the impression that higher entropy states correspond to more constrained, lower-variance reorganisation magnitudes. Compared to the cosine hexbin, this plot exhibits a wider vertical density structure, indicating that L2 flux captures variability in reorganisation strength that is largely invisible to directional metrics.

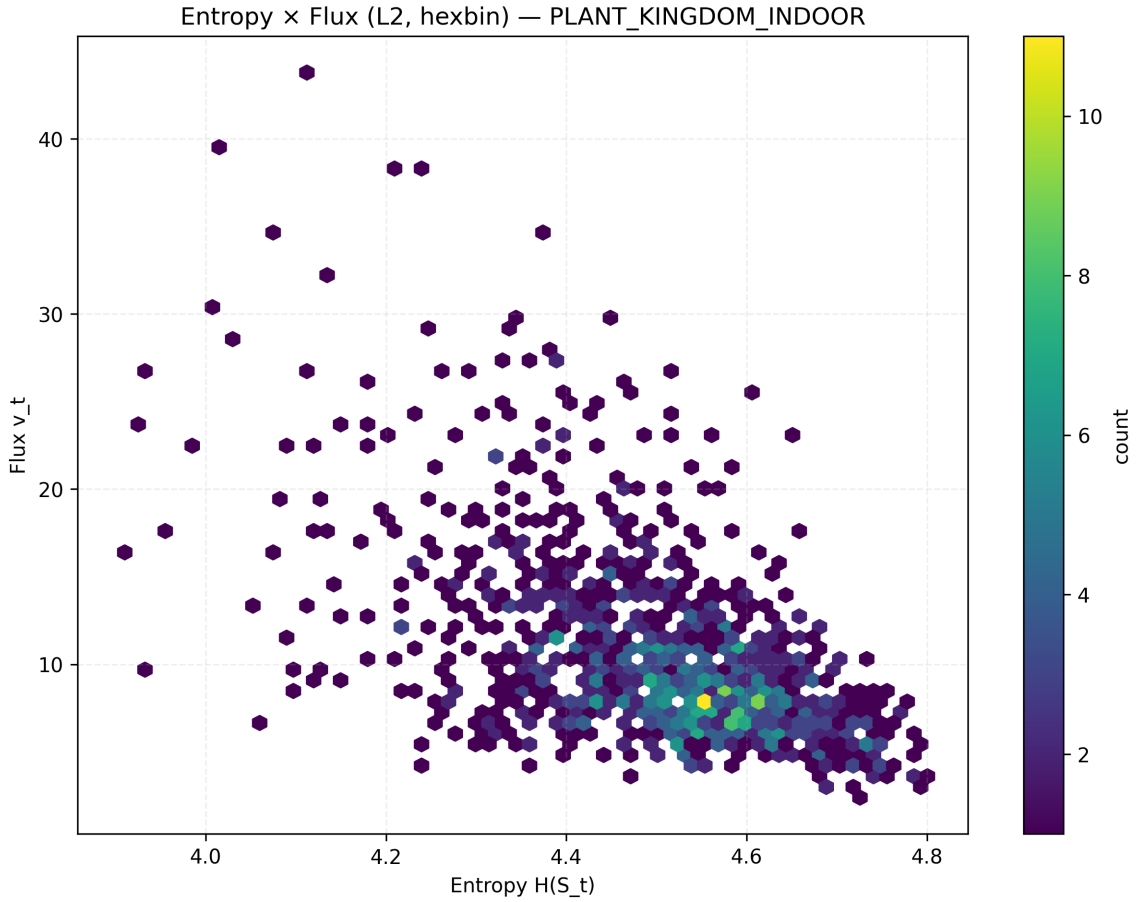

Figure 91: Plant Kingdom indoor: entropy vs flux (ℓ_2), hexbin.

Entropy × Flux (Cosine) — PLANT KINGDOM OUTDOOR

This scatter plot shows the relationship between instantaneous entropy $H(S_t)$ and cosine-based flux magnitude for the outdoor Plant Kingdom session. Most observations cluster at higher entropy values (roughly 4.6–4.9), with low to moderate flux values, forming a dense, right-skewed cloud. As entropy increases within this band, flux remains relatively constrained, suggesting that high-entropy states are typically associated with small incremental directional changes rather than abrupt reconfigurations.

A small number of points extend upward to substantially higher flux values, indicating rare but pronounced state transitions occurring at comparable entropy levels. These outliers are not associated with low entropy, but rather appear embedded within the high-entropy regime, implying that large reorganisation events can occur without a reduction in entropy. Overall, the plot highlights a dominant regime of high entropy with restrained flux, punctuated by sparse, high-magnitude excursions.

This figure is useful for visualising the full dynamic range of outdoor state transitions but may be visually dense for publication without aggregation.

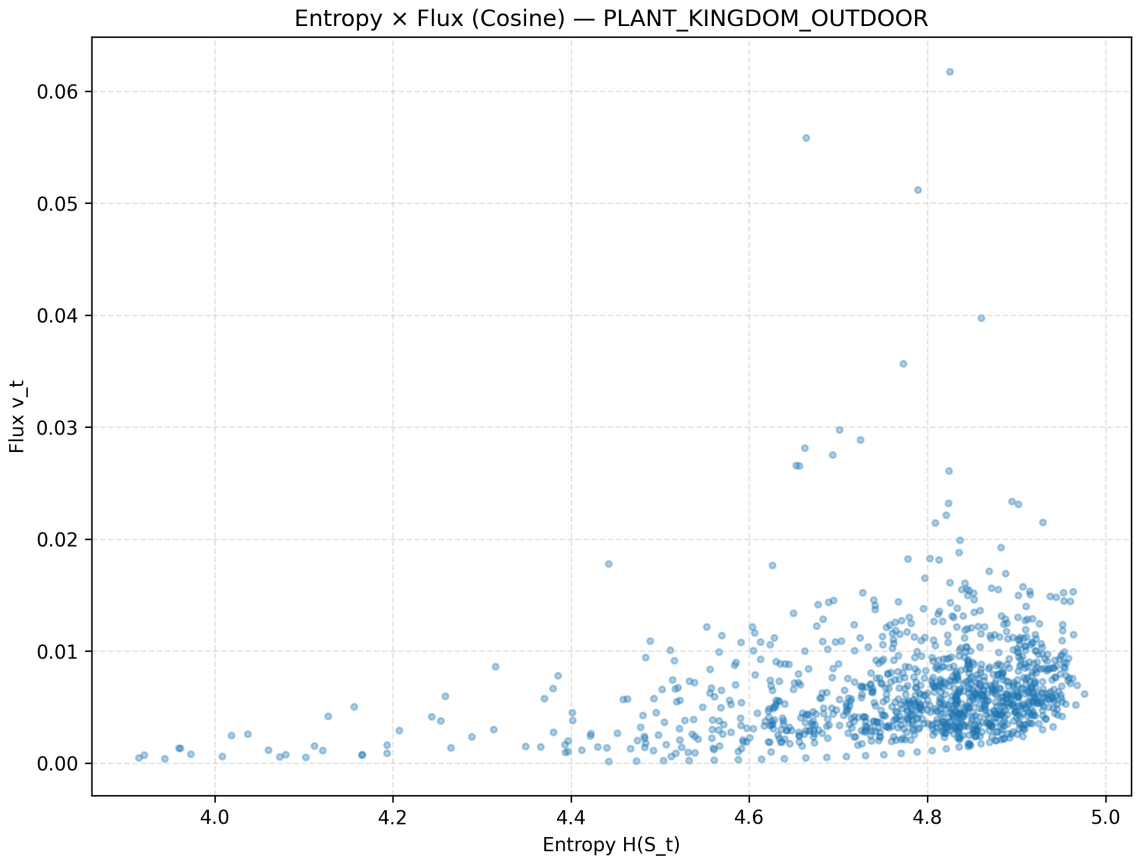

Figure 92: Plant Kingdom outdoor: entropy vs flux (cosine distance), scatter.

Entropy × Flux (Cosine, hexbin) — PLANT KINGDOM OUTDOOR

The hexbin representation of cosine flux versus entropy reveals the density structure underlying the scatter plot. A clear high-density basin appears at high entropy (approximately 4.7–4.9) combined with low flux values, indicating that the majority of time points occupy a stable, high-entropy–low-flux regime. This basin is sharply defined, suggesting temporal persistence rather than transient clustering.

The hexbin view also makes clear that the higher-flux events seen in the scatter plot are genuinely sparse, occupying isolated bins with very low counts. There is no secondary high-density mode at elevated flux, reinforcing the interpretation that large directional state changes are rare in the outdoor condition. This plot is particularly effective at distinguishing dominant dynamical regimes from outliers and may be a strong candidate for inclusion in a paper due to its clarity.

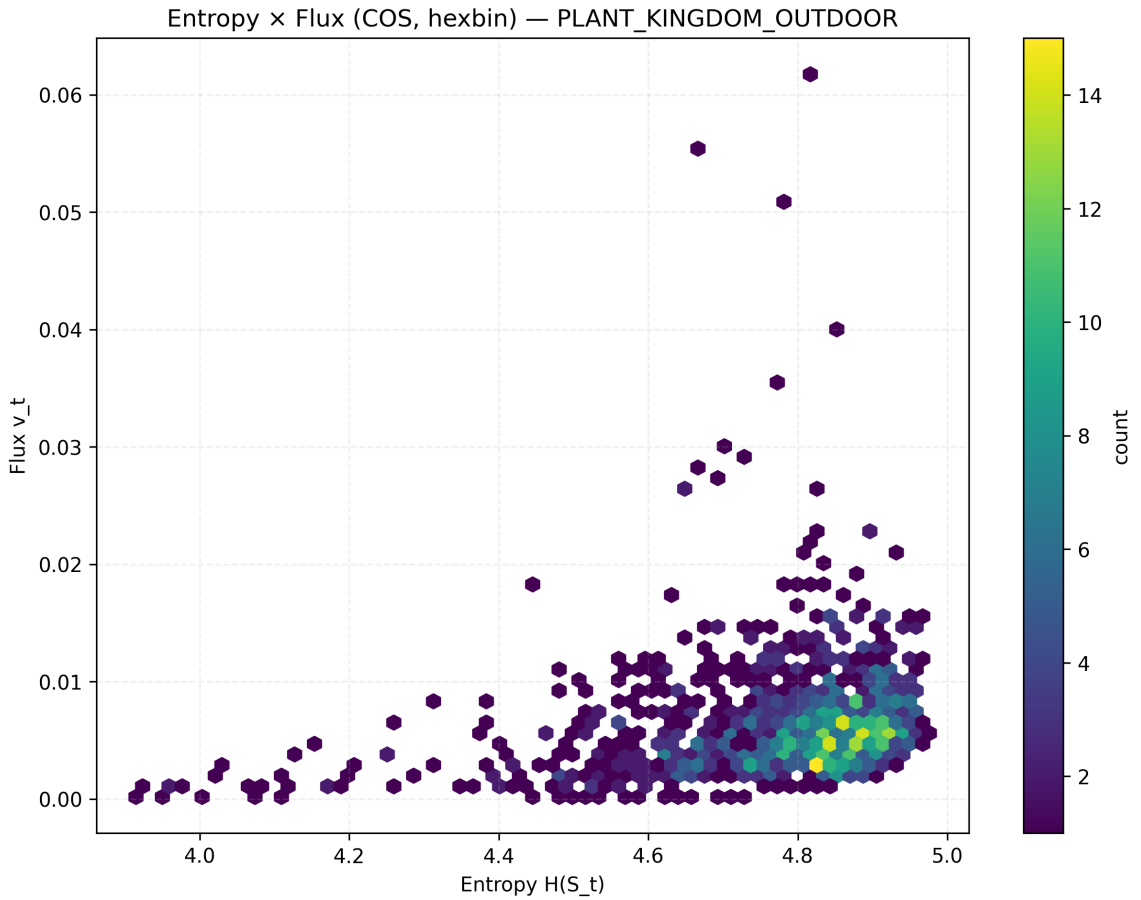

Figure 93: Plant Kingdom outdoor: entropy vs flux (cosine distance), hexbin.

Entropy × Flux (L2) — PLANT KINGDOM OUTDOOR

This scatter plot shows entropy against L2-norm flux, which captures the magnitude of regional reorganisation irrespective of direction. Compared to the cosine flux plot, the vertical spread is substantially larger, indicating sensitivity to total reconfiguration magnitude rather than alignment. Despite this broader range, the dominant pattern remains similar: most points cluster at high entropy with relatively low L2 flux values.

A long upper tail of high L2 flux values is present, extending to markedly larger magnitudes than the cosine metric. These events are scattered across the entropy range but still predominantly occur at higher entropy values. This suggests that large-scale reconfigurations in the outdoor session tend to occur within already complex states, rather than emerging from low-entropy baselines. The figure emphasises variability and intermittency in reorganisation magnitude.

This chart is informative for illustrating the full scale of state-space movement but may benefit from a density-based complement for clearer interpretation.

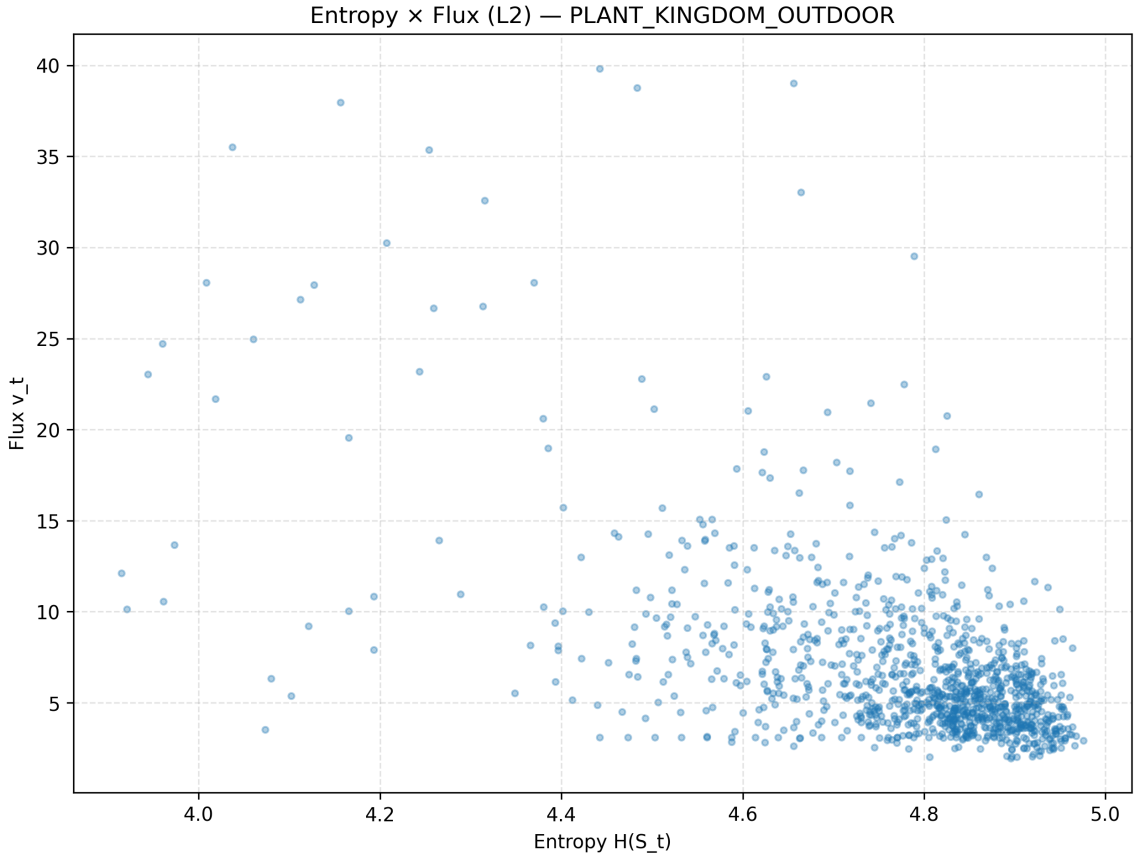

Figure 94: Plant Kingdom outdoor: entropy vs flux (ℓ_2), scatter.

Entropy × Flux (L2, hexbin) — PLANT KINGDOM OUTDOOR

The hexbin plot of entropy versus L2 flux reveals a concentrated core at high entropy and low-to-moderate flux, mirroring the cosine-based density structure but with a broader vertical footprint. The highest-density region sits around entropy values near 4.7–4.9 with flux values in the lower portion of the scale, indicating that most time points involve modest reorganisation within a complex state.

Above this dense core, bins thin rapidly, confirming that high-magnitude L2 flux events are infrequent and not sustained. Unlike the scatter view, the hexbin representation makes it clear that these extreme values do not form a secondary regime but instead represent isolated excursions from the dominant dynamical state. This figure is particularly strong for conveying the balance between stability and occasional large-scale reorganisation and is a good candidate for later inclusion.

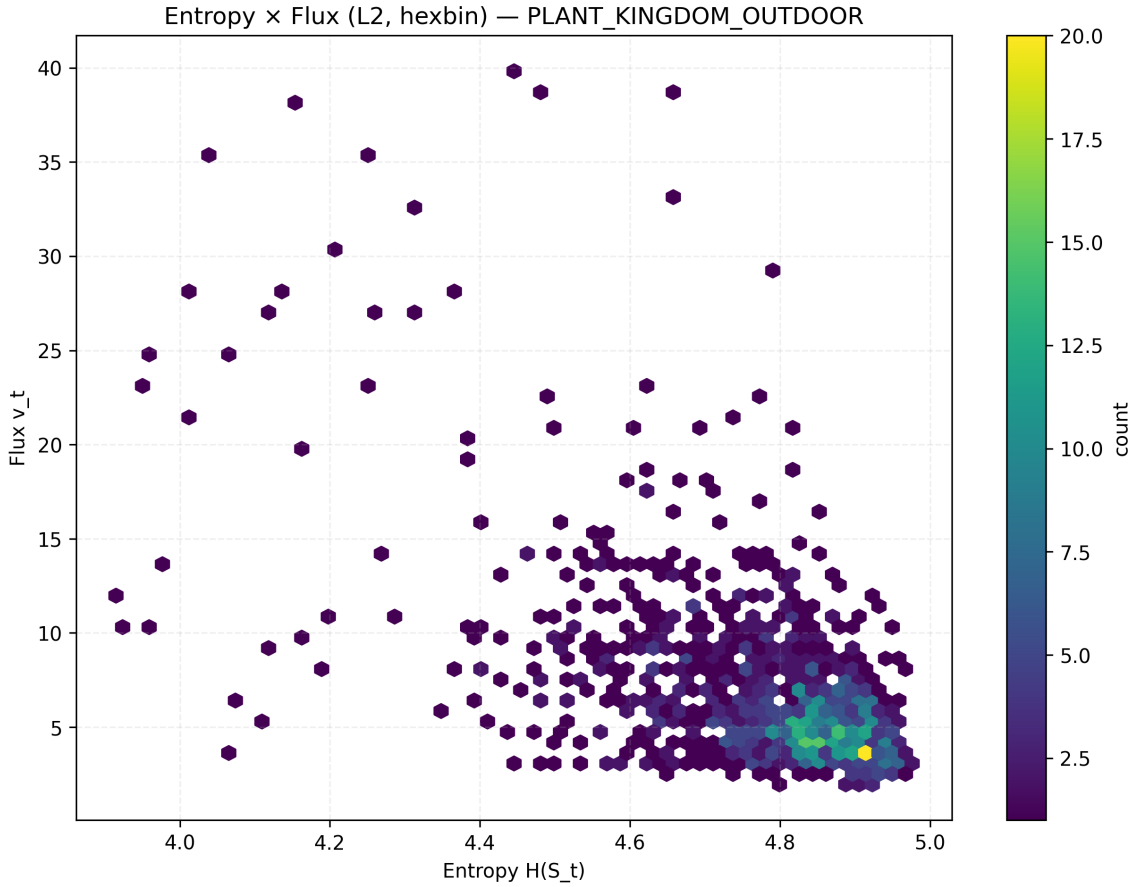

Figure 95: Plant Kingdom outdoor: entropy vs flux (ℓ_2), hexbin.

Final Summary

This analysis explores the complex and dynamic neural processes underlying the Plant Kingdom sessions through a variety of EEG metrics, focusing on entropy, cross-frequency coupling, state-space flux, and temporal stability. By comparing baseline resting conditions (eyes-closed) with the indoor and outdoor sessions, we gain valuable insights into how environmental factors modulate neural organization and reorganization at both the regional and band-specific levels. Key findings include:

1. **Entropy and Power Dynamics:** The Plant Kingdom sessions show a marked departure from baseline resting dynamics, with significant shifts in entropy and power distribution. Notably, the indoor condition revealed increased variability in higher-frequency bands (Beta and Gamma), while the outdoor condition demonstrated pronounced shifts in power toward high-frequency activity, especially in the Gamma band, and reduced Alpha activity.

2. **Cross-Frequency Coupling (PAC):** Phase-amplitude coupling (PAC) between low-frequency (Theta) and high-frequency (Gamma, Beta) bands was observed to increase during both the indoor and outdoor conditions. This coupling is more pronounced in frontal and parietal regions, particularly during the outdoor condition, highlighting how environmental factors can modulate the interaction between different frequency bands, further supporting the dynamic nature of brain state organization.

3. **State-Space Reorganisation:** The analysis of reorganisation velocity (state-space flux) revealed that both indoor and outdoor conditions exhibit increased reconfiguration rates compared to baseline. The indoor condition showed intermittent bursts of reorganisation, with higher variability than baseline, while the outdoor condition presented more pronounced bursts of reconfiguration, suggesting a more dynamic neural state under environmental modulation. Despite these bursts, the system showed overall temporal stability.

4. **Temporal Stability and Persistence:** Temporal persistence metrics highlighted that reorganisation during the indoor condition occurred in both gradual and episodic bursts, while the outdoor condition exhibited greater variability in both state and reorganisation magnitude. Importantly, both conditions showed that larger reorganisation events were rare, occurring in brief episodes rather than continuous shifts, reinforcing the importance of understanding temporal structure in neural dynamics.

In summary, this study provides a detailed empirical account of how different environmental settings impact neural dynamics. It emphasizes the crucial role of both spatial and temporal organization in understanding neural system reactivity and stability, which has significant implications for understanding brain function in naturalistic settings. Further, these findings underscore the potential of environmental influences to shape brain function beyond simple resting-state dynamics, offering new perspectives on the relationship between cognitive states, neural reorganization, and environmental contexts.

Conclusion

This study presents a comprehensive exploration of how environmental conditions influence neural dynamics, with a specific focus on entropy, cross-frequency coupling, state-space reorganization, and temporal stability within the Plant Kingdom sessions. By investigating both indoor and outdoor conditions against a baseline resting state, we've demonstrated that environmental factors can profoundly modulate neural activity at various levels, including regional power dynamics, cross-frequency interactions, and the overall tempo of reorganization. The findings suggest that the brain is highly adaptive to its environmental context, as evidenced by the shifts in power distribution, particularly the enhanced high-frequency activity observed in the outdoor condition. Furthermore, our analysis of phase-amplitude coupling (PAC) and state-space flux provides insight into how different frequency bands interact and reorganize in response to external stimuli. The indoor condition highlighted more episodic reorganization events, while the outdoor condition revealed more pronounced and sustained changes, with specific areas of the brain exhibiting higher levels of reorganization activity. This work highlights the importance of examining not just the amplitude or static power within specific bands, but also the temporal and spatial dynamics that shape the brain's response to its environment. The study underscores the need for further exploration into how environmental and contextual factors influence neural systems, and offers a valuable framework for understanding brain function in more naturalistic settings. In conclusion, by mapping how environmental changes impact neural organization, this research contributes to a deeper understanding of the brain's dynamic adaptability. It paves the way for future studies examining the impact of various environmental and experiential contexts on neural systems, with potential applications in cognitive neuroscience, neuroplasticity, and real-world brain-computer interface design.

Additional Data and Resources

The full set of analyses, including additional charts generated through the Spectral scripts, are available for further exploration in the project's GitHub repository. The supplementary data sets, charts, and scripts can be accessed via the following link:

GitHub Repository:

`https://github.com/thelinegroupltd/Neural-Reorganisation-Plant-Kingdom-EEG`

We encourage readers to review the extended analyses, as the GitHub repository houses supplementary material that may provide additional context and insights into the results presented in this paper.